Novel approaches
to study the biomechanics
of intact central nervous tissue

Der Fakultät für Physik und Geowissenschaften

der Universität Leipzig

eingereichte

D I S S E R T A T I O N

zur Erlangung des akademischen Grades

Doktor der Naturwissenschaften

Dr. rer. nat.

vorgelegt

von Valentina Dallacasagrande

geboren am 21. Oktober 1980 in Piacenza

Leipzig, den 31.03.2015

Dedicato alla mia famiglia

Bibliographische Beschreibung

Dallacasagrande, Valentina

Novel approaches to study biomechanics of intact central nervous tissue

Universität Leipzig, Dissertation

151 S., 313 Lit., 67 Abb., 4 Tab.

Referat

In nature, cells are not randomly clustered to form tissues. The tissue is a more complicated system with functions that go beyond what any single cell type could accomplish. While studying single-cell mechanics and dynamics is relevant from an investigative point of view, this approach loses, or fail to gather information about the tissue.

The tissue investigated in this study is the neurosensory retina which seeing as extension of the brain is a very convenient model for the central nervous system due to its accessibility. The retina is constantly subjected to different mechanical stresses from development to adulthood. Although the majority of the phenomena where mechanical stresses are involved are well-studied, the mechanics behind them is not well understood. However, knowledge about the ability of the retina to adjust to mechanical stresses is essential, for example, for improving retinal surgery.

Establishing a method to mechanically probe the retina is a challenge due to the extremely delicate nature of this multilayered neural tissue and to the short-time survival *ex vivo*. The organotypic tissue culture is a powerful tool because it allows to maintain with high accuracy the complex multicellular anatomy and the microenvironment of the original tissue. One of the limitations of the organotypic culture techniques has been until recently due to the ability to use only post-natal/juvenile tissues for long-term culture. The importance of using adult tissue is incontestable when the investigation focuses on age-related pathologies such as vitreous shrinkage or macula degeneration.

In this work, TiO_2 nanotube arrays are presented as the innovative substrate for long-term organotypic culture of adult neural tissue. The retinal whole-mount of adult guinea pig and the brain slices of adult mouse were cultures for 14 days without showing any sign of edema or swelling. Furthermore, in order to study the behavior of the retinal tissue under shear stress new set-ups were designed. For the first time, the behavior of the retinal layers were observed showing that the retina does not act as an homogeneous material in response to an applied stress. The methods developed here can be used for future quantitative studies, to provide an exact knowledge of retinal biomechanics which will help retinal surgeons to optimize their methods.

Contents

Contents

List of Figures

List of Tables

1 Introduction

The vertebrate eye is an extremely complex organ in which biomechanics plays a central role, nonetheless it is rarely considered as a biomechanical structure. Intraocular pressure, intraocular and extraorbital muscles and external forces exert mechanical loading to the eye. Indeed, its ability of tracking objects in movement or of deforming the lens to focus near and far, is due to forces applied by several muscles. Although the retina is constantly subjected to several different types of mechanical stress, biomechanical eye researchers have concentrated their attention on more motile structure such as lens, or recently on sclera and cornea. During development, the retina is stretched due to expansion of the eyeball. This tension is preserved in the adult eye by the intraocular pressure and the photoreceptor-RPE adhesion to assure integrity and function of the retinal tissue (Yao et al., 1994; Taylor et al., 2013). In addition to these physiological mechanical forces, under pathological conditions the retinal tissue undergoes mechanical stress which can cause several retinal disorders such as retinoschisis and retinal detachment. Although the majority of these phenomena are well-studied, the mechanics behind them is not well understood. Knowledge about the ability of the retina to adjust to mechanical stresses is essential, in particular to improve retinal surgery (see Figure 1.1).

Data on the material properties of the neural retina are almost lacking due to its highly delicate nature. To date, an increase in the number of studies focusing on the mechanical characterization of the retinal tissue, as well as individual glial and neuronal cells have been reported (Reichenbach et al., 1991; Lu et al., 2006; Lindqvist et al., 2010; Chen et al., 2010 Chen and Weiland, 2010; Franze et al., 2011; Chen and Weiland, 2012; Taylor et al., 2013; Worthington et al., 2014). The experimental techniques employed to study the mechanical response of single cells (Mofrad, 2009) are not suitable to analyze a complex structure such as the retina. The absence of established standard methods to mechanically probe tissues motivated the design of new set-ups as described in the second part of the present work. In addition, the work addressed the question whether the retinal tissue acts as homogeneous material or whether it is possible to distinguish the behavior of the different retinal layers when a shear stress is applied employing the novel methods.

The aim was also to design new methods to mechanically probe the retinal tissue with the possibility to use adult animal tissue and to apply mechanical stress over an extended period of time. The importance of using adult animals is incontestable when the investiga-
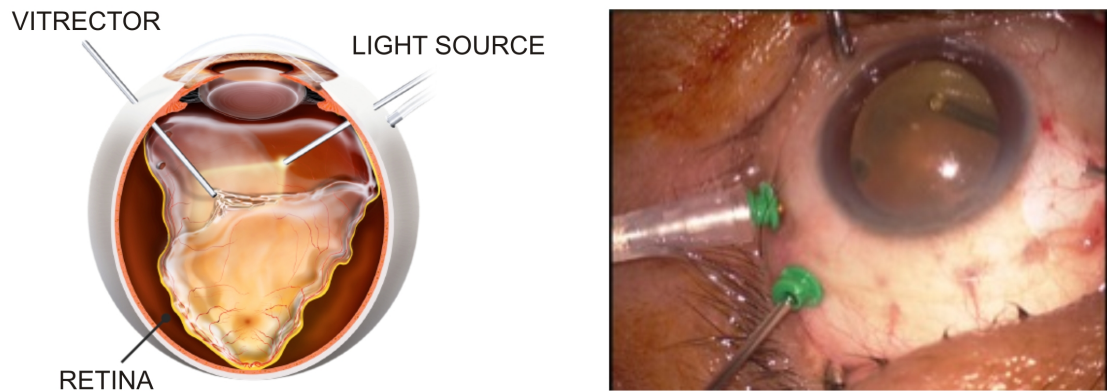
Figure 1.1: Illustration of retinal vitrectomy. The vitrectomy is a microsurgical procedure used to repair retinal disorders. The vitreous body is removed with a vitrector and then replaced with a special saline solution.

tion focuses on age-related pathologies such as vitreous shrinkage or macula degeneration. In addition, trying to prolong the survival time for mature tissue is essential to making progress in exploring regenerative mechanisms *in vitro*, for example. A cause of a decrease of plasticity of the adult animal the degeneration of the mature explant, in culture, occurs earlier than for the postnatal/juvenile tissue.

The air-liquid interface system, introduced by Stoppini (Stoppini et al., 1991), combined with the employment of cellulose filter or insert as culture substrate (Mosinger Ogilvie et al., 1999; Caffé et al., 2001; Johansson and Ehinger, 2005) is, up to date, one of the most efficient methods for organotypic culture of adult neural tissue. One of the limitations of this culture technique is the inability to guarantee a long-term survival of mature tissue. Consequently, the first part of this work was aimed at improving the organotypic culture of adult tissue, preserving the interface system which proved its effectiveness. The element which crucially influences the achievement of a stable long-term organotypic culture is the substrate material.

The idea developed was to introduce a novel substrate as a principal requisite of enhancing the survival of the entire tissue, while preventing the single cells to grow and to migrate out of the tissue. Considering that a change in morphology is a good indicator of tissue damage, the study focused on observing any alteration in the neural tissue structure.

The data extracted from this study are mainly qualitative since the main focus is on the morphological changes of the tissue. Nevertheless this work lays the foundations for understanding the complex mechanical response of the neurosensory retina and presents an efficient method for organotypic culture of adult neural tissue.

2 Background

In this chapter I will give an overview of how mechanics can help in the understanding of many biological processes. First, the morphology of the neural tissue, in particular the retina, is described. In the second part, I will introduce some fundamental concepts of mechanics of the continuum. Then, I will go into more details reviewing the models and the methods used in biophysics to describe mechanical properties of living cells and tissues.

2.1 The Retina

2.1.1 Morphology of the Inverted Retina

The human eye is one of the most sensitive and complex organ. Leonardo Da Vinci defined it as the window of the soul (Pevsner, 2002). Indeed, human beings rely on sight more than on any other sense. Three different layers can be distinguished in the eye: the outer region consisting of the cornea and the sclera, the middle region composed of the iris, the choroid and the lens, and the inner segment represented by the retina and the retinal pigment epithelium (RPE) (Willoughby et al., 2010) (see Figure 2.1).

The cornea acts as the major refractive component of the eye and protects it from infection and structural damage. Together with the crystalline lens and the aqueous vitreous body, the cornea is responsible for forming the optical image on the retina. The sclera is a coat of connective tissue surrounding the eye, and its function is to protects and maintain the eye's shape. The visible portion of the sclera is commonly known as the 'white' of the eye (Li and Jain, 2009). The choroid, located between the sclera and the retina, is composed of capillaries, small arteries and veins. Its function is to supply the back of the eye with oxygen and nutrients. The aqueous humor is a clear watery fluid that fills the chamber between the cornea and the iris, and nourishes them. The vitreous humor is gel-like substance that fills the cavity between the retina and the lens, maintaining the intraocular pressure (Li and Jain, 2009, Weale, 1974).

The retina represents the multilayered sensory tissue of the posterior eyeball. The light hitting the retina is converted into nerve signals (Hubel, 1995). The average thickness of the retina is around $200 - 250\,\mu\text{m}$ and it consists of multiple layers. The retinal layers from the vitreous to the choroid are shown in Figure 2.2. The *inner limiting membrane* (ILM)
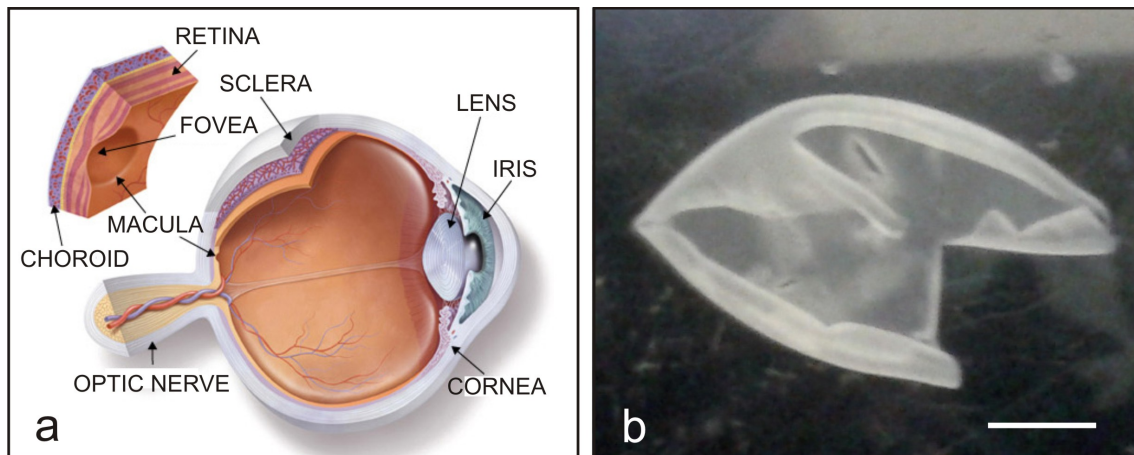
Figure 2.1: The structure of the eye. (a) A schematic drawing of the eye showing the main structures that compose this organ. The retina is the tissue located in the back of the eyeball which is in contact with the choroid. Image from www.aapos.org website. (b) Picture of a fresh isolated guinea pig retina. Scale bar $200\,\mu$m.

defines the boundary between the retina and the vitreous body. The *nerve fiber layer* (NFL) contains the axons of the ganglion cells. These axons form bundles and leave the retina as the optic nerve. The cell bodies of the ganglion cells represent the *ganglion cell layer* (GCL). The *inner plexiform layer* (IPL) consists of synaptic connections between the ganglion cells and cells, whose cell body is located in the *inner nuclear layer* (INL). In this layer the nuclei of amacrine cells, horizontal cells, bipolar cells and Müller cells are present. The *outer plexiform layer* (OPL) is made up of synapses formed between the cells of the INL and the photoreceptors. The nuclei of the cones and rods are located in the *outer nuclear layer* (ONL) . The *outer limiting membrane* (OLM) displays a row of junctional complexes between the photoreceptor nuclei and their inner segments. The segments of the photoreceptors compose the *photoreceptor segment layer* (PRS). The outermost retinal layers is the *retinal pigment epithelium* (RPE).

The retinal cells can be divided into neurons and glial cells. Six major classes of neurons are present in the retina: bipolar cells, horizontal cells, amacrine cells, ganglion cells, rod photoreceptors cells and cone photoreceptors cells (rods and cones). Rods are generally used at low-light conditions and cones for day-light, bright colored vision (Kolb, 2003). The main glial cells are the Müller cells. In addition, microglia and astrocytes can be found in the retina, with the latter being present if the retina is vascularized. In this type of retina one can also identify the pericyte contractile cells which wrap the endothelial cells of the retinal blood vessels.

The Müller Cells

Müller (radial glial) cells are the predominant glial cells of the vertebrate retina (Bring-mann et al., 2006). Each Müller cell represents the center of a so-called columnar unit of retinal neurons (Reichenbach and Robinson, 1995) (see Figure 2.3). This glia-neuron structure represents the smallest functional unit of the retina contributing to the imaging processing. Thus, the retina is considered to be composed of a repeating structure of these columnar units which do not depend on the local topography for their specialization (Bringmann et al., 2006). Müller cells are the only cells which span the entire thickness of the retina, anatomically and functionally connecting the retinal neurons with the different retinal compartments. In the last decades the role of these radial glial cells has been intensely investigated, highlighting their contribution to neuroscience understanding. They play a pivotal role in the biochemical processes and mechanical activity of the retina. Müller cells support homeostasis and the metabolism of the retinal neurons (Tsacopoulos and Magistretti, 1996; Bringmann et al., 2004, Bringmann et al., 2009b). They maintain the inner blood-retinal barrier and regulate the retinal blood flow (Tout et al., 1993, Metea and Newman, 2006). Neurotransmission and synaptic activity are controlled by the release of gliotransmitters (Newman, 2003). Müller cells stabilize the structure of the retina and protect the retinal neurons. A lack of this neuroprotective function could also be the cause of neuronal degeneration (Bringmann et al., 2009a, Bringmann and Wiedemann, 2012). Recently, it has been recognized that the radial glial cells act as living optical fibers that guide the light through the entire retina minimizing the scattering of light (Franze et al., 2007, Agte et al., 2011). It has also been shown that Müller cells are twice as soft as neurons. Thus, Müller cells could act like an 'air-bag' protecting the neurons from mechanical trauma or from tractional forces due to vitreous shrinkage (Lu et al., 2006). Because of their viscoelastic properties, they are considered an appropriate substrate for neurite outgrowth which leads to the conclusion that Múller cells are involved in retinal development and adult synaptic plasticity (Lu et al., 2010). In reactive gliosis, the retinal glial cells become stiffer due to the upregulation of the intermediate filaments (see Section 2.2.2). This suggests that these cytoskeleton polymers are involved in the retinal biomechanics. Lu et al. (2010) demonstrated that Müller cells of mice lacking intermediate filaments do not change their biomechanics under pathological conditions (Reichenbach and Bringmann, 2013).

The Fovea Centralis

The fovea centralis is a particular area of the human retina which is located exactly on the visual axis of the vertebrate eye. Indeed if a beam would be projected perpendicular to the center of the eye, it would hit the foveal pit (Hendrickson, 2005). The fovea lies

in the center of the macula, a central retinal region which can be identified by its yellow pigmentation (see Figure 2.1 a). The central area of the fovea in turn is called foveola which is characterized by the absence of retinal blood vessels, and by the centrifugal shift of the inner retinal layers , resulting in the lack of ganglion cell layer and the inner nuclear layers. Thus, incoming light directly hits the densely packed cone photoreceptor area (rod photoreceptors cells are absent) (see Figure 2.4) (Provis et al., 2013). Therefore, the fovea is the area of the retina with the maximal acuity vision (Helmholtz, 2005). A large portion of the visual cortex is dedicated to processing the information gathered from the fovea (Hendrickson, 2005). Because of the foveal structure, the inner processes of the foveal cones are elongated centrifugally in order to reach the synapses of the bipolar and horizontal cells located in the zone surrounding the foveola (see Figure 2.4 b) (Polyak, 1941). The margins of the depression that constitutes the fovea are composed of an accumulation of ganglion cells due to the displacement of the cells during the foveal development (Hendrickson and Yuodelis, 1984, Ma and Tc, 1995).

The mechanisms involved in the formation of the fovea are still not well understood. The foveal development is a long process that starts during fetal development and continues until years after birth (Springer and Hendrickson, 2004). The mechanical forces involved in retinal development are essentially tangential forces that stretch the retina due to organ growth, as well as orthogonal forces generated by intraocular pressure (Springer and Hendrickson, 2004). For more details see section 5. Among vertebrates, only primates, such as humans and some monkeys, as well as some species of fish, birds and reptiles possess a fovea centralis.
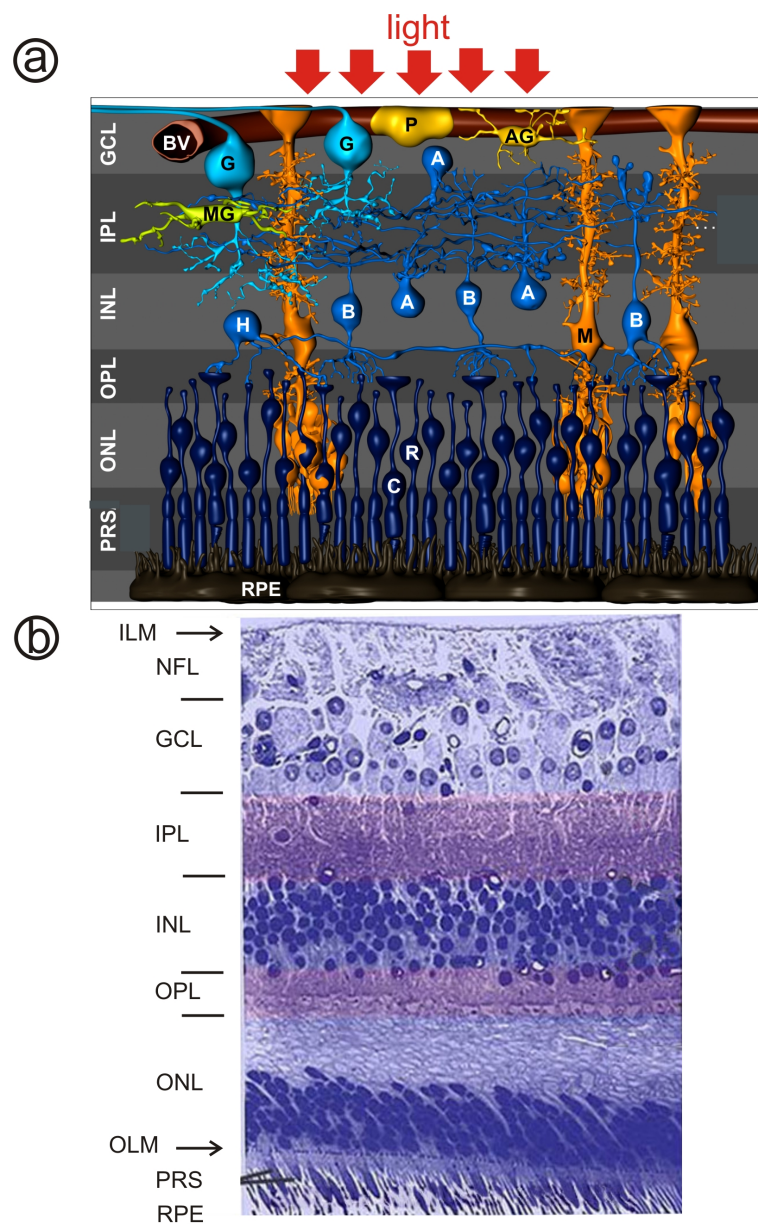
Figure 2.2: The structure of the inverted vertebrate retina. (a) Three-dimensional reconstruction of the retina which highlights the layers and the cells composing the retina. The layers starting from the bottom are the retinal pigment epithelium (RPE); the photoreceptor segments layer (PRS); the outer nuclear layer (ONL); the outer plexiform layer (OPL); the inner nuclear layer (INL); the inner plexiform layer (IPL) and the ganglion cell layer (GCL). The cells colored in blue shades represent the neurons: cones (C); rods (R); horizontal cells (H); bipolar cells (B) and amacrine cells (A). The glial cells are the Müller cells (M); microglia cells (MG) and astroglia cells (AG). A blood vessel (BV) and a pericytes (P) are also shown. (b) A light micrograph of a human retina (Richardson's methylene blue stain). The inner and outer limiting membrane are also shown (ILM and OLM). Adapted image from WebVision website.
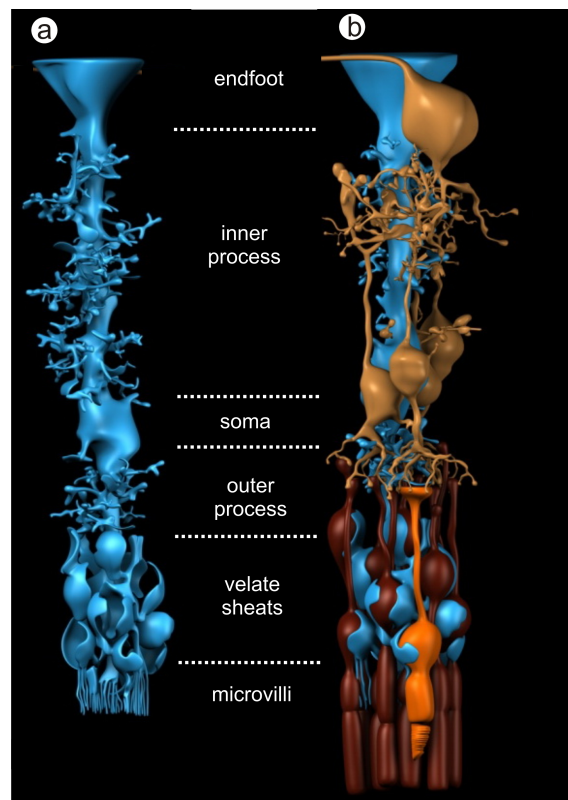
Figure 2.3: Morphology of a Müller cell. (a) Three-dimensional reconstruction of a single Müller cell showing its diversified morphology along the entire retinal thickness. (b) Three-dimensional reconstruction of a retinal columnar unit, in which the neurons (yellow, red) tightly enwrap the central Müller radial glial cells (blue).
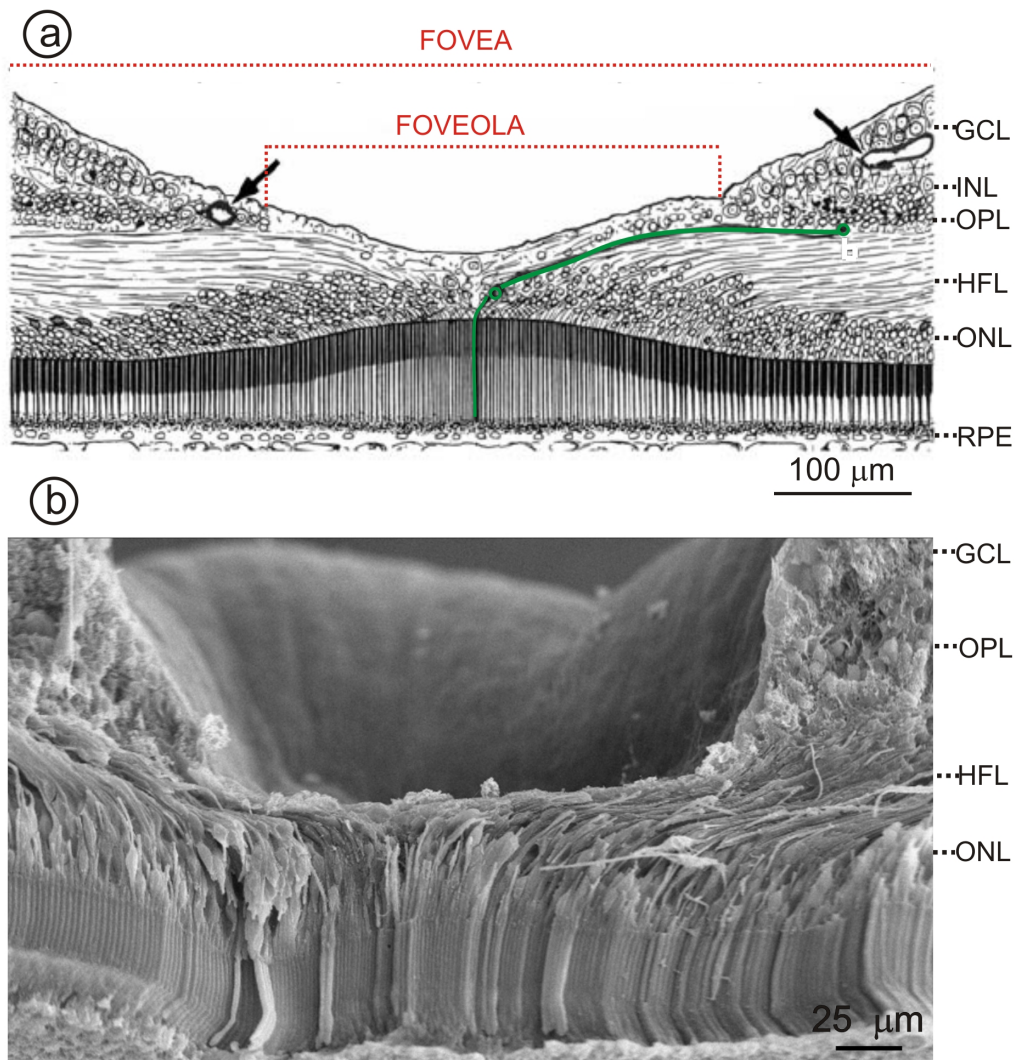
Figure 2.4: The ultra-structure of the fovea. (a) The drawing of the fovea and its central foveola shows the bending and the centrifugal elongation of the axon of the cone photoreceptor cells (green line) forming the Henle fiber layer (HFL) in order to retain their synaptic connection with the cells in the INL. All inner retinal layers (GCL, IPL and INL) are laterally shifted to the side such that the fovea forms a pit. The arrows indicate blood vessels which are absent within the foveola. Image of the fovea of a macaque monkey modified from Polyak, 1941. Scale bar 100 μm. (b) Scanning electron micrograph of the fovea of a macaque monkey. Image modified from Reichenbach and Bringmann, 2010. Scale bar 25 μm.

2.2 Mechanical Properties of Cells and Tissues

2.2.1 Rheology: Introduction to Viscoelasticity

The science of rheology was introduced by Professor M. Reiner and Professor E. Bingham in the mid-20's and was inspired by the Greek philosopher Heraclitus quotation Πάντα ρεῖ- *everything flows*. Rheology is a pluridisciplinary science describing the flow properties of various materials with complex structures, i.e. muds, sludges, suspensions, polymers, food and biological materials. Rheology encompasses viscosity measurements, characterization of flow behavior and determination of material structure.

In the field of rheology, the material is classified at *viscous*, *elastic*, or *viscoelastic* based on properties such as *relaxation time* defined as the time it takes a material to go back to its original shape once deformed.

An ideal elastic material stores all applied deformation energy and will consequently completely recover upon the release of the stress. In a viscous material, the deformation energy will not recover because the energy will be dissipated by the material flow. A large number of materials show viscous as well as elastic properties, i.e. they store some of the deformation energy within their structure while some is lost by flow. These materials are called viscoelastic.

Mechanical stress is defined as the applied force divided by the area where the force is applied (see equation 2.1). It measures the intensity of the interatomic and intramolecular forces of a material in which a solid or fluid body is idealized as a mathematical continuum. Mechanical stress in a solid material generalizes the simpler concept of pressure in a fluid. Because real materials are not infinitely rigid, stresses produce deformations that are measured by the strain. The Cauchy strain or engineering strain is defined as the ratio of the total deformation to the initial dimension of the material that experiences the external forces (see equation 2.2) (Sasaki, 2012). Integration of strains through space gives displacements which quantify the movement of the intramolecular structure. As a result of the applied forces, the material body changes its size and shape, this behavior is described by kinematics (see Figure 2.5) (Kelly, 2013).

The concept of stress is based on the physical principle of the Newton's second law of physics. However, the concept of strain is based on geometry and trigonometry. Both stress and strain can be applied to all materials without distinction, however their relationship differs among various materials (Kelly, 2013).

$$stress = \frac{applied\ force}{area} \tag{2.1}$$
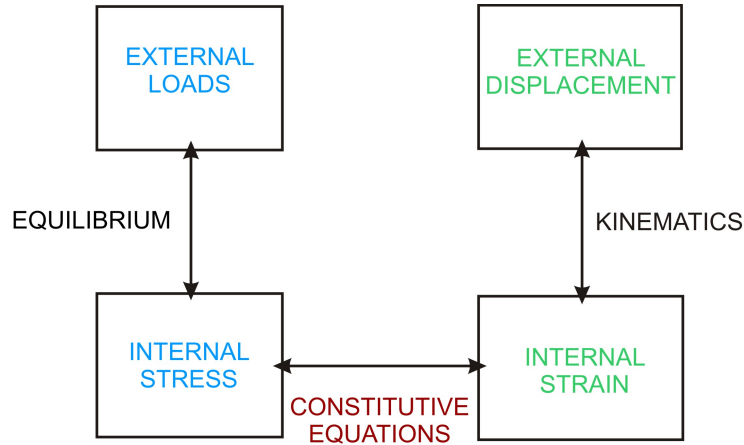
Figure 2.5: Schematic representation of the relationship between stress and strain due to constitutive equations. The internal forces induced by the applied external forces are indicated as internal stress. The internal strain measures the internal deformations which induce an external displacement. Consequently, the body deforms and/or moves. Image adapted from Kelly, 2013.

$$strain = \frac{dimensional\ change}{initial\ dimension} \qquad (2.2)$$

Mechanical stresses and strains are linked through the material properties (MP) of the body under consideration. The constitutive equations (see equations 2.3; 2.4; 2.6; 2.7; 2.8 and 2.9), also called material laws, characterize in mathematical terms the material behavior of the body.

The simplest constitutive law for solid materials is the one that assumes the stress to be proportional to the strain and vice versa (Fung, 1993). If a force is applied to a solid material, the solid can behave either as a rigid Euclidean material or as an elastic Hookean solid. In the first case, the body does not deform following an applied stress. In the second case, the deformation can increase linearly, i.e. the higher the stress the more the material alters its shape. The linear elastic law is ideal for predicting the response of materials undergoing small deformations.

An ideal elastic material does not undergo a permanent deformation when a load is applied, and it returns to its original shape when the load is removed. Usually the elastic behavior is represented by a linear spring, since a spring produces an instantaneous deformation proportional to the load (Fung, 1993). The unloading stress-strain path is the same as the loading path (see Figure 2.6). The body is considered stretched or compressed (see Figure 2.7, a and b) when an external force *F* is applied perpendicular to its cross-sectional area *A*. Therefore the *normal stress* σ is defined as,

LINEAR ELASTIC MATERIAL
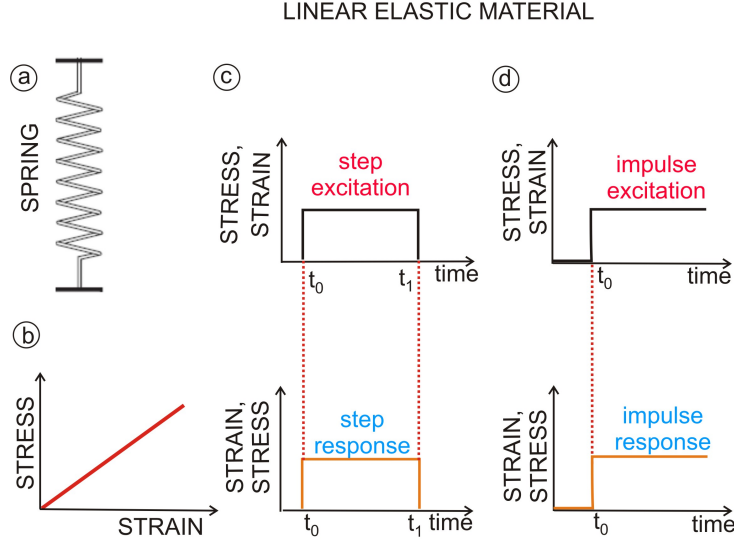
Figure 2.6: Stress-strain relationship in an elastic material. An elastic body can be modeled as a spring a) whereby after a deformation, the material completely recovers to its initial conformation. Stress and strain are directly and simply proportional to each other b). Under a given stress (or strain), the material responds proportionally to the deformation (or load) independent of the excitation being a step c) or an impulse d). For a given a step stress excitation, the strain for $t > t_1$ is constant and for $t < t_1$ results in zero. In the case of a given strain impulse the stress result is constant for $t > t_0$.

$$\sigma = \frac{F}{A}. \tag{2.3}$$

The deformation caused by the external load, as mentioned above, is the *axial strain ϵ*,

$$\epsilon = \frac{\Delta l}{l} \tag{2.4}$$

with Δl being the extension due to the tensional force and l the natural length of the body. The relationship between the stress and the strain can be described by

$$\sigma = C\epsilon \tag{2.5}$$

where C is a *tensor of the elastic moduli* (Fung, 1993).

For linear, homogeneous, isotropic materials, the coefficient of proportionality is called *Young's modulus* or *elastic modulus E*,

$$E = \frac{\sigma}{\epsilon}. \tag{2.6}$$

The Young's modulus measures the stiffness of a material, i.e. its resistance to defor-
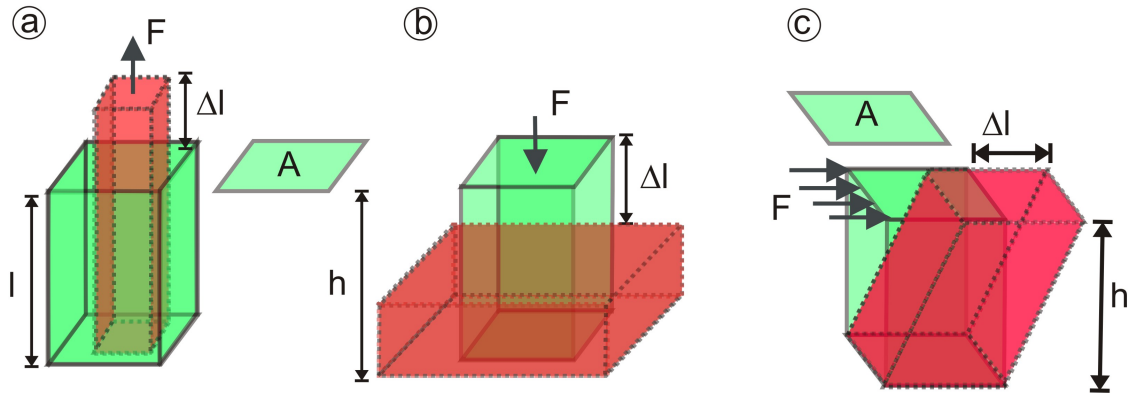
Figure 2.7: Schematic representation of tension, compression and shear. (a) A material is stretched (a) or compressed (b) when an external force F is applied perpendicular to the cross-sectional area A. A material is sheared (c) when an external force F is applied tangential to the cross-sectional area A. In the case where the body is not completely rigid or incompressible, it will be subjected to a deformation Δl.

mations. A material with a larger value of E is more elastic, therefore it is harder to permanently deform it.

In the case where the external force is applied tangential to the surface of an ideal elastic material, the material will become sheared (see Figure 2.7 c). The applied stress is described as a *shear stress τ*

$$\tau = \frac{F}{A} \tag{2.7}$$

and the related shear strain γ is defined as

$$\gamma = \frac{\Delta l}{h} \tag{2.8}$$

where h is the height of the material under analysis. In this case, the constant of proportionality is called *shear modulus* or *modulus of rigidity G*

$$G = \frac{\tau}{\gamma}. \tag{2.9}$$

A higher shear modulus indicates that the material is more stiff and more resistant to deformations. In rheology, the Young's modulus and the shear modulus can be controlled and calculated. Both parameters give information about the strength of the material under study. The *Poisson's ratio ν*, which is defined as the ratio between the relative change in thickness to the relative change in length when a normal stress is applied:

$$\nu = \left| \frac{transverse\ strain}{longitudinal\ strain} \right| \tag{2.10}$$

relates the Young's modulus and the shear modulus as follows (Fung, 1993)

$$G = \frac{E}{2(1 + \nu)} \tag{2.11}$$

$$E = 2G(1 + \nu). \tag{2.12}$$

The Poisson's ratio measures the deformation in two dimensions when the force is applied in the third dimension. If a material is stretched in the $\overrightarrow{x}$ direction, ν measures the tendency of the material to get thinner in the $\overrightarrow{y}$ and $\overrightarrow{z}$ directions. The Poisson's ratio is bounded by two theoretical limits: it must be greater than -1 and less than or equal to 0.5, however it is rare to encounter materials with negative Poisson ratios. Most materials will fall in the range $0.0 \leqslant \nu \leqslant 0.5$. A material which possesses a Poisson's ratio of 0.5 (e.g. water) is incompressible, i.e. it maintains its volume during a deformation.

In nature it is rare to find a purely elastic material. In fact, even at low load all materials will show at least some permanent deformation. In addition, the material response will not be exactly the same when the material is stretched at different speeds. However if these occurrences and differences are small enough, they can be neglected (Kelly, 2013).

As mentioned above, materials can also be classified by rheology as viscous if they dissipate the applied energy in viscous flow. For these materials the resultant stress is proportional to the rate of the strain, i.e. there is a dependence on the velocity of changing size and shape. The viscous behavior can be modeled using a dashpot which is supposed to produce a velocity proportional to the load (Fung, 1993)(see Figure 2.8 a).

If a force is applied to a fluid material, the fluid can behave either as an inviscid Pascalian material or as a viscous fluid where the stress increases linearly (Newtonian fluids) or non linearly (non-Newtonian fluids) with the strain rate. Considering the simplest case of linear viscous fluids, the shear stress σ is shown to be dependent on the loading time and its relationship with the strain rate $\dot{\gamma}$ is described by

$$\sigma = \eta\dot{\gamma}. \tag{2.13}$$

Here, η is the coefficient of viscosity which is a measure of the resistance of the fluid to the shear or to the flow. The faster the stretching, the larger the stress that is required.

Stress-strain diagrams are crucial to understand the behavior of the material under load. Hookean elastic solids and Newtonian fluids are abstractions; no real material is known to behave exactly like these simplified models. Within certain boundary conditions, some ma-

PURE VISCOUS MATERIAL
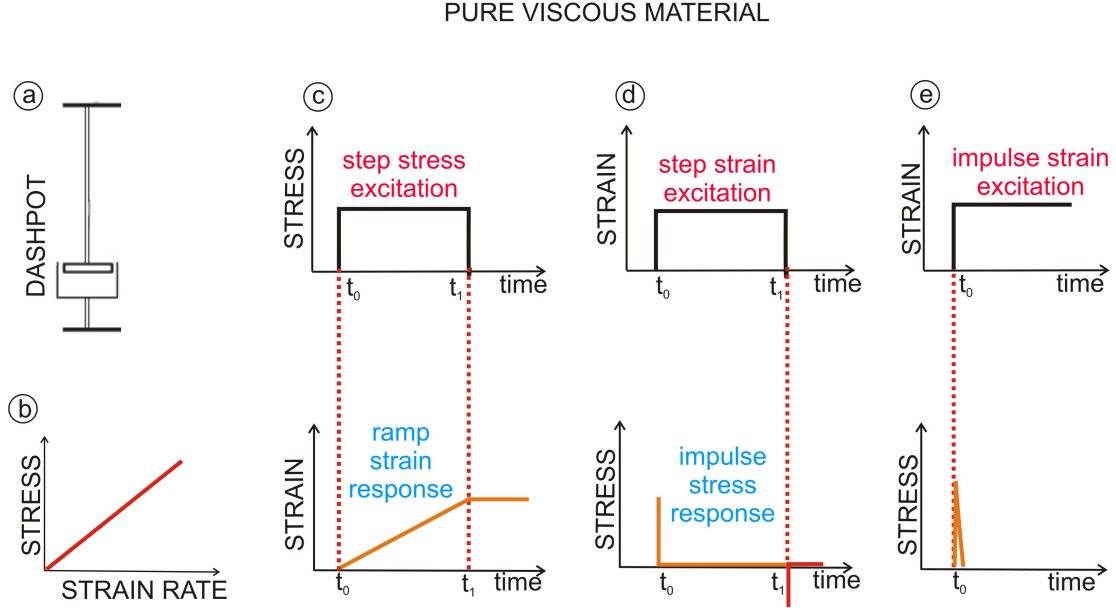
Figure 2.8: Stress-strain relationships in a viscous material. A viscous body can be modeled as a dashpot a). The stress has a linear relationship with the strain rate b) and the constant of proportionality is a measure of the material's viscosity. Under a given step stress excitation the material shows a ramp strain response c). The strain for $t > t_1$ increases linearly and for $t > t_2$ it stays constant. Under a step strain excitation d) the response is given by an impulse where the stress quickly reaches zero. Instead the stress response given a strain impulse is zero for $t > t_0$ e).

terials may follow these simple laws. Almost any real material which combines both solid-like and fluid-like behavior is defined viscoelastic (Fung, 1993). The elastic and viscous components work in concert to store and dissipate energy in a load and time dependent fashion (Müller Holt, 2011). For a viscoelastic material, the loading and unloading curves do not coincide; instead they form a hysteresis loop (Kelly, 2013)(see Figure not shown) showing a dependence on the time. The stress-response depends on both the applied strain and the rate of the strain at which it is applied.

To understand viscoelastic behavior and to provide insights into the connections between solid and viscous material behaviors, it is necessary to introduce three basic linear viscoelastic models, namely, the *Maxwell model*, the *Voigt model*, and the *Kelvin model* (*standard linear solid model*). The models contain different combinations of linear springs with spring constant μ and dashpots with coefficient of viscosity η (Müller Holt, 2011).

When a force F is acting on these elements, the resulting responses are seen in the spring and dashpot, respectively,

$$F = \mu u \tag{2.14}$$
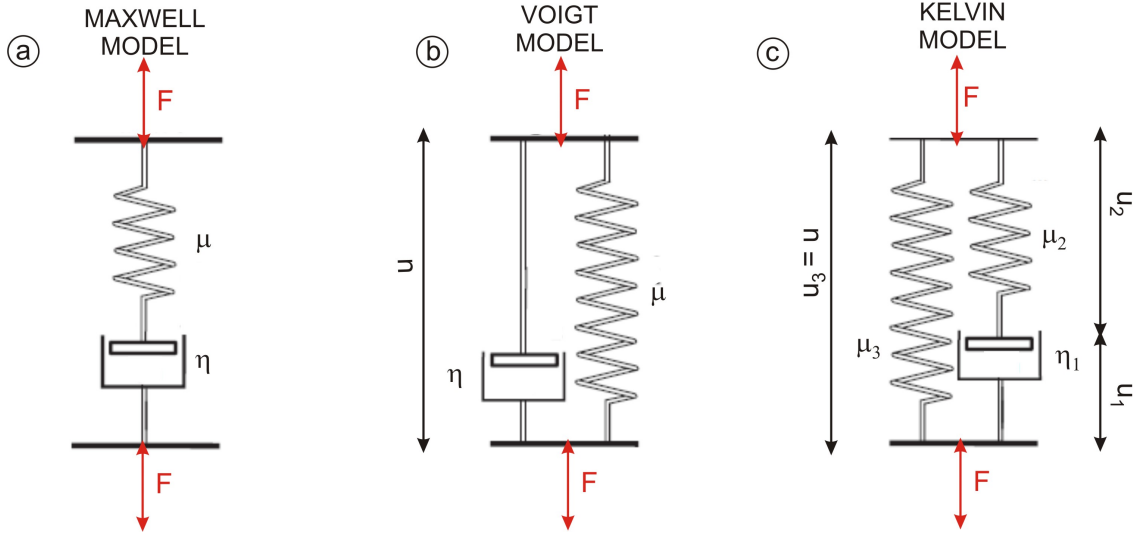
Figure 2.9: Simple spring and dashpot models. The viscoelastic material behavior is generally described with three models. The Maxwell model a) is composed of a spring with constant μ and a dashpot with coefficient of viscosity η in series. A The spring and a dashpot in parallel define the Voigt model b). The Kelvin model, also known as the linear standard solid model, c) is described by a Maxwell model in parallel with a spring.

$$F = \mu \dot{u} \tag{2.15}$$

where, u is the displacement/extension of the spring and $\dot{u}$ is the velocity of the deflection of the dashpot (Fung, 1993).

The Maxwell model is represented by a spring and a dashpot in series (see Figure 2.9 a). The spring and the dashpot experience the same force F which generates in the spring a displacement of $\frac{F}{\mu}$ and a velocity of $\frac{\dot{F}}{\mu}$ and in the dashpot a velocity of $\frac{F}{\eta}$. Knowing these relationships, the Maxwell model is often represented as a summations of the velocities of the single components

$$\dot{u} = \frac{\dot{F}}{\mu} + \frac{F}{\eta} \tag{2.16}$$

where at time $t = 0$, the displacement in the spring and the deflection in the dashpot are equal to zero (Fung, 1993; Müller Holt, 2011).

The Voigt model is represented by a spring and a dashpot in parallel (see Figure 2.9 b). When an external force is applied, the spring and the dashpot experience the same displacement u and the same velocity $\dot{u}$. The forces within the spring and the dashpot are μu and $\mu \dot{u}$, respectively. Therefore, the total force F is

$$F = \mu u + \mu \dot{u}. \tag{2.17}$$

The Kelvin model or standard linear solid model is represented by a spring and a dashpot in series with an additional spring in parallel (see Figure 2.9 c). It can be viewed as a Maxwell model in parallel to another spring. Since the response of this system to an applied force is more complex, deconstructing the displacements and forces of each component will help to understand the behavior of the whole system. The total displacement u is equal to the displacement of the Maxwell body and it can be described by

$$u = u_1 + u_2 = u_3 \tag{2.18}$$

where u_1 is the displacement of the dashpot of the Maxwell body, u_2 is the displacement of the spring of the Maxwell body and u_3 the displacement of the spring in parallel (Fung, 1993). The total force of the system is the sum of the force of the spring F_{spring} and the force of the Maxwell body, F_{Maxwell} as follows

$$F = F_{spring} + F_{Maxwell} \tag{2.19}$$

with,

$$F_{spring} = \mu_3 u \tag{2.20}$$

and,

$$F_{Maxwell} = \eta_1 \dot{u}_1 = \mu_2 u_2 \tag{2.21}$$

where μ_3 is the spring constant of the spring in parallel to the Maxwell body, η_1 and $\dot{u}_1$ are respectively the coefficient of viscosity and the velocity of deflection of the dashpot of the Maxwell body, and μ_2 is the spring constant of the spring of the Maxwell body (Müller Holt, 2011). By substitution, replacement and simplification (Fung, 1993), the equation that represents the Kelvin model becomes

$$F + \tau_\epsilon \dot{F} = E_R(u + \tau_\sigma \dot{u}) \tag{2.22}$$

where τ_ϵ is the relaxation time for constant strain, τ_σ is the relaxation time for constant stress and E_R is the *relaxed elastic modulus* as shown (Fung, 1993)

$$\tau_\epsilon = \frac{\eta_1}{\mu_2} \tag{2.23}$$

$$\tau_\sigma = \frac{\eta_1}{\mu_3}(1 + \frac{\mu_3}{\mu_2}) \tag{2.24}$$

$$E = \mu_3. \tag{2.25}$$

Viscoelastic materials undergo three typical mechanical responses to external loads. When a step strain is applied to a body and maintained constant, the corresponding stresses induced in the body will show a nonlinear time dependence, i.e. the stresses decrease with time. The phenomenon is called *stress relaxation* (Fung, 1993)(see Figure 2.10 a, b and c). After the load is removed, at first the stress decreases quickly before it decelerates to finally reach a limiting value. If this limiting value is different from zero the material is described as viscoelastic solid. In contrast if the value is zero or approaches zero quickly the material is considered a viscoelastic fluid (Pipkin, 1986). When a body is stressed and the stress is maintained constantly, the deformation resulting from the applied stress will increase nonlinearly over time until the load is removed. This phenomenon is called *creep* (Fung, 1993)(see Figure 2.11 a, b and c). In viscoelastic solids the shear increases to a plateau or limiting value, while in viscoelastic fluids the shear begins to increase linearly after an initial rapid increase (Pipkin, 1986). When a body is subjected to a cyclic loading, the stress-strain relationship in the loading process is usually different from that in the unloading process, and this phenomenon is called *hysteresis* (Fung, 1993). Hysteresis, originating from the Greek word $\nu\sigma\tau\acute{\epsilon}\rho\eta\sigma\iota\varsigma$ for deficiency, explains the history dependence of physical systems and derives from internal resistance of the viscoelastic materials.
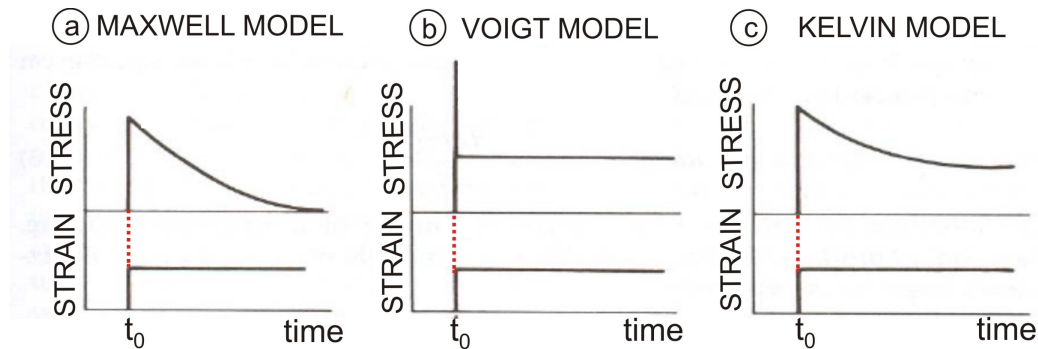
Figure 2.10: Relaxation experiment diagram. The graphs show the response in terms of force after an impulse deformation is applied for a Maxwell model a), a Voigt model b) and a Kelvin model c). In a Maxwell body the stress decreases with time starting from some high value to zero. In a Voigt body the stress stays constant for $t > t_0$. Instead a linear standard body behaves as the first model but the stress never reaches zero.
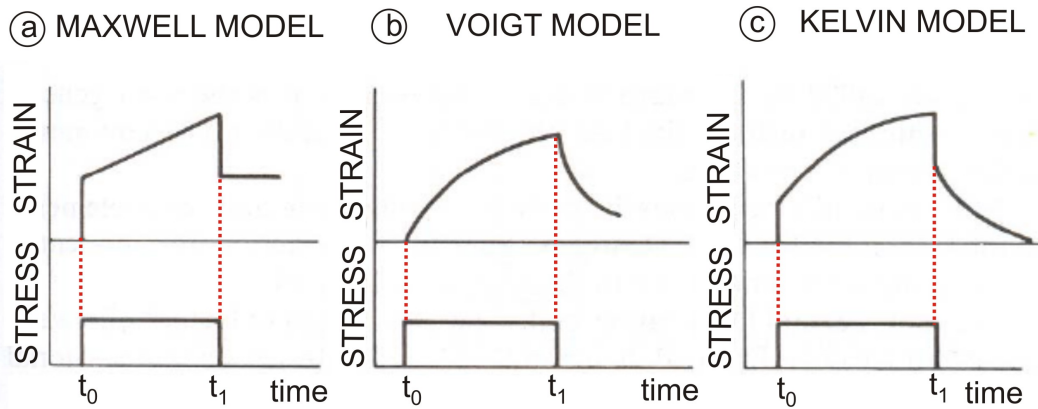
Figure 2.11: Creep experiment diagram. Creep is a time-dependent deformation under a certain applied load. In the Maxwell model a) the instantaneous response to the constant stress is elastic, where the body behaves as a linear viscous material. In the Voigt model b) the deformation increases non-linearly with time. For the Kelvin model c) it is possible to differentiate an istantaneous elastic response at time $t = t_1$ following a non linear viscous deformation. All the models for $t > t_2$ show a recovery zone where the material eventually reaches equilibrium.

Oscillatory Rheology

In mechanics there are two typical ways to establish the properties of viscoelastic materials: static and dynamic methods. Static methods, such as with as creep and relaxation experiments, usually provide test data as a function of time in ranging from 0 seconds to 10 years. To investigate the response of a viscoelastic material to very short term loading, it is more convenient to use an oscillatory loading. In order to predict the viscoelastic material behavior, it is necessary to formulate the theory based on oscillatory stresses and strains (Kelly, 2013).

When a sample is subjected to a strain γ,

$$\gamma(\omega, t) = \gamma_0 \sin \omega t \tag{2.26}$$

which varies sinusoidally with time at an angular frequency ω and has an amplitude γ_0, the response in terms of stress can be written as

$$\tau(\omega, t) = \tau_0 \cos(\omega t + \delta) \tag{2.27}$$

where τ_0 is the stress amplitude and δ is the phase angle (Schramm, 1994). In oscillatory rheology it is common to introduce the term *complex modulus G^** which represents the total resistance of a substance against the applied strain. It is described as

$$|G^*| = \frac{\tau_0}{\gamma_0}. \tag{2.28}$$

A quantity which varies periodically can be considered as a projection of a rotating vector on a real axis. Since a vector is specified by two components, it can be represented by a complex number composed of a real part and an imaginary part (Fung, 1993). Therefore, working on the Gaussian number level allows one to distinguish the elastic behavior and viscous behavior on a sample subjected to dynamic tests (Schramm, 1994).

The *complex modulus G^** can be defined by the complex number

$$G^* = G' + iG'' \tag{2.29}$$

where $i = \sqrt{-1}$ (Schramm, 1994). The parameter G' describes the *elastic or storage modulus* which indicates that the stress energy is temporarily stored during the test but it can be recovered afterwards. It is based on the amplitude of in-phase stress:

$$G' = G^* \cos \delta = \frac{\tau_0}{\gamma_0} \cos \delta. \tag{2.30}$$

The parameter G'' defines the *viscous or loss modulus* and indicates that the energy used

to start the flow is completely dissipated in heat. It is based on the out-of-phase stress:

$$G'' = G^* \sin\delta = \frac{\tau_0}{\gamma_0}\sin\delta. \tag{2.31}$$
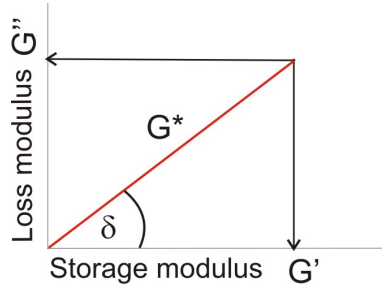
Figure 2.12: Geometric resolution of the complex G^* into its real component G' called storage modulus and its imaginary component G'' also known as loss modulus. δ is the phase angle.

The relationship between G' and G'' is given by

$$\tan\delta = \frac{G''}{G'} \tag{2.32}$$

which defines the dimensionless *loss tangent*. The loss tangent is a measure to which extent the sample is elastic ($\delta \approx 0$) or viscous ($\delta \approx 90°$).

In a pure elastic substance, the phase shift angle δ is zero (see Figure 2.13 a) whereby the equation 2.32 is simplified to:

$$G' = G^* \quad G'' = 0. \tag{2.33}$$

The response of stress caused by the applied strain is immediate. Stress and strain are in phase, that results in a maximum value for the stress when the strain reaches its maximum. For a pure viscous material, the phase shift angle δ is 90° (see Figure 2.13 c), simplifying the equation 2.32 results in the following:

$$G' = 0 \quad G'' = G^*. \tag{2.34}$$

For this case, stress and strain are out-of-phase, implying maximum stress when strain rate is maximum. Consequently, in viscoelastic materials the phase angle between the applied strain (or stress) and the resulting stress (or strain) varies between 0° and 90° (see Figure 2.13 e). In particular, for linear viscoelastic materials the amplitude of stress is proportional to the amplitude of strain. The stress alternates sinuisoidally at the same frequency as the strain, but there is a lag between the applied strain and the resultant stress (Schramm, 1994). The same conclusions can be drawn by observing the Lissajous

curves which graphically show the direct relationship between the sinusoidal stress and strain. For Hookean materials, stress plotted against strain results in a straight line in the Lissajous-diagram. The point of greatest stress (denoted by the stars in Figure 2.13 b) is achieved at $2\gamma_0$. For Newtonian materials, the resulting stress-strain Lissajous figure is a circle (see Figure 2.13 d). There, the maximum stress is obtained at the point where the material has acquired γ_0 strain. Consequently for a linear viscoelastic material the Lissajous curve assumes an elliptic shape and the response has the stress maximum somewhere intermediate to these limits (see Figure 2.13 f)(Vincent, 2012).

Using the *complex modulus* G^*, it is useful to define the *complex viscosity* η^*:

$$\eta^* = \frac{G^*}{i\omega} \tag{2.35}$$

which describes the total resistance to a dynamic shear. It can also be broken into an elastic component $\eta^{''}$ (*storage viscosity*)(Schramm, 1994):

$$\eta^{''} = \frac{G^{'}}{\omega} = [\frac{\tau_0}{\gamma_0\omega}]\cos\delta \tag{2.36}$$

and a viscous component $\eta^{'}$ (*dynamic viscosity*)(Schramm, 1994):

$$\eta^{'} = \frac{G^{''}}{\omega} = [\frac{\tau_0}{\gamma_0\omega}]\sin\delta. \tag{2.37}$$

Now the stress response in the dynamic test can be written in terms of moduli or of the viscosities (Schramm, 1994):

$$\tau(t) = G^{'}\gamma_0\sin\omega t + G^{''}\gamma_0\cos\omega t \tag{2.38}$$

$$\tau(t) = \eta^{''}\gamma_0\sin\omega t + \eta^{'}\gamma_0\cos\omega t. \tag{2.39}$$

Over the past decades, several different techniques and rheological models have been developed to quantify the mechanical behavior of cells in response to external conditions and forces. Before going into details on this, it is necessary to elucidate which cellular components are directly involved in the mechanics of the cells and tissues.
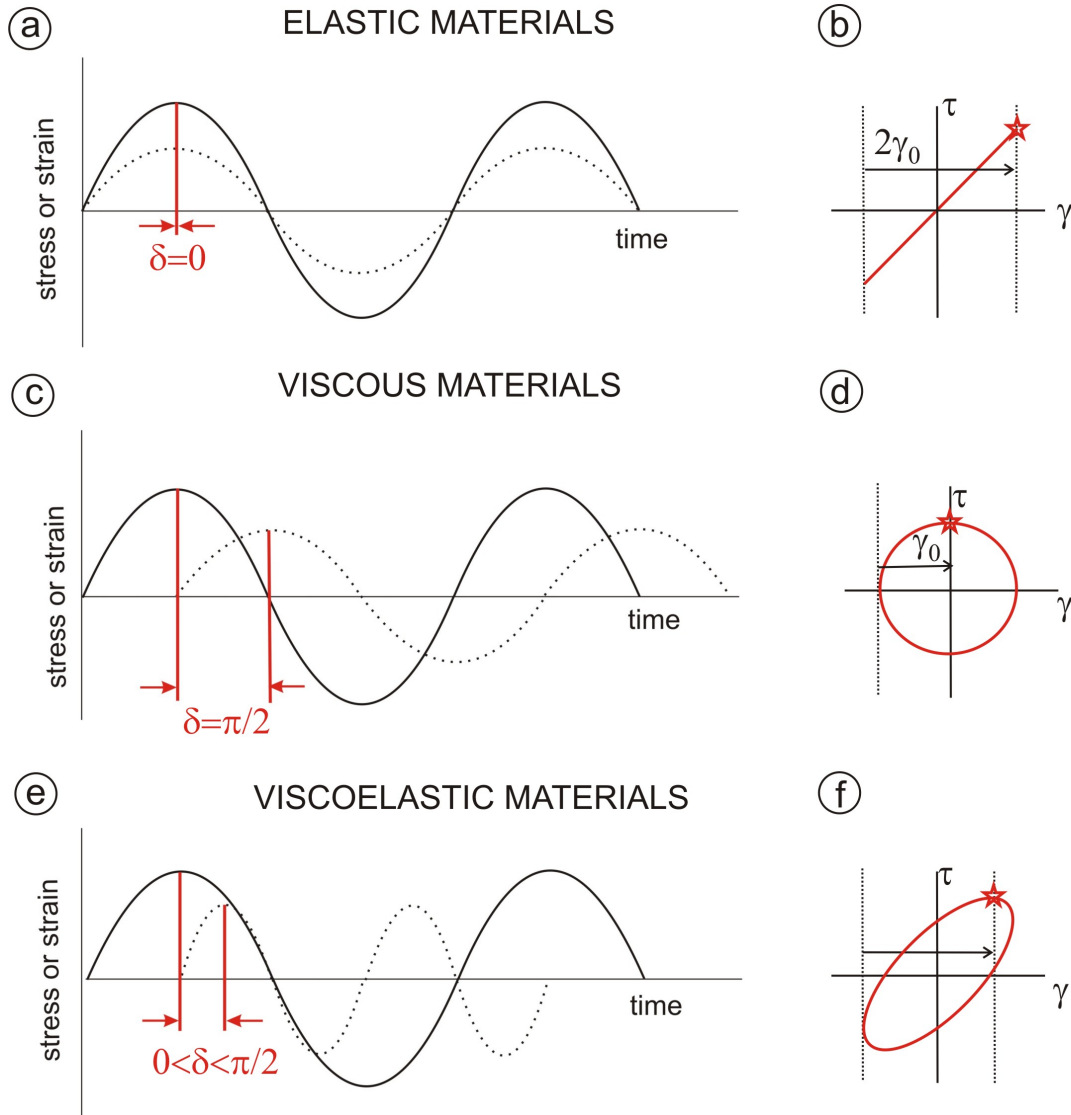
Figure 2.13: Sinusoidal strain and resulting stress diagram. For an elastic material the strain and the stress are in phase ($\delta = 0$) (a) and the Lissajous-Bowditch representation of the stress plotted against the strain is a line (b). The stars denote the maximum stress. The stress and the strain in a viscous material are out of phase ($\delta = \pi/2$) (c) and the resulting stress-strain Lissajous figure is a circle (d). The response of the viscoelstic material is partly viscous and partly elastic, so its response to a sinusoidally varying strain is a combination of preceding two extremes ($0 < \delta < \pi/2$) (e). The shape of the Lissajous diagram in this case is elliptical (f).

2.2.2 Biomechanical Properties of Living Materials

Cells are considered to be living materials with a complex microstructure and viscoelastic properties. Their behavior can be described as a solid-like or fluid-like material with a frequency-dependent response. They are enclosed by a phospholipid bilayer membrane reinforced with protein molecules. The inside of the cell includes the liquid cytosol, a nucleus, the cytoskeleton and organelles of different sizes and shapes. The cell motility, adhesion, deformation and the maintenance of the cell shape are based on micro- and nano-mechanical phenomena related to the dynamics and rheological properties of the cytoskeleton (Geiger et al., 2009). In fact, the cytoskeleton is able to sense mechanical signals and transduce them into a cascade of biochemical signals (Kamm et al., 2010). The distribution of the cytoskeleton components (actin filaments, microtubules and intermediate filaments) differs depending on the type of cells (see Figure 2.14) and cell cycle stage. In epithelial cells, the actin filaments are concentrated within the microvilli and the cortex. In migrating cells, the actin mainly forms the lamellopodia and filopodia.
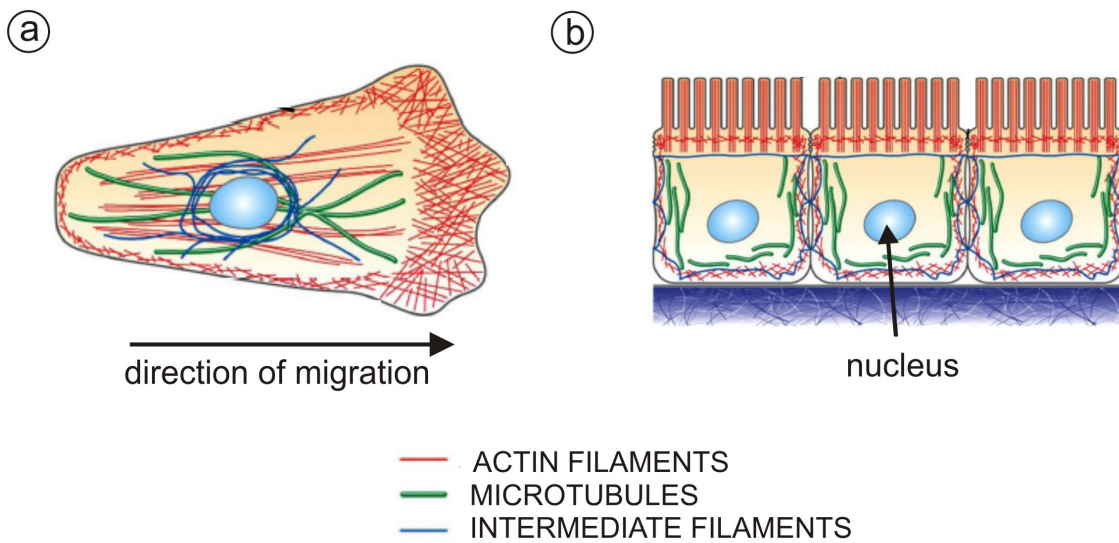
Figure 2.14: Distribution of the cytoskeleton components in different types of cells. (a) In migrating cells, the actin filaments tend to occupy the cell cortex. The intermediate filaments and microtubules fill up the area in the proximity of the nucleus. (b) In epithelial cells, the actin filaments predominately occur within the microvilli. The other cytoskeleton components surround the nucleus with a certain distance.

The Cytoskeleton

The cytoskeleton is formed by a complicated network of three biopolymers : microtubules, actin filaments (also called microfilaments) and intermediate filaments, see Figure 2.15 (Amos and Amos, 1991). These polymers are also dynamically connected, cross-linked and pre-stressed by different types of proteins (Howard, 2001; Alberts, 2008). The structure of the cytoskeleton can be compared to LEGO, the popular children's toy . As with LEGO, the cytoskeleton is composed of a copy of few key pieces that can be combined to build various structures with different functions depending on the need. However, only the cytoskeleton has the property of self-assembly (Fletcher and Mullins, 2010). The cytoskeleton performs mainly three functions:(i) it spatially organizes the structure of the cell, (ii) it connects the cell physically and biochemically to its environment; and (iii) it generates forces to keep the cell moving and changing its shape (Fletcher and Mullins, 2010).

Microtubules (see Figure 2.15 a) are composed of a single type of globular protein, called tubulin. Tubulin dimers (α-tubulin and β-tubulin) polymerize to form hollow tubes with an external diameter of 25 nm (Valiron et al., 2001). Microtubules are the stiffest of the three biopolymers. In fact their persistence length (L_p), defined as a basic mechanical property quantifying the stiffness of a polymer, is very large ($L_p \approx 5$ mm). Despite their stiffness, microtubules do not seem to dictate the mechanics of the cytoskeleton, probably because they are not stably crosslinked to the other filaments or to each other (Wen and Janmey, 2011). Nevertheless they indirectly influence the elasticity of the actin network through myosin-II (Pelletier et al., 2009; Bhat et al., 2012). In neuronal cells, their contribution in cell mechanics is more evident (Chen et al., 1992; Conde and Caceres, 2009). Microtubules can span the entire length of the cell and assume the shape of a rigid rod. They are highly dynamic and they undergo constant polymerization and depolymerization; in fact their half-life is just a few minutes. They can stably grow and rapidly shrink. This 'dynamic instability' allows the microtubules to reorganize the cytoskeleton (Mofrad, 2009; Fletcher and Mullins, 2010). The viscoelasticity of microtubules is due to a combination of the concentration and cross-linking of its subunits (Bhat et al., 2012).

Actin filaments (see Figure 2.15 b) are polymerized from global actin monomers which spiral around the filament axis in a structure reassembling a double helix with a diameter of approximately 8 nm (Otterbein et al., 2002). Microfilaments are semi-flexible polymers. Their L_p is several micrometers, approximately the same order of magnitude of their contour length L, defined as the physical extension of the polymer chain. They possess an effective Young's modulus of $1 - 3 \times 10^9$ Pa, comparable with that of polystyrene and nearly equal to that of bone (Mofrad, 2009). Even if actin filaments are less rigid than microtubules, they are highly organized stiff structures forming isotropic, bundled and branched networks. That occurs because of the presence of a high concentration of
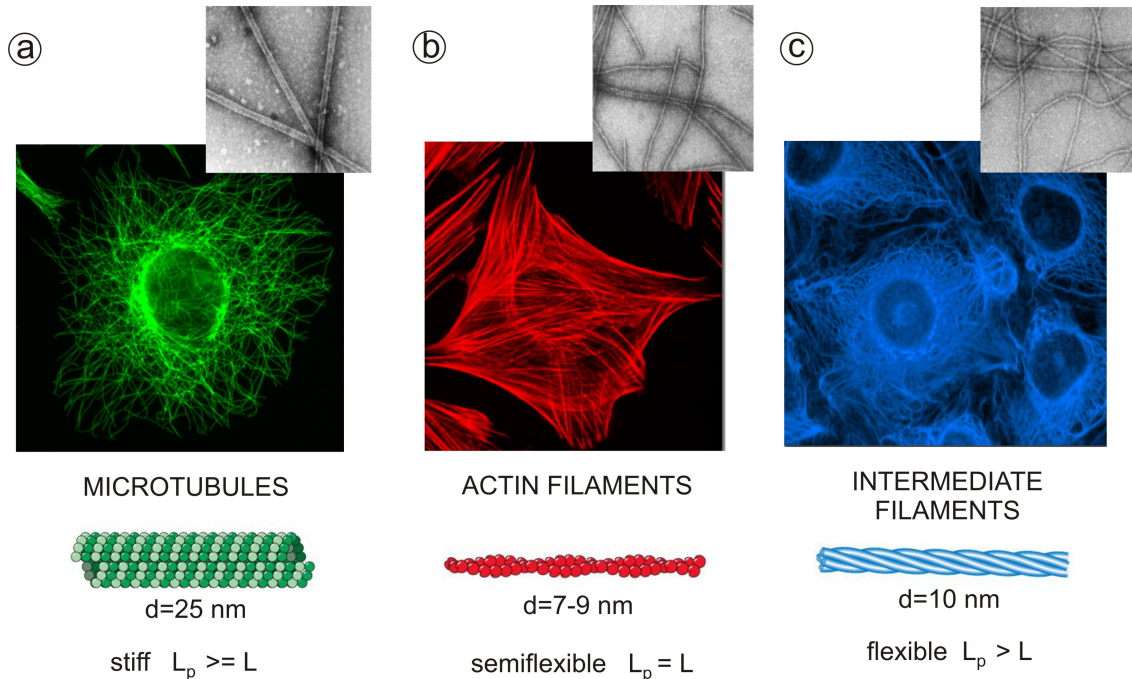
Figure 2.15: The three principal components of the cytoskeleton. The cytoskeleton is mainly assembled by three polymers. (a) The microtubules are hollow cylinders made by tubulin subunits. They are the stiffest of the three filaments since their persistence length (L_p) is greater than their contour length (L). The fluorescent microscopy image represents human lung carcinoma cells. (b) The actin filaments are twisted and have a pearl-string-like structure, made of F-actin polymers. They are less rigid than the microtubules ($L_p = L$). The fluorescent microscopy image represents fibroblast cells. (c) The intermediate filaments are flexible ($L_p < L$) rope-like structures made of different polymers (keratin, desmin, vimentin or lamins) depending on the cell type. Their diameter is around 10 nm, between the microtubules ($d = 25$ nm) and the microfilaments ($d = 7 - 9$ nm) diameter values. The fluorescent microscopic image represents rat kangoroo epithelial cells. The small images on top are electron microscopy pictures taken from Howard, 2001. The schematic drawings at the bottom are taken from Lodish, 2013. The fluorescent microscopy images are taken from the *Nikon MicroscopyU* website.

proteins which bind the actin filaments together (Fletcher and Mullins, 2010). More than one hundred proteins promote the formation of a single actin filament (Bhat et al., 2012). In fact, actin represents 10% of all proteins within most of the cells. Therefore, it can be considered the primary structural component. Actin filaments do not switch between states of polymerization and depolymerization like microtubules; instead, they show a steady elongation that helps them to respond rapidly to external forces. This property makes them have a the principal role in cell migration (Pollard and Borisy, 2003; Fletcher and Mullins, 2010). They are continuously assembled and disassembled in response to the local signaling of the cell (Fletcher and Mullins, 2010; Bhat et al., 2012). Actin filaments are considered to be semi-flexible polymers with a linear and nonlinear response to external

forces (Gardel et al., 2004; Lin et al., 2011; Bhat et al., 2012).

Intermediate filaments (see Figure 2.15 c) are composed of a huge variety of proteins (i.e. keratin, lamins, vimentin, desmin and neurofilament) expressed in different cell types (Schweizer et al., 2006). Intermediate filaments are rope-like structures containing approximately eight protofilaments with an average diameter of 10 nm which is smaller than the diameter of microtubules but larger than the diameter of actin filaments (Renner et al., 1981). Intermediate filaments are flexible polymers with an L_P of approximately 1 μm which is smaller than their contour length (Mofrad, 2009). In contrast to other cytoskeleton filaments, intermediate filaments have a long-term stability because they can be crosslinked to each other as well as to microtubules and actin filaments (Wiche, 1998). In addition, they are not directly involved in directional movements of the cells since they are not polarized like the other main components of the cytoskeleton. Intermediate filaments are less resistant to compressive forces than tensile ones. Their basic role is to provide mechanical strength to the cell and the tissue, considering that many cell types assemble intermediate filaments in response to mechanical stresses (Flitney et al., 2009; Fletcher and Mullins, 2010). Intermediate filaments also act like guide wires providing a lateral elastic support to microtubules stabilizing them against buckling (Brodland and Gordon, 1990).

Models of the Cellular Mechanical Response

Modeling the mechanical properties of a highly complex and heterogeneous structure as the cell is challenging. A wide range of models have been introduced over the years to explain the rheology and mechanics of the cytoskeleton. A complete model should account for all the cell mechanics phenomena, describing molecular networks and cellular substructures, remaining at the same time generic in its formulation. Each existing model only explains a particular series of experiments. Additionally, in most cases the different models appear to be mutually incompatible (Mofrad, 2009, Hoffman and Crocker, 2009).

Numerous experimental studies (Sung et al., 1988; MacKintosh et al., 1995; Satcher Jr and Dewey Jr, 1996; Coughlin and Stamenović, 2003) have shown that the physical properties of a cell are mainly governed by two phenomenological principles: (i) the cytoskeletal components are under a pre-existing tension also called pre-stress. This state is critical for maintaining cell shape and to control cell rigidity; and (ii) the rheological cytoskeleton behavior depends on time and frequency, according to a weak power law (Stamenović, 2008). The models which better describe the mentioned phenomena in a satisfying way are the tensegrity (tension-integrity) model (Ingber, 1993) and the soft glass rheology (SGR) model (Fabry et al., 2001a). The power-law viscoelasticity and the cytoskeleton pre-stress described by these models are conceptually two very different phenomena, but

they seem to coexist in the living cells (Stamenović, 2008).

The pre-stress condition is given by the generation of a tensile force due to myosin motor proteins cross-linked to actin filaments through ATP-processes. Based on that assumption, Ingber proposed the tensegrity model where the cytoskeleton is considered to be self-equilibrated mechanical system due to the balance between tension and compression forces (Ingber, 1993; Stamenović, 2008).
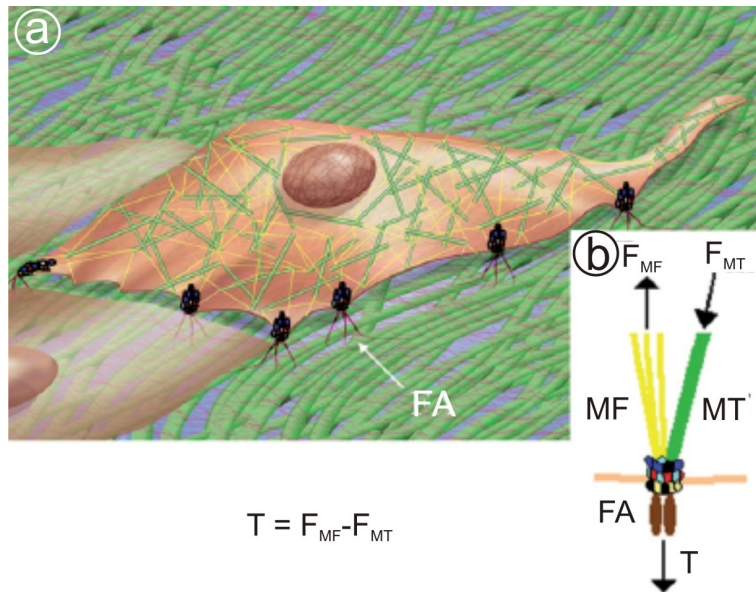
Figure 2.16: Schematic illustration of the tensegrity model. (a) Drawing of the distribution of the cytoskeletal elements (microtubules, green; microfilament, yellow) in a cell. The focal adhesion points (FA) between the cell and the extracellular matrix are highlighted. (b) Schematic representation of the forces that play a role in the cellular tensegrity model. The tension force (F_{MF}) of actin microfilaments (MF) is counterbalanced by the compression force (F_{MT}) of microtubules (MT) and the fraction force (T) due to the focal adhesion clusters. Image from Stamenović, 2008.

In this model, cytoskeletal microfilaments and intermediate filaments carry the tensional forces that are balanced by microtubules and the extracellular matrix through focal adhesions (FAs) (Ingber, 1993; Ingber, 1997). The whole cell is stabilized by the tensional pre-stress, generated by the actomyosin structure (Ingber, 1993). The traction force (T) generated at a FA can be described by a simple relationship: $T = F_{MF} - F_{MT}$, where F_{MF} describes the tensil force of actin microfilaments and F_{MT}, the compression force of microtubules (see Figure 2.16)(Stamenović, 2008). In tensegrity structures, the pre-stress confers stability and the tensile elements counterbalanced by compression elements create a self-equilibrated stable mechanical system which will collapse without pre-stress. The break down of this structure in the absence of pre-stress occurs due to the fact that its rigidity and connection between its elements are not sufficient to contrast motion and to

stabilize the system. When a tensegrity structure is subjected to external forces, before reaching an equilibrium state, it deforms, resulting in the geometrical rearrangement of its elements. If the material is stiff, the deformation is smaller, as the pre-stress is greater, i.e. stiffness increases with increasing pre-stress. There exists a linear relationship between pre-stress and stiffness (Wang et al., 2001; Wang et al., 2002a; Stamenović, 2005). The same relationship is shown in experiments on various types of cells which strongly suggests that tensegrity mechanisms govern the stiffness of the cell (Stamenović et al., 2002; Fabry et al., 2003; Deng et al., 2006; Stamenović, 2008). The pre-stress is an important factor for cell migration and proliferation as it is used by the cells to sense their physical environment and to react (Discher et al., 2005; Engler et al., 2006; Trepat et al., 2008).

The second model, based on the soft glass rheology theory, was developed by Bouchaud (Bouchaud, 1992) and extended by Sollich (Sollich, 1998). This theory considers the material as an ensemble of a large number of elements trapped in wells by their neighbors (Sollich, 1998; Mofrad, 2009). Each trap is at a different energy depth $E = 1/2kl^2$ (see Figure 2.17). From the deepest wells, the element is not able to escape just by thermal fluctuations. The hypothesis is that the element hops the well by agitation due to the mutual interactions within the neighboring elements (Sollich, 1998; Fabry et al., 2003). The physical origin of this non-thermal agitation is still unknown but it can be represented by a non- dimensional parameter indicated as *effective temperature* or *noise level x* (Sollich, 1998; Fabry et al., 2001a; Stamenović, 2008). If the system is perfectly elastic, the elements are not able to escape their wells which is indicated by $x = 1$. Instead the elements can hop between the wells when $x > 1$, generating flow and disorder (see Figure 2.17). Upon increasing the effective temperature the elements tend to hop out from a well in order to fall into the next one. This jump can be seen as a rearrangement of the system under fluid-like behavior. In this case, the system tends to melt. When the elements are trapped in the deeper wells, the hopping phenomenon is slowed down. In this case the system tends to freeze and to approach the glass transition (Kollmannsberger and Fabry, 2011).

The elements which assume the behavior described above are defined as soft glass materials: they behave like solid when they do not undergo external mechanical pertubation, and they soften and fluidize when a shear is applied to them (Weitz, 2001; Semmrich et al., 2007; Trepat et al., 2008). The category of soft glasses contains various types of materials (i.e. foams, emulsions and pastes) with a geometrically disordered and metastable structure (Sollich, 1998; Fabry et al., 2001a; Stamenović, 2008; Trepat et al., 2008). They are considered soft because their mechanical moduli are in the range of Pa to kPa. Their storage $G^{'}$ and loss $G^{''}$ moduli increase with a weak power-law dependency upon the frequency of the applied load. Instead, their loss tangent $G^{''}/G^{'}$ is nearly constant for a wide range of frequencies and of the order of 0.1 (Fabry et al., 2003; Trepat et al., 2008; Mandadapu
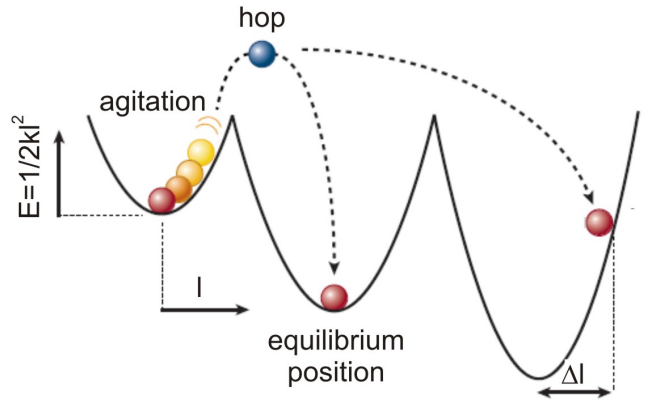
Figure 2.17: Schematic illustration of the soft glass rheology model. Elements hop between wells of different energy depths *E* that depends on the distance *l* from the position of trap minimum and the spring constant *k*. The elements in the deeper wells usually approach to the solid phase and unlikely are able to hop to another well. Instead the elements that hop from one well to another are in the fluid-like phase. Image from Kollmannsberger and Fabry, 2009.

et al., 2008).

The mechanical behavior of the cells is similar to that of soft glass materials as shown in the experimental data from Fabry et al (Fabry et al., 2001a). They measured the relaxation modulus, $G(t)$, the frequency dependence of the storage modulus $G'(\omega)$, and the loss modulus $G''(\omega)$ of the cytoskeleton. They observed that the G' and G'' increased weakly with increasing frequency ω in the range of $0.01 - 10$ Hz, according to the power law $\sim \omega^{x-1}$ (Fabry et al., 2001a; Mofrad, 2009). In contrast, they also showed that the loss tangent was insensitive to the frequency change, remaining almost constant between 0.3 and 0.4 (Fabry et al., 2001a). Following this discovery, the cytoskeletal elements (i.e. protein complex) of the living cells became considered to be the elements of the soft glass rheology model, trapped by the molecular crowding or by the weak chemical bonding (Fabry et al., 2003; Trepat et al., 2008). The non-thermal agitation that occurs is probably due to ATP-dependent mechanisms such as binding energies between cytoskeletal neighboring proteins (Bursac et al., 2005) or due to mechanical stretch (Trepat et al., 2008).

For living cells, the power law exponent α describes the viscoelastic behavior of the cells depending on the frequency and on the time of imposed deformations after applied static or dynamic loads (Balland et al., 2006). If α approaches zero, the cell behaves like a Hookean elastic solid and the deformation energy is elastically stored in the body. If α approaches unity, the cell acts like a Newtonian viscous fluid. In this case, the body dissipates the energy deformation since it is not able to store it elastically. In cells, α typically assumes values between 0.1 and 0.5 (Stamenović, 2008; Kollmannsberger and Fabry, 2011).

In consideration of the fact that cells can be regarded as soft glass materials, the exponent α can assume the formulation of $x - 1$.

Although the soft glass rheology model was designed to describe the behavior of inert materials, it has been shown that this model can characterize the linear rheology and the fluidification in response to the stretching of living cells (Fabry et al., 2001a; Trepat et al., 2007; Trepat et al., 2008)

The remaining question is whether the tensegrity and the soft glass rheology models can be linked to each other. It is relatively simple to show how soft glass materials such as foams and emulsions exhibit tensegrity-like (Stamenović, 1991; Reinelt and Kraynik, 1993) and SGR-like (Jiang et al., 1999; Koehler et al., 1999) behaviors. For a complex and dynamic biological material such as the cell, it is less intuitive. The best approach would be to see these two models as complementary to each other rather than mutually incompatible.

Experimental Methods for Measure Cell Mechanics

The continuous remodeling and biochemical changes of the cytoskeleton have been studied using a variety of experimental techniques (Mofrad, 2009). The measurement methods can be divided into two different categories: passive techniques (i.e. particle tracking microrheology) that monitors the thermal fluctuations of the cells without any mechanical engagement, and active techniques (i.e. atomic force microscopy, magnetic twisting cytometry, optical stretcher, magnetic tweezers, micropipette aspiration, microneedle and microplate rheometer) that measure the response of the cell after applying a direct external force (Janmey and Schmidt, 2006). The techniques can also be classified depending on if they probe a portion of the cell, the entire cell or a cell population (Bao and Suresh, 2003).

The atomic force microscopy or scanning force microscopy (AFM) (see Figure 2.18 a) produces images by applying a mechanical force across a sample surface. It quantifies the stiffness of the sample and the surface topography (Binnig et al., 1986; Van Vliet et al., 2003). The viscoelastic response of the cells is probed by applying force in the range of $0.1 - 1$ nN and indentations of about 50 nm or less (Henderson et al., 1992; Radmacher et al., 1996; Pullarkat et al., 2007). The AFM scans the specimen surface using a tip (probe) located at the end of a cantilever. The interactive force between the tip and the sample surface produces a displacement of the tip that is tracked via a laser. The laser reflects off of a device that converts laser light into voltage. Thus, tip deflection is converted to a force through Hooke's law. The maximum force is given by the spring constant of the cantilever, whereby the resolution of the instrument is given by its thermal fluctuation.

Often for AFM measurements of cells, a bead of a few micrometers is glued to the tip. In this way, it is possible to modify the stress range by changing the diameter of the bead (Mahaffy et al., 2000; Smith et al., 2005; Pullarkat et al., 2007). The advantage of using this technique is that the AFM can probe cells within their physiological environment (Van Vliet et al., 2003; Pullarkat et al., 2007). The AFM is a valid instruments to study elastic deformation of the cells and cellular components such as the cytoskeleton (Rotsch and Radmacher, 2000; Alcaraz et al., 2003; Van Vliet et al., 2003,Kirmizis and Logothetidis, 2010).

The magnetic twisting cytometry (MTC) (see Figure 2.18 b) technique uses beads ranging in diameter from 250 nm to 5 μm to measure their pointwise displacements. The cells in part phagocytose the beads that can be coated with specific ligands to bind to cell surface receptors (Van Vliet et al., 2003). First the beads are permanently magnetized almost parallel to the cell surface and then an homogeneous magnetic field twists them in the vertical direction (Pullarkat et al., 2007). The MTC technique allows to study the mechanical response of cells to sinusoidal perturbations, including the estimation of the storage and loss moduli for frequencies between 0.01 to 10^3 Hz (Fabry et al., 2001a; Puig-De-Morales et al., 2001; Van Vliet et al., 2003; Pullarkat et al., 2007). Originally, this method was developed to study the cytoplasm (Crick and Hughes, 1950) but it has also been used to investigate the mechanics of the cell membrane and the cytoskeleton (Puig-De-Morales et al., 2001; Maksym et al., 2000; Wang et al., 1993; Fabry et al., 1999; Fabry et al., 2001b).

The optical stretcher is a novel instrument used to micro-manipulate single cells and probe their mechanical properties (Guck et al., 2001; Wottawah et al., 2005) (see Figure 2.18 c). The single cells are held in suspension by two laser beams located diametrically opposite to each other. (Van Vliet et al., 2003). An optimized microscopic analysis optically measures the cell deformation (Pullarkat et al., 2007). The radiation damage of the lasers is reduced since the laser beams are not focusing on the same plane of the cell. Strains of 160% can be attainable for PC12 cells and neutrophils (Guck et al., 2002). The excellent sensitivity in detection and the high throughput of this technique allows for an analysis of the cell deformation with respect to cancer progression (Guck et al., 2005).

In magnetic tweezers, paramagnetic and ferromagnetic microbeads (250 nm to 5 μm in diameter) are used to apply large forces to the surface of the cell and to the intracellular environment (Mofrad, 2009) (see Figure 2.18 d). An electromagnetic field imposes a force on these beads causing their displacement (Smith et al., 1992; Bausch et al., 1998; Van Vliet et al., 2003; Kollmannsberger and Fabry, 2007). For single cell studies, the beads can be coated to adhere to the cell surface (Bausch et al., 1999, Alenghat et al., 2000). The

beads can also be forced through the cellular matrix or engulfed by phagocytosis (Mofrad, 2009). The forces applied can range from piconewtons (Karcher et al., 2003; Vonna et al., 2003) to nanonewtons (Trepat et al., 2003; Trepat et al., 2007).

The micropipette aspiration is a technique that uses suction pressure ranging from 0.1 to 10^3 Pa to partially or wholly suck a single cell into a glass pipette (see Figure 2.18 e). The pipette has a diameter between 1 and 10 μm and is coated with 1% agar in order to inhibit cell adhesion (Evans and Yeung, 1989; Hochmuth, 2000; Van Vliet et al., 2003; Lim et al., 2006). The displacement of the cell membrane is recorded and visualized by light microscopy. This method, first introduced by Mitchison and Swann (Mitchison and Swann, 1954), correlates the applied pressure and the cell deformation in a real time scale, which allows for the calculation of elastic modulus and apparent viscosity for the cell membrane of many cell types (Rand, 1964; Shao, 2001).

The microneedle technique is one of the earlier experimental approaches using a cantilever to deform adherent cells as well as single molecules (Van Vliet et al., 2003) (see Figure 2.18 f). It also represents the first technique employed to study the sliding forces between microtubules (Kamimura and Takahashi, 1981, Shao, 2001). The stiffness of the microneedle can be as small as 0.09 pN/nm. Between all the mechanical cantilever approaches, microneedle is the softest, with a force maxima on the order of 200 pN. The force resolution is around 0.6 pN (Ishijima et al., 1991) and the displacement maxima is on the order of μm (Van Vliet et al., 2003). The microneedle is loaded with a force on its tips and will bend with a deflection that is linearly proportional to the force (Shao, 2001). The displacement is measured using optical imaging (Felder and Elson, 1990). This techniques has been used in many studies, e.g to calculate the force of a small number of myosin molecules interacting with a single actin filament (Waugh and Bauserman, 1995) and to estimate the bending stiffness of erythrocyte membranes (Kishino and Yanagida, 1988,Shao, 2001).

The microplate rheometer is another instrument to quantify the viscoelastic properties of the cells. It is composed of two glass microplates with narrow flat tips (Thoumine and Ott, 1997) (see Figure 2.18 g). The cells are placed in between the two plates which can be coated with specific adhesion proteins. By displacing one of the plates, a uniaxial stretch is applied to the cells. Hereby, an optical fiber technique is used to measure the bending of the plate. The forces are typically in the range of 10 nN - 10 μN and the frequencies range between 0.01 Hz and 10 Hz (Pullarkat et al., 2007). With this technique it is possible to study the non-linear behavior and the creep response of the cells over long time scales (Fernández et al., 2006; Desprat et al., 2005).

In contrast to the previously described methods, the particle tracking microrheology is classified as a passive technique because it does not apply any external force. It moni-

tors the Brownian motion of fluorescent beads due to their environments (see Figure 2.18 h). These nanoprobes ($< 1\mu$m) are inserted into the cytoplasm of living cells through microinjection. Consequently, this technique is able to measure frequency-dependent viscoelastic parameters by observing the displacement of the beads (Tseng et al., 2002; Wirtz, 2009; Bhat et al., 2012). A laser can be used to detect the fluorescent beads obtaining a nanometer spatial resolution over a frequency range from 1 Hz to 50 Hz (Yamada et al., 2000; Crocker et al., 2000; Jonas et al., 2008).

The development of microrheological techniques just described above, allows for the production of quantitative mechanical measurements of single living cells. Each technique measures different parameters of cell rheology, and each technique has advantages and limitations (Kollmannsberger and Fabry, 2011). Biological systems are intrinsically different from synthetic material systems, and despite the apparent simplicity of the force-displacement law on which these techniques are based on, the quantification of their mechanical response is not obvious (Van Vliet et al., 2003).
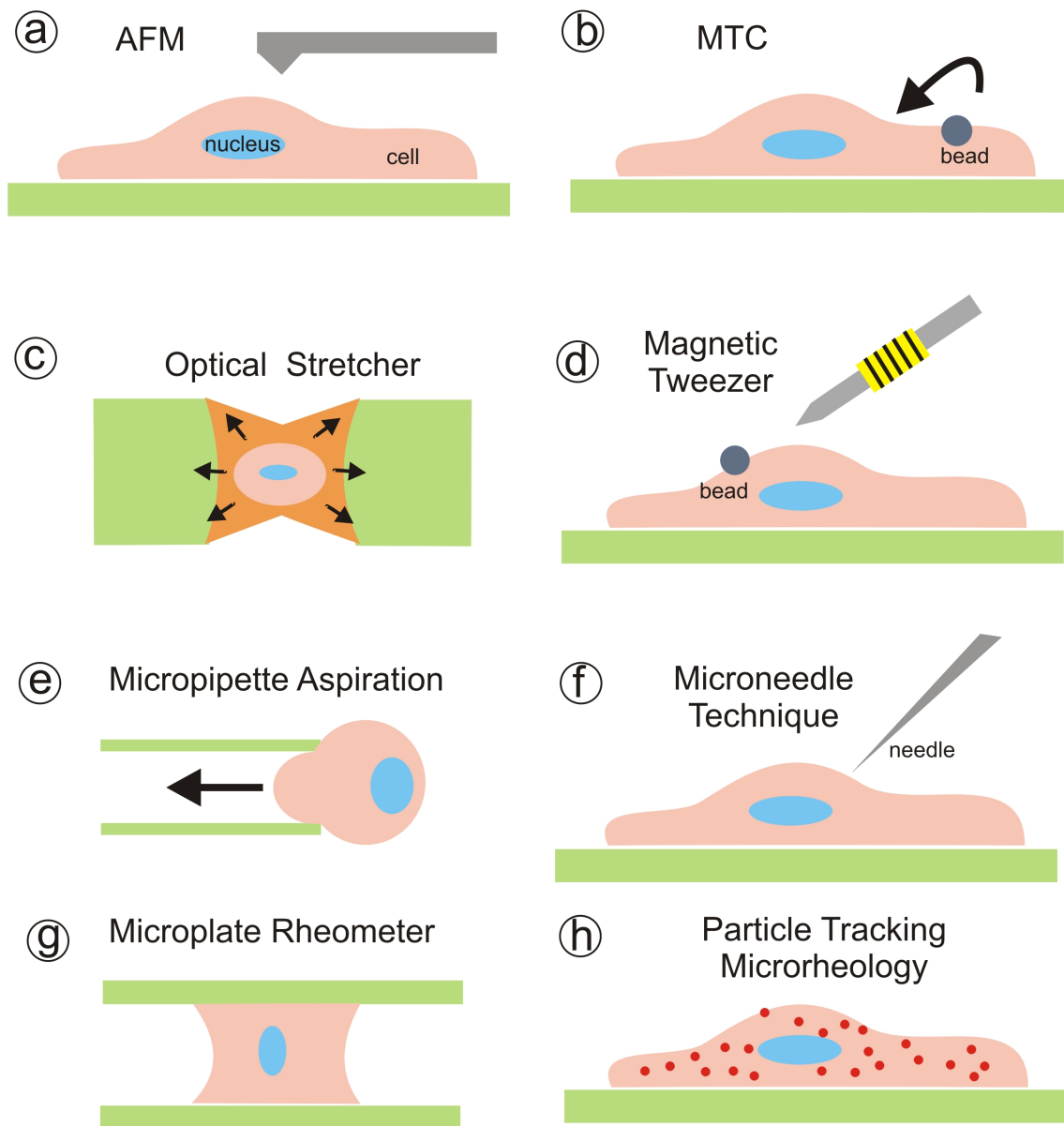
Figure 2.18: Schematic representation of the common methods used to measure cell rheology. (a) The atomic force microscopy (AFM) is a technique that uses a cantilever with a microtip or polystyrene bead to poke the cell and study the cell response. (b) The magnetic twisting cytometry (MTC) uses magnetic beads that turn under a magnetic field and apply force to the cells. (c) The optical stretcher is a recent technique that uses two laser beams to probe the cell in suspension. (d) The magnetic tweezer uses magnetic beads moved by magnetic field to apply forces to the cell surface. (e) Micropipette aspiration is a relatively simple technique that employs a micrometer tip to suck a portion of the cell applying negative pressure. (f) Microneedle technique probes the elastic properties of the cell with a calibrate glass needle. (g) The microplate rheometer applies uniaxial stretch to the cell located in between two glass plates. (h) Particle tracking microrheology is a passive technique able to extrapolate the viscoelastic parameters tracking the random Brownian movements of organelles or microinjected particles (red). [Original image].

3 Material and Methods

In this chapter, I will present the methods used to study the behavior of the retinal cells under mechanical alterations of their natural environment, as well as a new innovative method to culture adult neural tissue. In the first part, preparation and handling of the retinal tissue and brain is explained in detail. In addition, the methods used to visualize the structure of the retina, such as immunofluorescence and live staining, are described. In the second part, a new simple and effective methods for organotypic culturing of retinal whole-mount and brain slices will be described. In the third part, the different setups employed to apply shear stress or to stretch the retina are introduced.

3.1 Tissue and Cell Preparation

3.1.1 Animals Used - Guinea Pig Retina and Mouse Retina as Model Systems

Pigmented guinea pigs and C57BL/6 mice have been used as animal models in this work. Both animal models are commonly used for neuroscience research, e.g. pain studies (Mogil, 2009), stroke, epilepsy, inflammatory disorders (Lythgoe et al., 2003), and retinal ischemia (Pang and Clark, 2010) to cite some examples.

The retinae of most mammalians, including humans and also mice, receive their nutrients from two types of circulations: intra-retinal vascular and choroidal circulation (Delaey and Voorde, 2000). For this reason, this type of retinae are identified as vascular retinae. Instead, in some mammalian species, such as the rabbit and guinea pig, the retinal metabolism depends almost exclusively on the choroidal circulation (Pournaras et al., 2008) since these animals lack retinal blood vessels. In the choroidal circulation, oxygen diffuses from the choroid through the retinal pigment epithelium and reaches the outer layer of the sensory retina (Uga and Smelser, 1973; Delaey and Voorde, 2000) mostly where the photoreceptors are located.

In animals with an avascular retina, the thickness of the retinal tissue is influenced by a reduction of the outer nuclear layer and is limited by the availability of oxygen, the supply of other nutrients and the removal of waste products (Buttery et al., 1991; Yu et al., 1996). The guinea pig retina with a thickness of d $\approx$ 100 μm is around three times thinner in comparison to other rodent retinae, e.g. mouse (d $\approx$ 300 μm) (Dreher et al., 1992).

Another difference between the guinea pig retina and mouse retina is due to a slightly different organization of the outer nuclear layer. In the first species the photoreceptor nuclei are arranged in columns containing between five and seven nuclei, in the second animal the number of nuclei per column is duplicated.

The advantages of using the guinea pig retina in my experiments are that a thin retina is more suitable for slice preparation and for culture. Since the Müller cells in the guinea pig have a wider trunk, their detection is less complicated. This is a crucial point in the investigation of the mechanical properties of the retinal tissue since the Müller cells span the entire thickness of the retina and can give information about the layers.

The choice of also using murine retina is due to the possibility to investigate genetically engineered animals, e.g. knockout mice where existing genes can be inactivated by replacing or disrupting them with artificial pieces of DNA. The mouse was also employed to investigate long-term culture of brain slices.

The animals were retained in size- and species-appropriate cages with free access to water and food in dedicated rooms under 12-hour light and 12-hour dark cycles. All animals were handled in accordance with the European Directive 86/609/EEC and the Association for Research in Vision and Ophthalmology (ARVO) Statement for the Use of Animals in Ophthalmic and Vision Research. Furthermore all the experiments were additionally approved by the German law of animal protection.

3.1.2 Preparation of the Retinal Tissue

Immediately after the animals were sacrificed with carbon dioxide, their eyes were removed. The technique to isolate the retinal tissue is identical for the mouse and guinea pig. The aqueous solutions used differ by experiment types. For long-term experiments, the eyes were enucleated and put in phosphate buffered saline (PBS) at 4°C, briefly rinsed in ethanol 70 %, washed in PBS and lastly kept in Ames medium (A1420, Sigma-Aldrich, Germany). For short-term experiments, the only compound used was an extracellular solution (ECS) consisting of sodium chloride (NaCl), potassium chloride (KCl), calcium chloride ($CaCl_2$), magnesium chloride $MgCl_2$, HEPES and D-glucose (pH 7.4) (see Table 3.1). In all experiments the solutions were aimed to reproduce the physiological environment in order to avoid deterioration of the fragile biological tissue. After the eyes were enucleated, the connective tissue was removed (Figure 3.1, a and b). An incision was made behind the ora serrata to release the pressure allowing to hold the eyeball easily (Figure 3.1 c). Following the laceration, the eye was cut in half to separate the cornea, iris and lens from the posterior part of the eye (Figure 3.1, d and e). With a gentle compression, the vitreous body was removed (Figure 3.1 f) and ultimately the retina was cautiously separated from the pigment epithelium (Figure 3.1, g and h).

Table 3.1: Composition of extracellular solution. All chemicals are dissolved in bi-distilled water and the pH is adjusted to the physiological value 7.4 by using 1 M TRIS-Buffer (pH = 10.4).

Substance	Concentration [mM]
NaCl	136
KCl	3
CaCl$_2$	2
HEPES	10
MgCl$_2$	1
D-Glucose	11
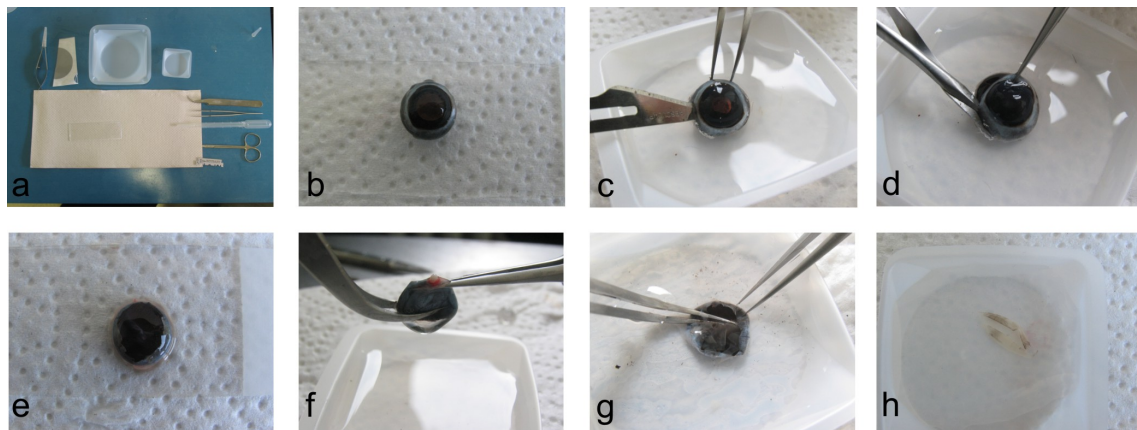
Figure 3.1: Preparation of the guinea pig retina. (a) The tools used during the isolation are mainly tweezers, scissor, pipette and blade. (b) The freshly enucleated eye is immediately transferred into aqueous solution. (c) To release pressure, an incision of the eye behind the ora serrata is made with a sharp razor. (d) Following the incision, a cut made with Vannas scissors separates the anterior part of the eye from the posterior part (e). (f) The vitreous body is gently removed with tweezers. (g,h) The retina is carefully detached from the retinal pigment epithelium.

For long-term experiments, the entire isolation of the retina was performed under the laminar flow hood to guarantee sterilized conditions necessary for tissue culturing. The instruments used for dissection were sterilized in an autoclave and the solutions were filtered using a membrane with a pore size of 20 μm (18058, Sartor Lab P Plus). After isolation the retina was carefully transferred on a titanium dioxide (TiO$_2$) nanotube substrates (see section 3.2.3) with the photoreceptors side down. To permit the adhesion of the retina to the surface of the TiO$_2$ nanotubes and to ensure an air-liquid interface system, the solution remaining from the transport on top of the membrane was removed by suction.

After the preparation, the tissue was kept in an incubator at 37°C and 5% CO_2 for at least 3 days. It was crucial to prevent retinal degeneration processes ensuring a correct exchange of gas and nutrients between the system and the incubator. For short-term experiments the retina was lying on top of a nitrocellulose filter (10407132, Whatman) with the photoreceptors side down. A sharp razor blade (Apollo, Solingen, Germany) was used to cut this assembly in long rectangular pieces for short-term shear stress experiments (see Section 3.3.2). Also in these cases the solution was quickly removed to allow the tissue to adhere to the filter, paying attention not to dry the retina out.

3.1.3 Preparation of the Brain Tissue

Immediately after exposure to the carbon dioxide, the mice were decapitated under sterile conditions. The technique adopted for the isolation of the brain is commonly used in my laboratory. To expose the cranium, the skin (from the base of the neck to the forehead in the proximity of the eyes) is cut with sharp scissors (see Figure 3.2 a). In this way it is possible to wrap the mouse ears around the index of one hand keeping the animal head still during the procedure. The skull is carefully lifted up making a coronal cut from one ear to the other and then a horizontal cut in each side from the ear to the eye (see Figure 3.2 b). The skull is removed with the help of forceps (London Forceps, Fine Science Tool, F.S.T.) paying attention not to damage the brain. At this point the brain is free and can be isolated (see Figure 3.2 c). The brain is kept for a few minutes in ice cold PBS to remove the debris. A vibration microtome (HM 650 V: Micro-International, Walldorf, Germany) was used to slice the tissue. To firmly fix the brain on top of the vibratome stage with common glue, the cerebellum is cut out creating a flat surface (see Figure 3.2 d). The brain was sectioned in coronal slides of 200 μm in thickness. Each of the slices was placed in a customized six-well plates connected to the carbon dioxide tank, kept in a box of ice and filled with chilled culture medium.
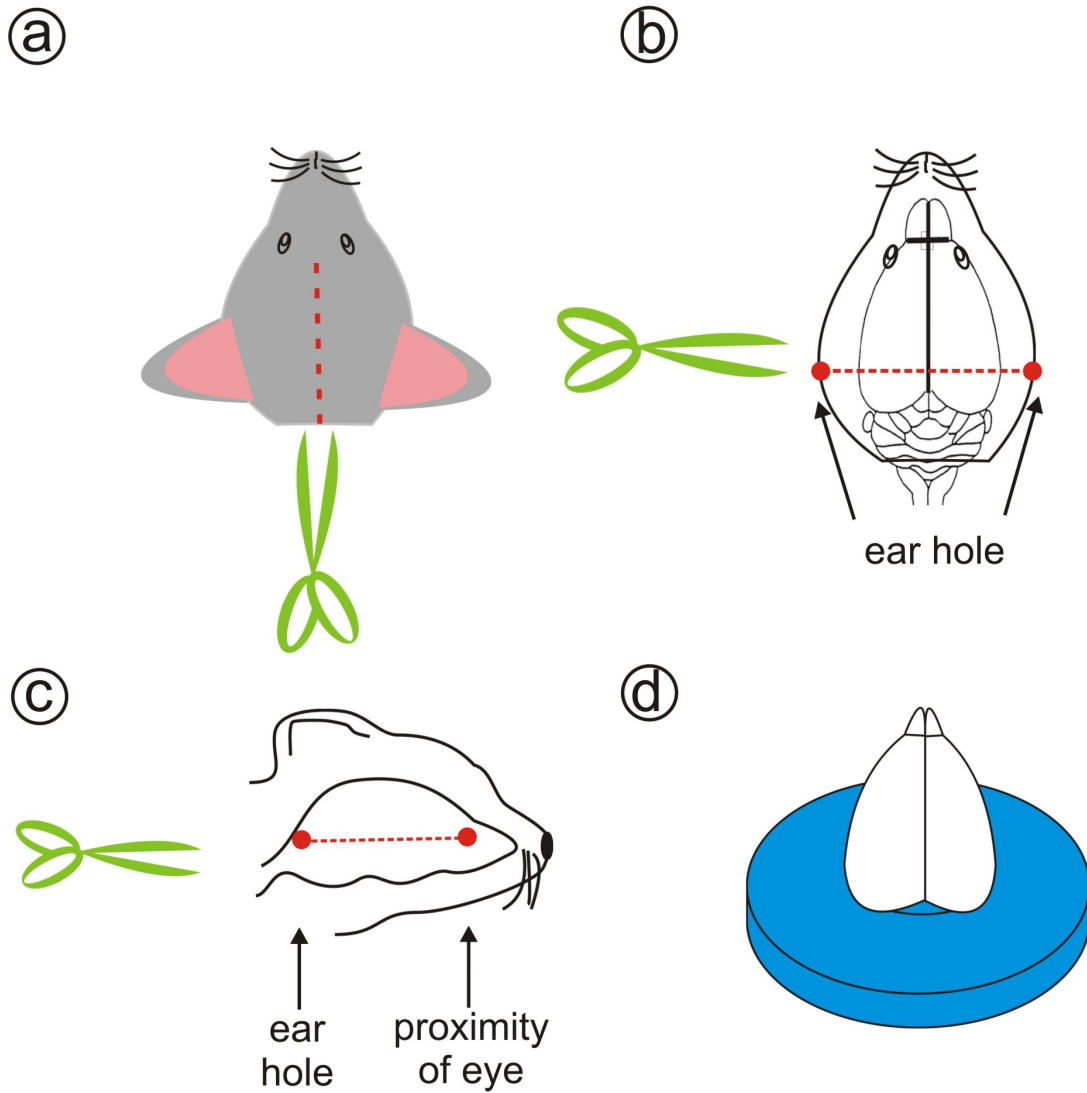
Figure 3.2: Preparation of the mouse brain. (a) After sacrificing the mouse, the head was removed, and to expose the skull, the skin was cut on the sagittal plane. (b) The skull is first cut with a coronal incision from ear to ear. (c) Then to completely remove the skull, another incision was made in each side, from ear to eye. (d) Finally the isolated brain deprived of the cerebellum was glued to the stage of a vibratome, ready to be sliced in coronal sections.

3.1.4 Staining of the Vital Cells in the Retinal Tissue

As previously mentioned (see Section 2.1.1), the retina is composed of a myriad of cells that can be simply divided into two categories of cells which are well organized in layers: neuronal and glial cells. The only cells that span throughout all the retinal layers are the Müller radial glial cells, the predominant glia of the vertebrate retina (Uckermann et al., 2004). Because of their advantageous position within the retina and their rapid activation in response to pathological and non-pathological stimuli (Bringmann et al., 2006), Müller cells are an appropriate target to study the behavior of the tissue during shear stress experiments, for example. To visualize the retinal radial glial cells during an experiment, the vital MitoTracker dyes were chosen. It has been shown that Müller cells take up the thiol-reactive vital dye while neuronal cells are not labeled (Figure 3.3) probably due to the presence of binding sites for the thiol groups in the Müller cells (Uckermann et al., 2004).

Müller Cell endfeet

Müller Cell nuclei

Photoreceptor autofluorescence
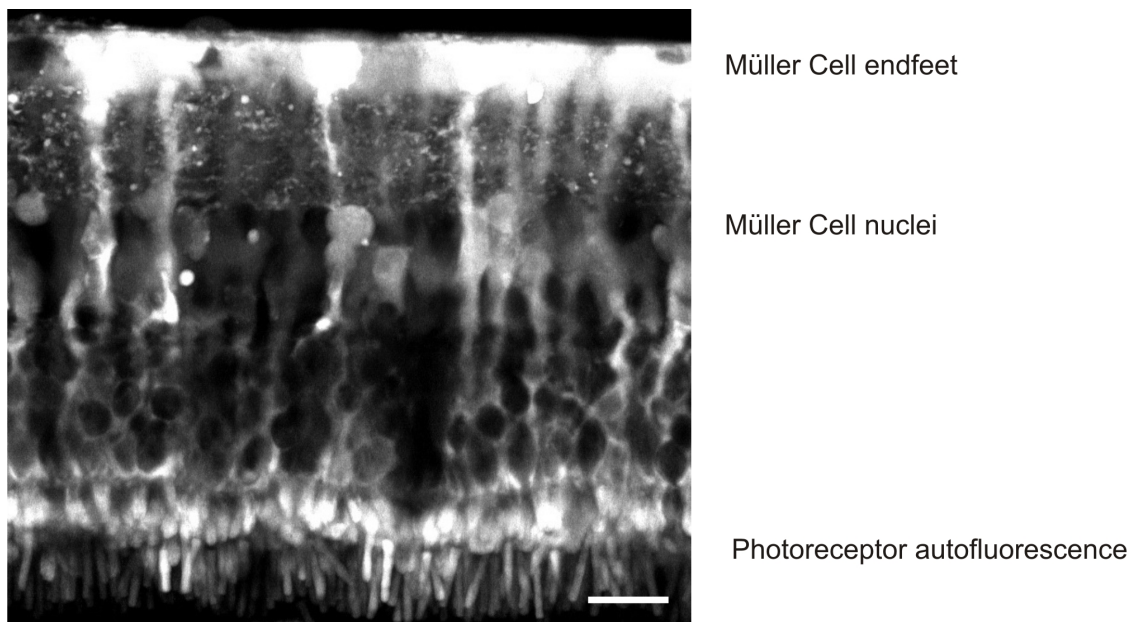
Figure 3.3: Guinea Pig retina stained with vital dye. The isolated retina was incubated within the MitoTracker Orange for 15 min and washed with PBS afterward. To allow for the detection of the retinal cross section, the tissue was fixed onto a nitrocellulose filter with the photoreceptors side down. The Müller cells filled with the vital dye are shown using a laser scanning microscope equipped with a $40x$ water immersion objective. The endfeet, nuclei, outer and inner processes are clearly visible. Scale bar $20\,\mu$m.

A stock solution with a concentration of $1\,mM$ was prepared with $50\,\mu g$ of the lyophilized dye in $50\,\mu l$ anhydrous dimethylsulfoxide (DMSO, D2650, Sigma-Aldrich, Taufkirchen, Germany). Then $10\,\mu l$ of the dye was diluted in 5 ml of ECS or PBS depending on the

experiment. The isolated retinae were incubated for $15 - 30$ min in darkness at room temperature, washed three times with ECS or PBS and examined using a confocal laser microscope LSM 510 (Zeiss, Oberkochen, Germany).

3.1.5 Immunohistochemistry

The cell is the basic building block of all tissues. The plasma membrane, that surrounds the cell, anchors surface proteins called antigens (see Figure 3.4 a). These surface proteins can serve as cell identifiers by defining characteristics about a cell. The antigens are targeted and bound very tightly by another type of proteins, the antibodies (see Figure 3.4 b). Each type of antibody has a distinct antigen-binding site. Each antibody recognizes its antigen with great specificity (Odell and Cook, 2013).

To estimate any change in the different retinal layers in response to the mechanical stress, which is used to verify the tissue structure after organotypic culture, samples were analyzed by immunohistochemistry. The method used is called indirect immunofluorescence, a two-step technique that requires an unlabeled primary antibody which reacts with the tissue antigen and with a labeled secondary antibody (see Figure 3.4 c and d).

The pieces of retinae were fixed in 4% paraformaldehyde overnight at 4°C. Thereafter, the tissue was washed three times in PBS, embedded in 3% agarose (05073,Sigma-Aldrich Fluka, Germany) and cut in thin slices ($d = 50\,\mu m$) with a vibration microtome (HM 650 V: Micro-International, Walldorf, Germany).

In order to detect intracellular antigens, cells must first be permeabilized especially after fixation with cross-linking agents such as formaldehyde and glutaraldehyde. Permeabilization provides access to intracellular or intraorganellar antigens.

To permeabilize the tissue I have used Triton X-100, the most common detergent that improves penetration of the antibodies. The permeabilization solution is composed of $0.3\,\%$ or $3\,\%$ Triton X-100 and $1\,\%$ dimethylsulfoxid (DMSO) diluted in PBS (PBS-TD). Slices were permeabilized for 1 hour at room temperature in PBS-TD. Therefore, to block unspecific binding of the antibodies, the slices were incubated in $5\,\%$ goat or donkey normal serum (Sigma-Aldrich, Germany) in PBS-TD for 1 hour at room temperature on a shaker. Retinal slices were maintained overnight at 4° C in a solution of PBS-TD containing primary antibodies chosen between the following: anti-vimentin (1 : 200, clone V9, Sigma-Aldrich, Germany) which shows the intermediate filaments in the Müller cells, anti-glutamine synthetase (MAB302, Chemicon, Germany) for localizing the radial glial cells, and anti-ACTIVE caspase-3 pAb(G7481, Promega, Germany) for recognizing the apoptotic cells. The tissue was also stained with peanut agglutinin (PNA) (L6135, Sigma Aldrich, Germany) specific for cone photoreceptor cells, not considered an antibody.
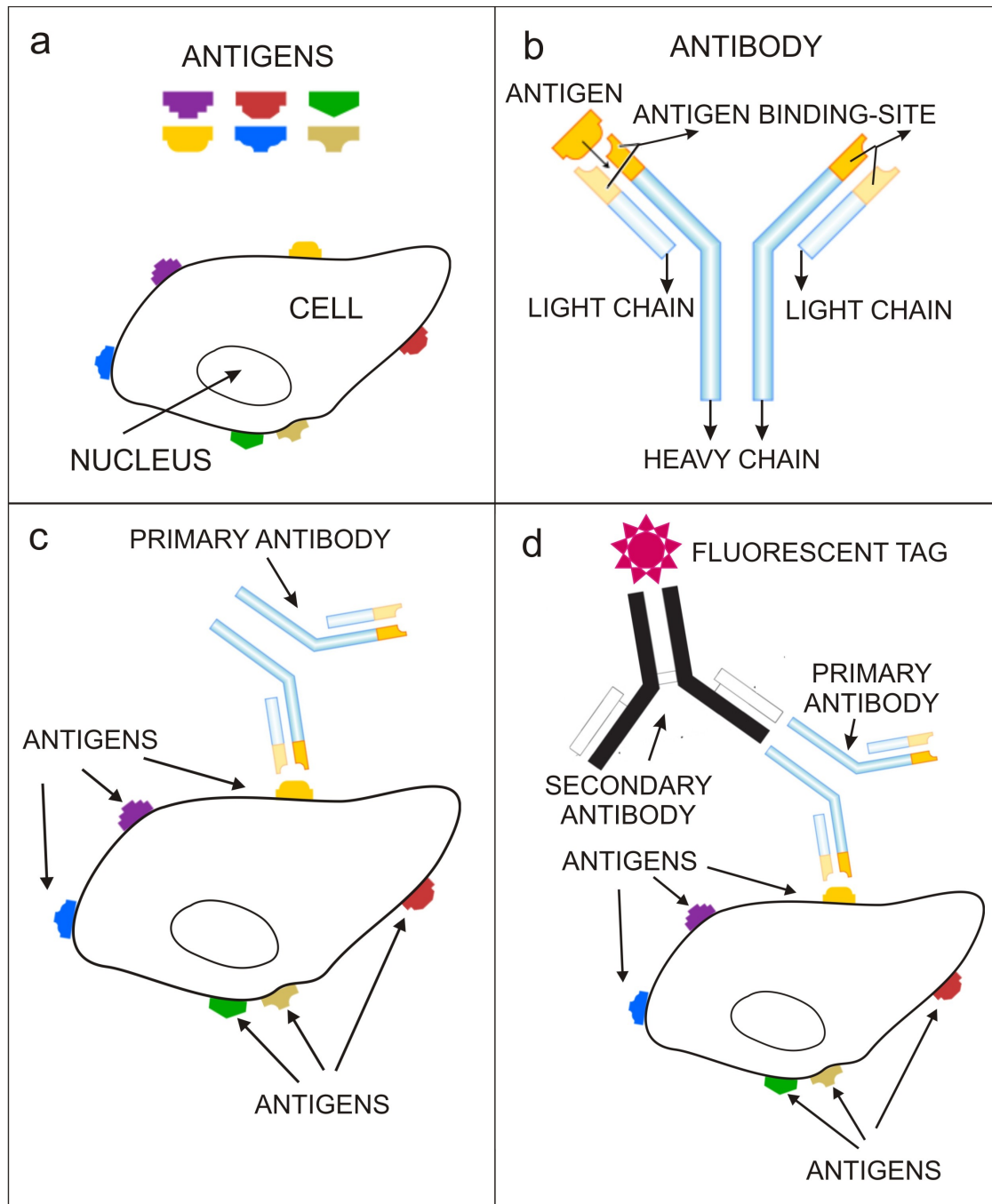
Figure 3.4: Schematic representation of indirect immunofluorescence. The cell membrane is covered with different type of surface proteins called antigens (a). The antigen is recognized and bound by an antibody, a large Y-shaped protein composed of a light chain and a heavy chain. The heavy chain defines the class or isotype of the antibody (b). The unlabeled primary antibody specifically binds the antigen (c) and the secondary antibody, which carries the fluorophore, recognizes and binds to the primary antibody (d). (Original image).

Afterwards, the slices were washed with PBS-TD for 3 hours on the shaker, and the solution was changed every hour. The secondary antibodies conjugated with a fluorescence dye (Jackson Immunoresearch, USA) were in contact with the tissue overnight at 4° C. During the following day, the slices were washed for 1 hour with PBS-TD, before they were either incubated with the nuclear dyes Hoechst 33258 (Molecular Probes,) or To-Pro-3 iodide (642/661, Invitrogen, USA) for 1 hour at 4°C. Hereafter the retinal slices were washed 3 times with normal PBS and mounted on a coverslip coated with some drops of mounting medium (Immunomount). Finally the slices were let to dry overnight in a dark place. The slices were observed using a confocal microscope (LSM 510, Meta, Zeiss, Jena, Germany) with a 40x objective (c-Achroplan, 1.2 W Corr M27, Zeiss, Jena, Germany).

3.2 Organotypic Culture of Adult Neural Tissues

The retina and the brain, the neural tissues used during my work, belong to the central nervous system (CNS). One of the conventional techniques used to culture these tissues is based on an air-liquid interface system (Stoppini et al., 1991; Gähwiler et al., 1997; Moritoh et al., 2010). In addition to observing strict sterile conditions and to keeping the culture at a constant temperature, the necessary conditions for a healthy culture are (i) firmly attaching the tissue to a substrate, supplying them with (ii) suitable growth medium and (iii) sufficient oxygenation (Gähwiler et al., 1997). In the air-liquid interface system, the tissue is placed on a semiporous membrane (Millicell, Millipore) inserted in a six-well plate (Stoppini et al., 1991). The medium is added to the bottom of the culture dish, feeding the tissue from below and leaving the top of the tissue directly in contact with the air (Gähwiler et al., 1997). In my work I used the same technique, replacing the semiporous membrane with a TiO_2 nanotube arrays (see Section 3.2.3) for reasons that I will explain later. To be able to feed the tissue without covering it, I inserted a stainless steal grid into a Petri dish (or in a six-well plate), on top of which I positioned the TiO_2 nanotube arrays (see Figure 3.5).
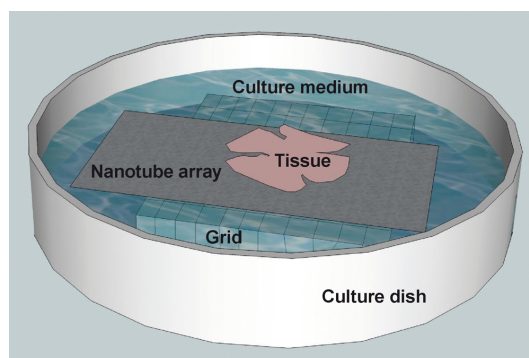
Figure 3.5: Schematic illustration of the culture setup. The setup used to culture retinal whole-mount and brain slices is relatively simple. It is composed of a culture dish containing a stainless steal grid on top of which the nanotube arrays lay (see section 3.2.3). The explants are positioned on top of the nanotube arrays. The culture dish is filled up with culture medium up to the edge of the membrane without covering the sample.

After isolation and preparation, the tissue is carefully transferred to the top of the nanotube membrane with a glass pipette or a brush. The medium in excess on top of the TiO_2 nanotube arrays is gently removed by aspiration. This operation also helps to securely attach the tissue to the substrate. Finally the culture dish is filled up to the edge of the nanotube membrane.

3.2.1 Retinal Whole-mount Culture

The retinal tissue was isolated as described in section 3.1.2. To avoid any risk of contamination, the entire procedure was executed under the laminar flow hood in the cell culture room. To flatten the tissue and consequently to facilitate its adhesion to the TiO_2 nanotube arrays, four incisions were made to the optic nerve hole. Once the tissue was firmly attached to the nanotube membrane placed in a Petri dish (see Figure 3.5), the culture dish was filled up with retinal culture medium composed of Ames medium (A1420, Sigma-Aldrich, Germany), horse serum (H1270, Sigma-Aldrich, Germany) and gentamicin (1357, Sigma-Aldrich, Germany) (see Table 3.2).

Table 3.2: Supplements added to the retinal culture medium. The Ames medium was prepared from a 90% w/v powder in water formulation in the following way. It was measured out, with 7.5 % w/v of sodium bicarbonate. This solution was bubbled with 100 % of CO_2 for at least 15 minutes. The supplements were directly dissolved in Ames medium and the pH was adjusted to the physiological value of 7.4 by using hydrochloric acid (HCl) or sodium hydroxide (NaOH).

Substance	Concentration [%]
Horse Serum	20
Gentamicin	0.1

The tissue was immediately incubated in a humidified 5% CO_2 atmosphere at 37° C. The entire medium was replaced 24 hours after seeding and then every third day. The retinal tissue was cultured for 7 and 14 days. After the culture time, the tissue still attached to the TiO_2 nanotube arrays was fixed in 4% paraformaldehyde overnight at 4°C. After this fixing time, it was washed three times in PBS and, with the help of a blade and a pipette, it was gently and carefully removed from the substrate. At this point it was ready to be embedded in agarose for cutting and immunostaining as described in section 3.1.5.

3.2.2 Brain Slice Culture

The culture technique used for brain slices is very similar to the one for the retina previously described (see Section 3.2.1). The brain slices were prepared as explained in section 3.1.3. From the six-well plates, where the slices were kept oxygenated during the cutting, they were transferred on top of the TiO_2 nanotube arrays using a small brush. To facilitate the adhesion of the slice to the membrane, the extra solution on top of the substrate was removed by aspiration. The culture setup is the same used for the retina culture (see

Figure 3.5). The difference lies with the solution used to culture the brain slices. The culture medium was composed of DMEM/F-12 with L-Glutamine medium (11320, GIBCO) supplemented with horse serum (H1270, Sigma-Aldrich, Germany), D-Glucose, HEPES and gentamicin (see Table 3.3).

Table 3.3: Supplements added to the culture medium for brain slices. The supplements are directly dissolved in DMEM/F-12 with L-Glutamine medium and the pH is adjusted to the physiological value of 7.2 using hydrochloric acid (HCl) or sodium hydroxide (NaOH).

Substance	Concentration [%]
Horse Serum	24
20% D-Glucose	1
HEPES	2
Gentamicin	0.1

As mentioned previously, it is important not to cover the tissue with the culture medium, allowing for good oxygenation during the incubation. The tissue was moved into an incubator set at 5% CO_2 and 37° C. The medium was changed with fresh medium 1 day after the isolation and then every third day. To compare the neural tissue integrity with that to the retinal tissue, the brain slices were also cultured for 7 and 14 days. Before removing the slices from the TiO_2 nanotube arrays, they were fixed in 4% paraformaldehyde overnight at 4°C. The slices were carefully detached from the substrate with the pressure applied by a pipette to their edges and they were immunostained using the technique explained in section 3.1.5. To observe the immunoreactivity of the neo-cortex after long-term culture, nuclei and neurofilaments were fluorescently labeled with To-Pro-3 Iodide (T3605, Molecular Probes) and Anti-Neurofilament H Non-Phosphorylated SMI-32 (NE1023, Millipore), respectively.

3.2.3 TiO$_2$ Nanotube Arrays

Titanium dioxide (TiO_2) nanotubes were first described by Zwilling and colleagues in 1991, as 'columnar porous' titania layers formed electrochemically in a fluorinated electrolyte. Titanium (Ti) and its alloys have long been used in biomedical devices as implantable biomaterials and have an emerging role in soft and hard tissue engineering as well as in regenerative medicine. The beneficial effects of their surfaces on cells adhesion, cell proliferation and cell functionality have also been observed (Brammer et al., 2010). In fact

TiO_2 is known to be a non-toxic, environmentally friendly, corrosion-resistant and exceptionally biocompatible material (Roy et al., 2011). Synthesis of TiO_2 nanostructures may be achieved by different ways including sol-gel methods, template-assisted methods, hydro/solvothermal approaches and by electrochemical means. In this project, the conventional electrochemical anodization has been used to produce self-organized TiO_2 nanotubes layers (Fischer and Mayr, 2011).

An oxidation reaction, explained by $M \rightarrow M^{n+} + ne^-$ (where n is the number of electrons (e) lost during the reaction) occurs when metals (M) are exposed to a sufficiently anodic voltage in an electrochemical configuration (see Figure 3.6). Thus, this reaction depends on the electrolyte used and on the particular anodization parameters. The formation of TiO_2 nanotubes is the result of three simultaneous processes: (i) oxidation of Ti metal to form titanium dioxide; (ii) dissolution of Ti metal ions in the electrolyte and (iii) chemical dissolution of Ti and TiO_2 due to etching processes caused by fluoride ions (Brammer et al., 2012). The diameter of the nanotubes can be controlled linearly by the applied voltage. The anodization time and the etching rate define the tube length. It becomes obvious that the fastest growth conditions also represent the conditions for optimized ordering. Various nanoscale morphologies, such as free-standing membranes, nanobamboo, tube stacks and tube-to-pore transitions can be achieved (see Figure 3.6 d and e).

To be more specific, for this project the TiO_2 nanotubes were prepared by anodization in fluorine-ion containing electrolytes (Dallacasagrande et al., 2012). The Ti foils were first cleaned in an ultrasonic bath with distilled water and isopropanol for 10 min each and dried in a nitrogen stream. TiO_2 nanotube array substrates were synthesized by electrochemical anodization using a titanium foil as the anode (Advent Research Materials LTD.; 99.6%; 1.8cm x 2.8cm; 0.1mm thickness) and a platinum mesh as the cathode (Advent Research Materials LTD.; 99.9 %; 52 mesh per inch; 25mm x 25mm). The electrolyte employed a mixture of ethylene glycol (Merck, Emplury) containing 0.3 wt% ammonium fluoride (Merck, EMSURE-ACS) and 2 vol % distilled water. After anodization, the samples were rinsed with ethylene glycol and dried in air at 50°C. They were cleaned a second time for 20 minutes in an ultrasonic water bath and dried in air at 50°C. Some samples were anodized more than once. This means that after anodization, the tubes were removed by exposing the samples for 20 minutes to an ultrasonic water bath . After multiple anodization steps, the samples were post-treated as described (Dallacasagrande et al., 2012).
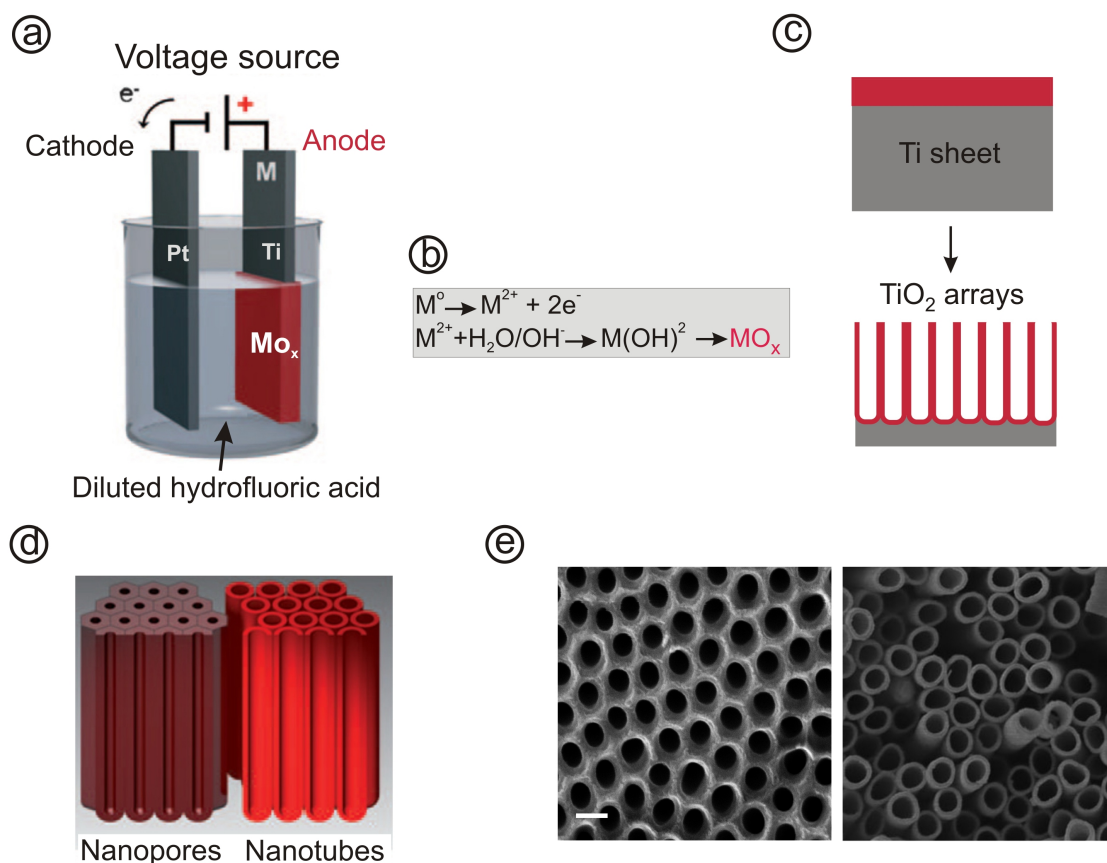
Figure 3.6: Schematic illustration of the electrochemical anodization used to fabricate TiO_2 nanotube arrays.(a) A titanium (Ti) sheet is used as the anode and a platinum (Pt) sheet is used as the cathode submersed in a fluoride-based electrolyte solution. (b,c) Anodization leads to an oxidation of metal species that forms a solid oxide (MO_x) on the metal surface and to the formation of TiO_2 arrays. (d) Depending on the anodization conditions (potential, electrolyte and temperature) the solid oxide layer can self-organize in a nanotubular shape (nanopores or nanotubes).(e) The pictures show TiO_2 arrays prepared in different solutions. The left image shows nanopores and the right image shows nanotubes. Scale bar $100\,\mu$m.

3.3 Mechanical Setup

3.3.1 Long-term Measurement Setup

Long-term Shear Stress Device

The device is mainly assembled from three components: a chamber made of polytetrafluoroethylene (Teflon), a stepping motor (C-663 Mercury Step, Physik Instrumente, Karlsruhe, Germany) and an actuator (M-228 Stepper-Mike Linear Actuator, Physik Instrumente, Karlsruhe, Germany) (see Figure 3.7 a). The stepping motor is attached to the chamber on the side through a metallic plate and both are fixed on a heavy metallic tray (see Figures 3.7 a). The tray is necessary for stabilizing the sample during the experiments since the device has to be moved from the laminar flow hood into the incubator. The metallic parts are made of stainless steel since the experiment requires sterilized conditions. For this reason, all the components placed on the plate have to be sterilized before use.
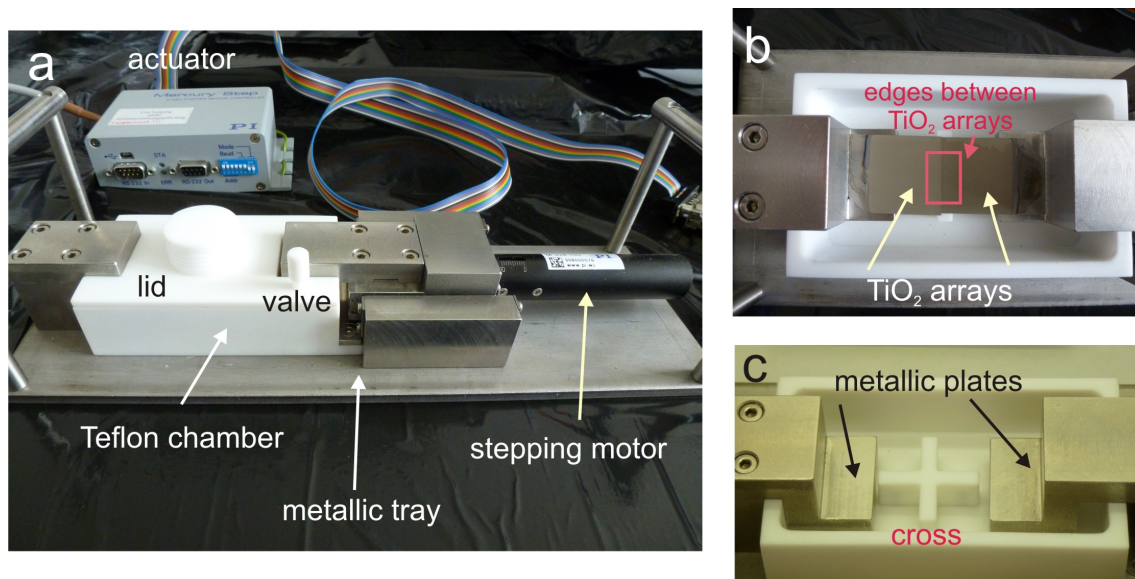
Figure 3.7: Device for long-term shear stress measurements. (a) The set-up is composed of a heavy stainless steal tray that holds the Teflon chamber and the stepping motor. The actuator connects the stepping motor to a computer. (b) Two TiO_2 nanotube arrays are glued on the stainless steal part of the Teflon chamber. The sample is positioned in the middle where the nanotubes substrates enter in contact with each other. The chamber is filled with culture medium until the edge of the TiO_2 arrays. (c) In the middle of the Teflon chamber a cross helps to avoid the bending of the substrate during the mounting of the explant.

The device components made of Teflon and all small metallic parts were washed in 1% of a special cleaning solution (Hellmanex, HellmaAnalytics) in an ultrasonic bath for 1 hour

(see Figure 3.8 a). All remaining parts were cleaned with 70% ethanol under laminar flow (see Figure 3.8 b). After cleaning, it was important to rinse all the component with bi-distilled water three times to remove any residues that could be harmful for a living tissue. In order to avoid any risk of infection, the number of pieces that constitute the device were reduced to minimum for easy disassembly and cleaning. The actuator connects the stepping motor to a laptop where a customized Labview program runs during the experiment (see Figure 3.8 c). During the experiment, the device was kept under the flow hood (see Figure 3.8 d).
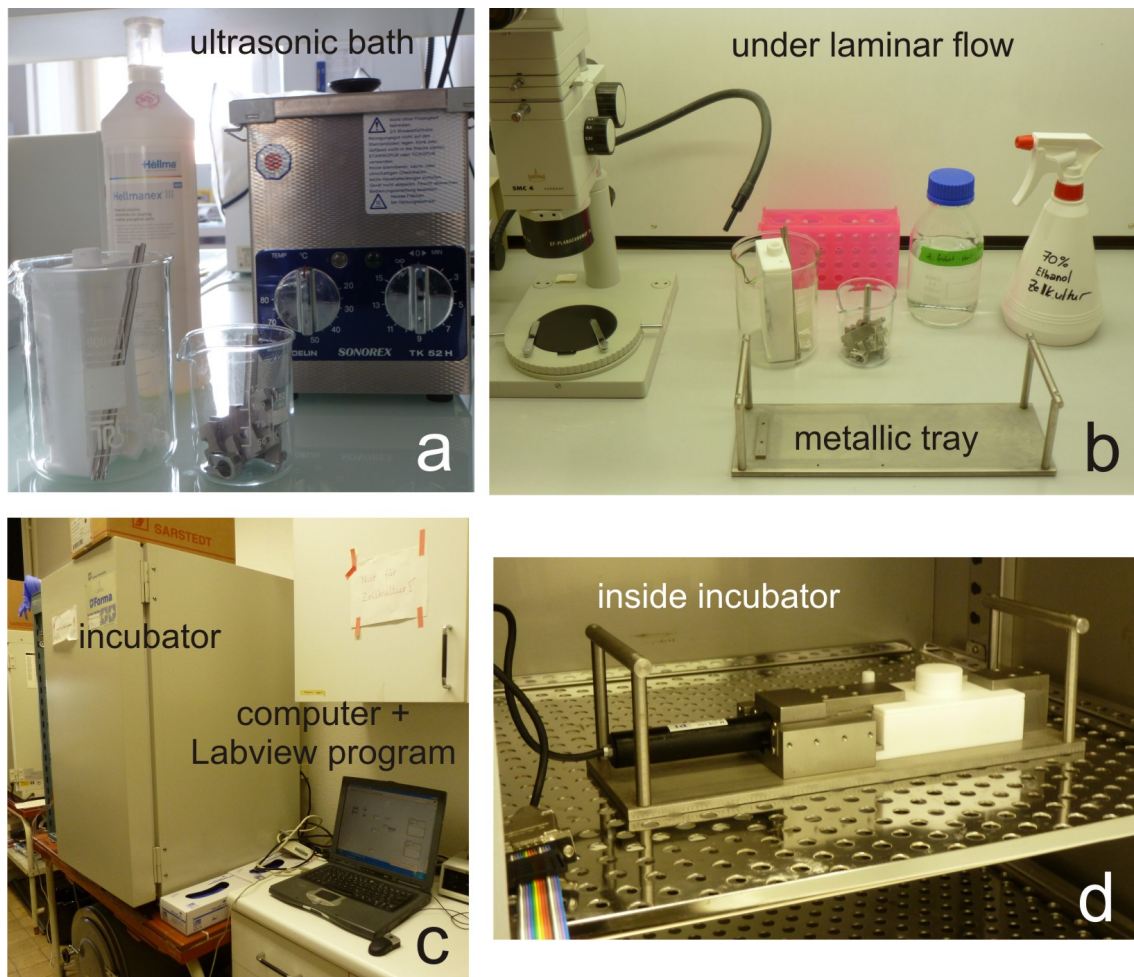
Figure 3.8: Cleaning procedure and setup for long-tern shear stress experiment. All the small components were disassembled and cleaned in the ultrasonic bath with a special detergent (Hellmanex)(a). Most of the metallic parts were sterilized with ethanol under the laminar flow hood (b). The experiment was controlled using a self customized LabView program (c). The device was kept inside an incubator during the experiment (d).

The device has been designed to ensure a long-term survival of the retinal tissue. In the described setup, the retinal whole mount is placed on two pieces of TiO_2 arrays (see Figure 3.7 b). The super-hydrophilicity of the Ti-substrate ensures the maintenance of a healthy retina during the experiment. The medium reaches the retina from below the side of the TiO_2 arrays in order to deliver the nutrients. The TiO_2 substrates are fixed with a special glue (Histoacryl Tissue Adhesive) on the metallic plates (see Figure 3.7 c) inside the chamber. The glue is biocompatible and can be removed easily but ensures a stable adhesion of the substrates throughout the experiment. TiO_2 arrays are placed on a cross (see Figure 3.7 c) made of Teflon (positioned in the middle of the chamber) to prevent the bending of the arrays during the mounting of the retina. The chamber is provided with an indispensable lid to maintain a clean environment for the tissue inside the incubator. A valve situated on top of the lid guarantees an adequate exchange of gas when opened properly (see Figure 3.7 a).

The experiment consisted in moving one membrane $1\,\mu$m every hour for 100 hours reaching a maximum displacement of $100\,\mu$m. After the fourth day of shearing, the retina was left rest for 24 hours. Following the settling, the retinal whole-mount, still attached to the $TiO_2$ nanotube arrays, was fixed in 4% paraformaldehyde over night. to assure a correct detachment, first with the help of a sharp blade the edge of the tissue were detached from the membrane, then melted agarose was poured on top of the sample and let it dry. In this way the agarose held together the retinal tissue facilitating the removal. Once fixed and removed, the retinal tissue was immunostained as a whole-mount or as a slices to allow to analysis the cross-section (see section 3.1.5).

3.3.2 Short-term Measurement Setup

Short-term Shear Stress Device

The guinea pig retina, after having been isolated (see Section 3.1) and stained with Mito-tracker Orange (see section 3.1.4), was fixed on a cellulose filter (MF-Millipore Membrane filter, HABG01300, Billerica, MA, USA) with the photoreceptors upside down. A razor blade was used to cut the retina in slices of 5 mm thickness. These slices were mounted within a chamber made of polydimethylsiloxane (PDMS) and filled with extracellular solution (see Figure 3.9 c). The chamber was placed on a motorized stage under a water immersion objective (40x Achroplan, *NA* 0.80W, Zeiss, Oberkochen, Germany) of an upright microscope (AxioScope FS2NOT, Zeiss, Oberkochen, Germany) equipped with a laser scanning unit (LSM 510 Meta, Zeiss, Oberkochen, German) (see Figure 3.9 a). A square-shaped piece of cellulose filter (5 mm x 5 mm) was glued to an extremity of a ceramic rod (see Figure 3.9 b). A micromanipulator (Luigs & Neumann, Ratingen, Germany) was used to gently guide the filter attached to the ceramic rod towards the retinal

slice. The motorized stage, controlled by a customized Labview program, was moved to apply the shear stress to the retina which was positioned between two cellulose filters and visible under the microscope because of the vital dye staining.
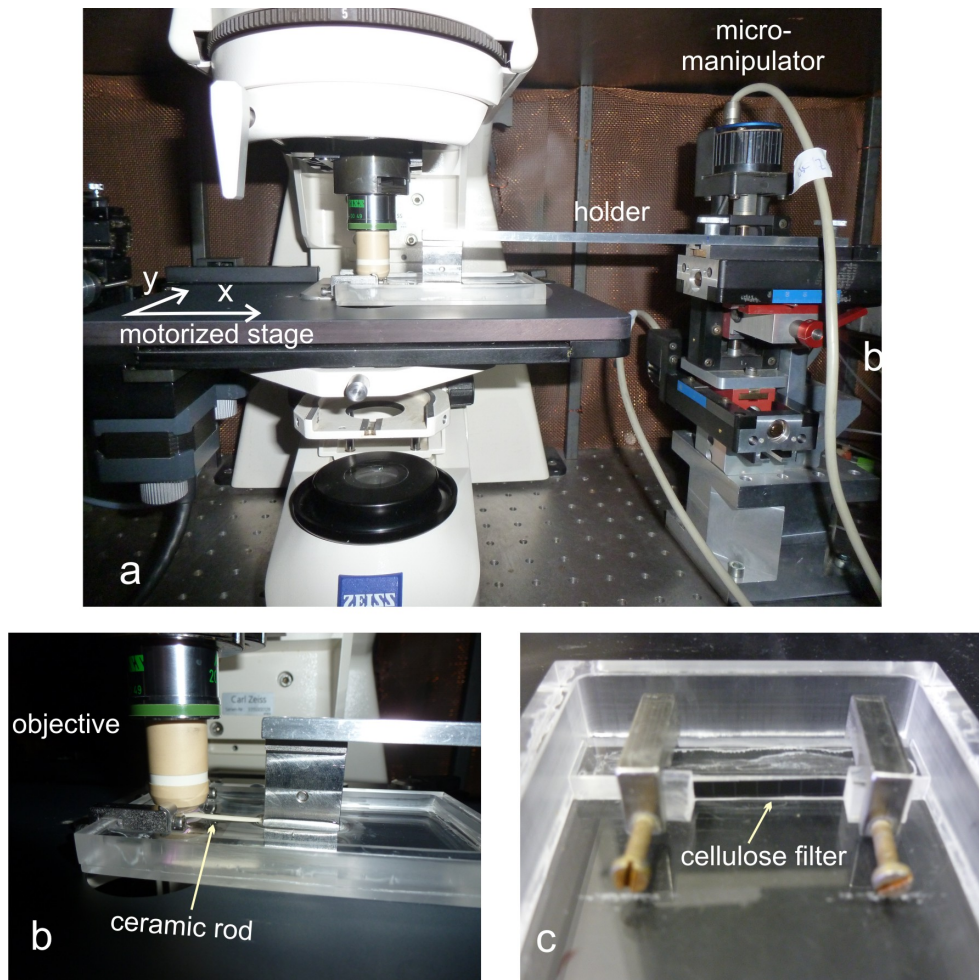
Figure 3.9: Device for short-term shear stress measurements. (a,b) The micromanipulator places the ceramic rod under the objective. A motorized stage controls the xy-movements of the sample. (c) The retinal slice, attached to the cellulose filter, is positioned inside the PDMS chamber which is filled with extracellular solution (ECS).

4 Experimental Results

The purposes of this work were first, to find a biocompatible membrane to extend the culture time of adult tissue and second, to design new set-ups to acquire a deeper knowledge of the behavior of retinal tissue in response to mechanical stimuli.

In the first part of this session a new method for long-term organotypic culture of adult neural tissue is presented. The system adopted for the tissue culture is already well established, however the innovation consists in employing TiO_2 nanotube membranes to support the tissue. That allowed to conserve the explants alive for up to 14 days, a satisfying result considering that adult neural tissue usually is cultured up to 6 days (Koizumi et al., 2007). In the second part new approaches to mechanically probe the retinal tissue are introduced. Using these methods, shear stress was applied to the retinal slices and to the retinal whole-mount with the goal to better understand the involvement of the mechanics in retinal processes such as retinal detachment or fovea development.

4.1 A New Method to Culture Adult Neural Tissue

The aim of this part of my research was to preserve adult neural tissue for an extended period of time in culture. The common method used to culture brain slices or retinal whole-mount, as mentioned previously, is based on an air-liquid interface system (Stoppini et al., 1991; Moritoh et al., 2010). Generally, the tissue is isolated and mounted on a Millicell insert or on a cellulose filter positioned on top of a stainless steal grid which both prevent the medium to cover the explant and, at the same time, allow the solution to reach the tissue from the bottom. The organotypic culture of neural tissue usually employs postnatal animals because of the low rate of survival in culture of the tissue of adult animals. In fact, using the conventional culture method, the adult brain slice or the adult retina whole-mount survive up to six days (Koizumi et al., 2007; Schrag et al., 2008; Su et al., 2011;). Adult retinas are difficult to culture, mainly because of the exceptionally high metabolism of the photoreceptor cells (Laughlin et al., 1998; Linsenmeier and Padnick-Silver, 2000).

My research was addressed to find a biocompatible membrane possessing the characteristics of stability and rigidity necessary to support mechanical stress without undergoing any type of deformation, and being able to guarantee long-term culture of neural tissue using the air-liquid interface system.

4.1.1 TiO$_2$ Nanotube Arrays as Membranes for Long-Term Culture of Adult Neural Tissue

After testing different types of membranes (i.e. silicon dioxide membrane) the amorphous TiO$_2$ nanotube arrays were found to be the more efficient membranes for a long-term culture of adult neural tissue.

To study the interaction of tissue explants with TiO$_2$ nanotube arrays, these substrates were synthesized by conventional electrochemical anodization as described in section 3.2.3 (Fischer and Mayr, 2011). A variety of nanobutes with different diameters and surface roughness were analyzed (Dallacasagrande et al., 2012). The necessity of this testing was dictated by the fact that these membranes were utilized until recently just for implants or for single cell culture but not yet for tissue culture (Peng et al., 2010; Park et al., 2012). One of the features of TiO$_2$ nanotube arrays is their tunability, for this reason it was necessary to test which were the best parameters for a long-term culture. Various diameters d, wall thicknesses t and surface roughness were examined . The surface roughness was estimated by AFM measurements of the variations of individual tube heights h_i and the characteristic length scale of the modulations λ (see Figure 4.1) (Mayr et al., 1999). The variations of the individual tube heights were characterized-normal to the surface plane by the standard deviation $\sigma = \sqrt{\langle h_i^2 \rangle - \langle h_i \rangle^2}$.

Interestingly, the retina and the brain could not be cultured on nanotubes with the same parameters for reasons that have still to be explained.

For long-term culture of the adult retinal tissue three different classes of nanotubes arrays resulted to have the right parameters for a successful cultivation. These were: (i) arrays composed of free-standing tubes (see Figure 4.2 a) with $d = (71 \pm 4)$ nm, $t = (7.5 \pm 2.0)$ nm and rough surface (see Figure 4.1 a) with $\sigma = 120$ nm and λ below 1.5 μm; (ii) nanoporous arrays (see Figure 4.2 b) with $d = (83 \pm 8)$ nm, $t = (8.5 \pm 2.5)$ nm and compact nanotube structure with a smooth surface ($\sigma = 85$ nm and $\lambda > 2$ μm); as well as (iii) largely heterogeneous arrays in term of nanotube diameters ranging from 33 nm to 63 nm and average diameters $d = (46 \pm 13)$ nm (see Figure 4.2 c and 4.1 b), very thick walls ($t = (32.5 \pm 4.5)$ nm) and considerable surface roughness ($\sigma = 111$ nm and $\lambda > 3$ μm) (see Figure 4.2 c).

Surprisingly, the brain slices preferred to be cultured on TiO$_2$ nanotube arrays with diameters greater than $100\,nm$ and with a smoother surfaces than for the retinae. Best organotypic culture was obtained for nanoporous arrays featured with $d = (100 \pm 12)$ nm , thin walls ($t = (8.0 \pm 1.5)$ nm) and considerably smooth surface ($\sigma = 63$ nm and $\lambda > 150$ μm) (see Figure 4.3).

The superhydrophilicity of the TiO$_2$ substrates was shown in a previous study (Balaur et al., 2005b) and was confirmed by our measurements of the contact angle. Using a
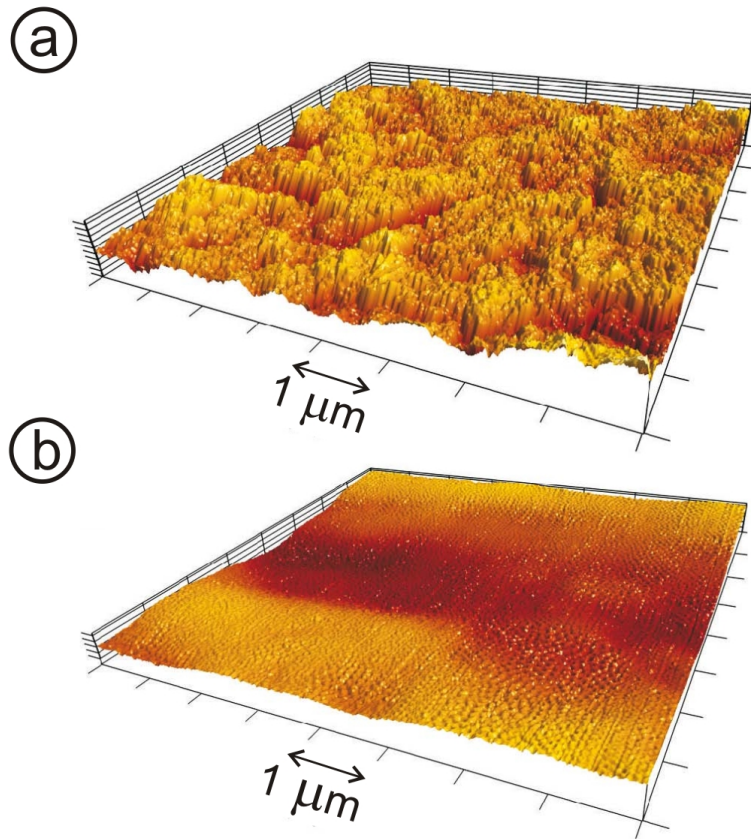
Figure 4.1: Surface morphologies of TiO$_2$ nanotube arrays. (a) Atomic force microscopic surface topographs of the rough surface of the free-standing nanotube substrates shown in Figure 4.2 a. This surface is characterized by sharp edges due to microcracks and by significant height variations of nanotubes. (b) Atomic force microscopic surface topographs of the smooth surface of the nanotube arrays shown in Figure 4.2c. The homogeneous length of the tubes generates a low curvature profile that characterized the smoothness.

droplet of distilled water and a droplet of culture medium, we calculated a contact angle of $(1.5 \pm 0.5)°$ and $0°$, respectively. Full nanotube wettability ensures the condition for the air-liquid interface system necessary for a healthy organotypic culture of neural tissue. Indeed, the explants were not covered with culture medium, instead they were fed from the bottom and the side of the nanotubes by diffusion, allowing the exchange of gas and nutrients and avoiding tissue edema and swelling.

Table 4.1: Parameters of the TiO$_2$ arrays for a long-term culture of neural tissue. Surprisingly the neuroretina and the neo-cortex preferred to be cultured on different membranes. The brain slices maintained their structure if cultured on TiO$_2$ nanoporous with tube diameter greater than 100 nm and smooth surface.

Retina			
type	**diameter [nm]**	**thickness [nm]**	**surface**
free-standing tubes	71 ± 4	7.5 ± 2.0	rough
nanoporous arrays	83 ± 8	8.5 ± 2.5	smooth
nanoporous arrays	46 ± 13	32 ± 4.5	rough
Brain			
nanoporous arrays	100 ± 12	8.0 ± 1.5	smooth
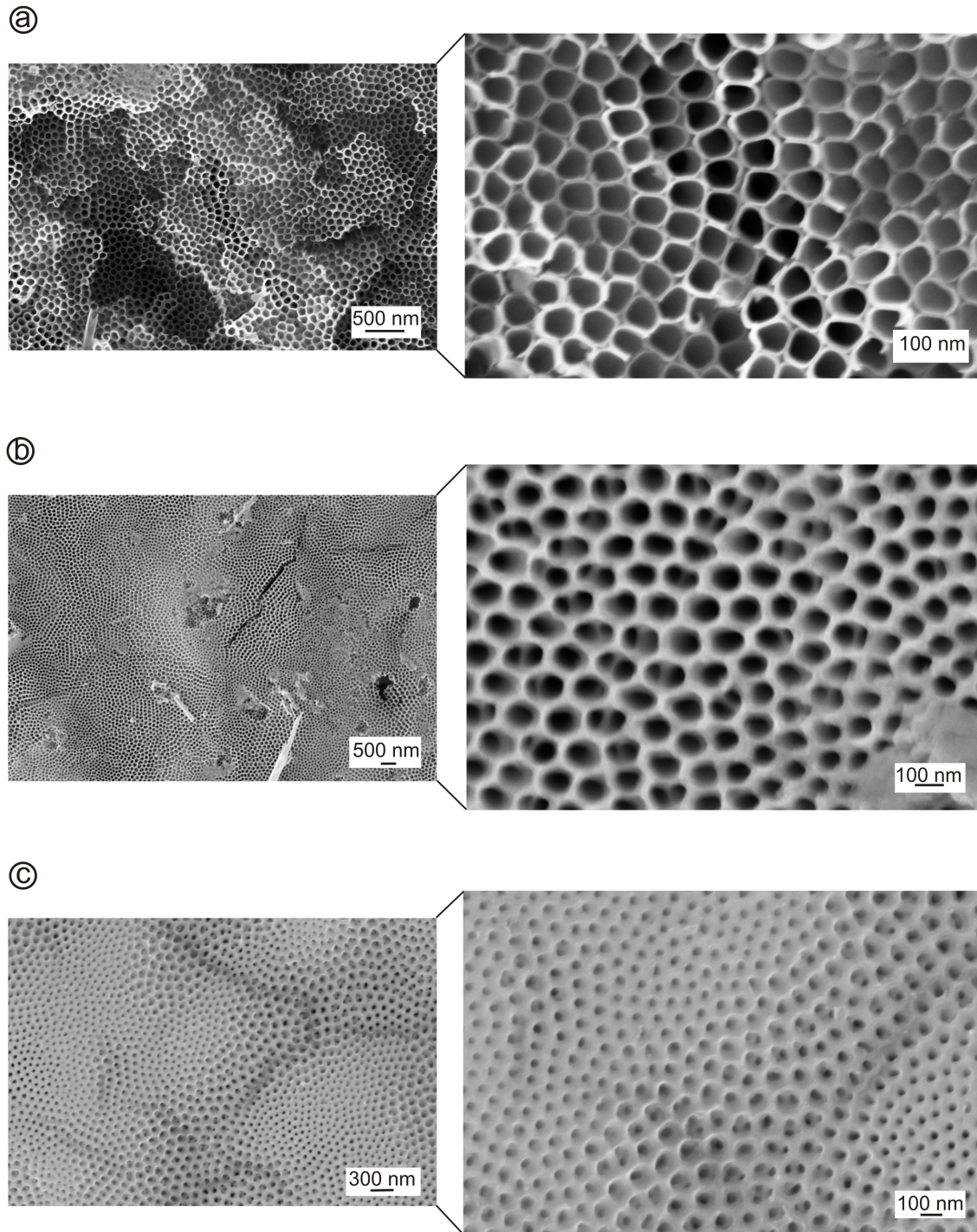
Figure 4.2: Scanning electron microscopic image of different TiO_2 substrates used for long-term culture of retinal tissue. The image shows the morphology of the nanotubes, before culture, with different scaling. (a) Free-standing TiO_2 nanotubes characterized by diameter of the tubes around 70 nm and a rough surface. (b) TiO_2 nanoporous with the diameter of the tubes in average 83 nm and a smooth surface. (c) The diameters of these tubes range from 33 nm to 63 nm. These substrates are characterized by thick walls and a smooth surface.
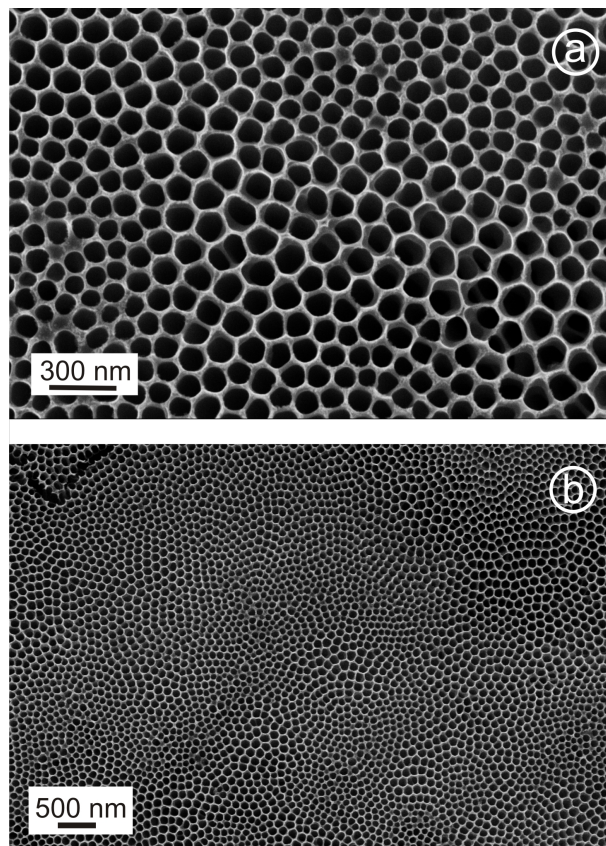
Figure 4.3: Scanning electron microscopic image of TiO$_2$ nanoporous arrays. The image shows the morphology before culturing with different scales (a-b). These substrates allow to achieve the best organotypic culture of brain slices. They have a average tube diameter around 100 nm, thin walls and significantly smoother surface compared to the nanoarrays used for retinal tissue culture.

4.1.2 Morphology of Adult Neural Tissue after Long-Term Organotypic Culture on TiO$_2$ Substrates

To test the properties of TiO$_2$ nanotube arrays as suitable membrane for long-term tissue culture, the retinal tissue was incubated using the culture setup illustrated in section 3.2. Initially, the retinal whole-mount was cultured for a few days, then for 7 days to overcome the maximum reached by the traditional method. Finally, I increased the days in culture until stopping at 14 days.

The possibility to increase the time in culture was given by the fact that the retina, cultured on top of TiO$_2$ nanotube arrays, showed a well conserved structure from the beginning. Indeed, the thickness and the layered network were wholly maintained after 7 and also 14 days of culture. In total, more than 20 tissue culture experiments were performed. The retinal thicknesses were obtained measuring thicknesses at 10 different positions. Quantitatively, the thickness of a freshly isolated retinal tissue (see Figure 4.4) was calculated to be 104.02 ± 1.03 μm and the thicknesses after 7 and 14 days of culture were determined to be 110.43 ± 0.88 μm and $97.54 \pm .48$ μm, respectively. Showing that, the thickness of the retinal explants remained constant during the culturing within a deviation of less than 6%. Furthermore, the organization of the nuclei within the inner and outer layers appeared to be unaffected. In fact, the retina cultured for 7 as well as for 14 days shown three nuclei atop within the inner nuclear layer and five nuclei atop in the outer nuclear layer (see Figure 4.5 a), as reported by control experiments (see Figure 4.4).

The preservation of the outer plexiform layer, as the site of synaptic connection between photoreceptors and neurons, is well shown in all the images (see Figure 4.5 b). In addition, it was demonstrated that the photoreceptor layer had maintained its integrity, revealing that the inner and outer segments of the photoreceptors survived well during two weeks of culture (see Figure 4.5 b). This is barely observed in long-term cultures (Mosinger Ogilvie et al., 1999; Reidel et al., 2006) when the retinal pigment epithelium is removed, as in these experiments. Considering that the Müller cells are the first cells to react in case of changes in the physiological environment, or due to degeneration and injury (Bringmann et al., 2006), they were employed as indicator of healthy and undamaged retina to verify the conservation and viability of the tissue in culture. The morphology and functional integrity of the Müller cells were shown by immunofluorescence. The radial retinal cells were stained with antibodies directed to glutamine synthetase and vimentin. With both markers, it was observed that the morphology of these cells remained intact (see Figure 4.5 c). There were no signs of tissue edema (Mosinger Ogilvie et al., 1999), migration or hypertrophy of Müller cells (Caffé et al., 1993). Finally, apoptotic cells within the adult retina after culture were visualized using the anti-Active Caspase-3 polyclonal antibody. The few apoptotic cells identified were mainly in the ganglion cell layer (see Figure 4.5
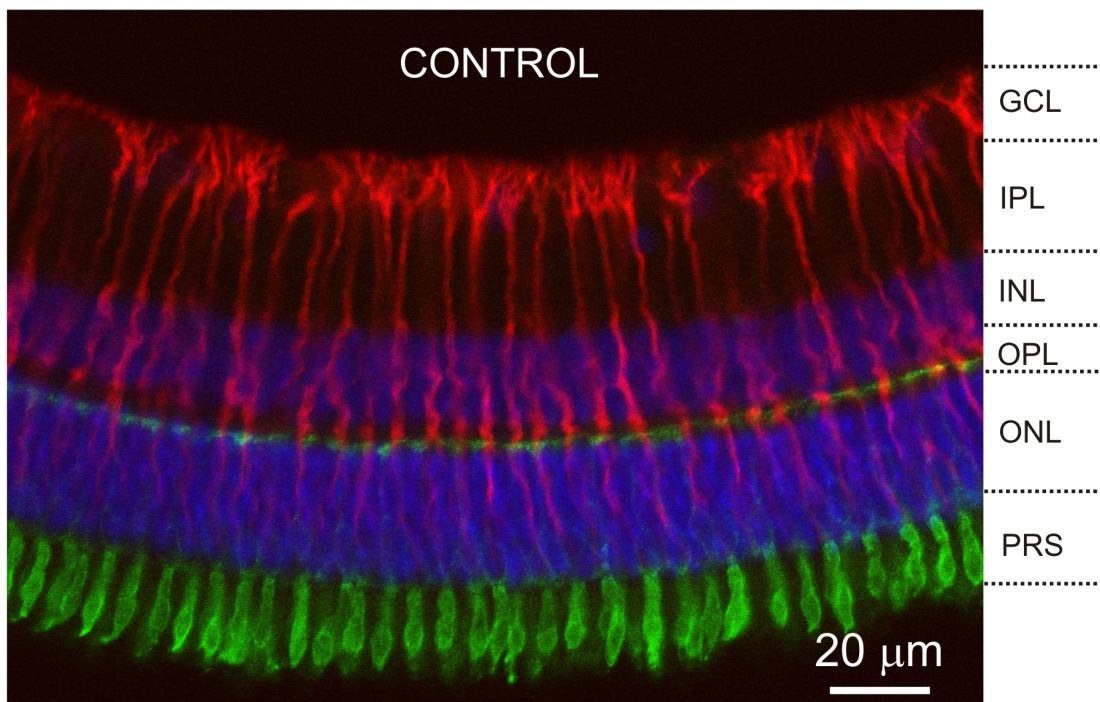
Figure 4.4: Fluorescent image of a freshly isolated adult guinea pig retina. Müller glial cells are fluorescently labeled in red, photoreceptor cones in green and nuclei in blue. All the layers are clearly discernible. GCL=ganglion cell layer, INL=inner nuclear layer, ONL=outer nuclear layer and PRS=photoreceptor segment layer.

d and e). This phenomenon is not uncommon due to Wallerian degeneration. Indeed, the axons of these cells were disconnected from their target during isolation. The fact that the apoptotic cells were located only in this area confirmed the well-maintained structures and cell density in the explants.

Supplementary experiments were performed on arrays with other nanotubes diameters, wall thicknesses and surface roughness than the ones mentioned in section 4.1.1 to verify their influence on tissue conservation. In the literature, data regarding experiments conducted on single cells using TiO_2 nanotube arrays are available. Those data proved that arrays with tubes diameters within $15 - 30$ nm are ideal for the viability of single cells, while larger diameters caused reduced adhesion and finally apoptosis at $d = 100$ nm (Park et al., 2007; Park et al., 2009b). Therefore, I chose to culture the retinal whole-mount and to test its viability on nanotubes with tube diameter ranging from 15 nm to 150 nm. It was possible to identify the diameters between $30\,nm$ and $85\,nm$ as optimal for culturing retinal explants, while variations of the other parameters were more tolerable within larger selections. At the lower tube diameter limit of $d = 30$ nm the retinal tissue structure was endangered.
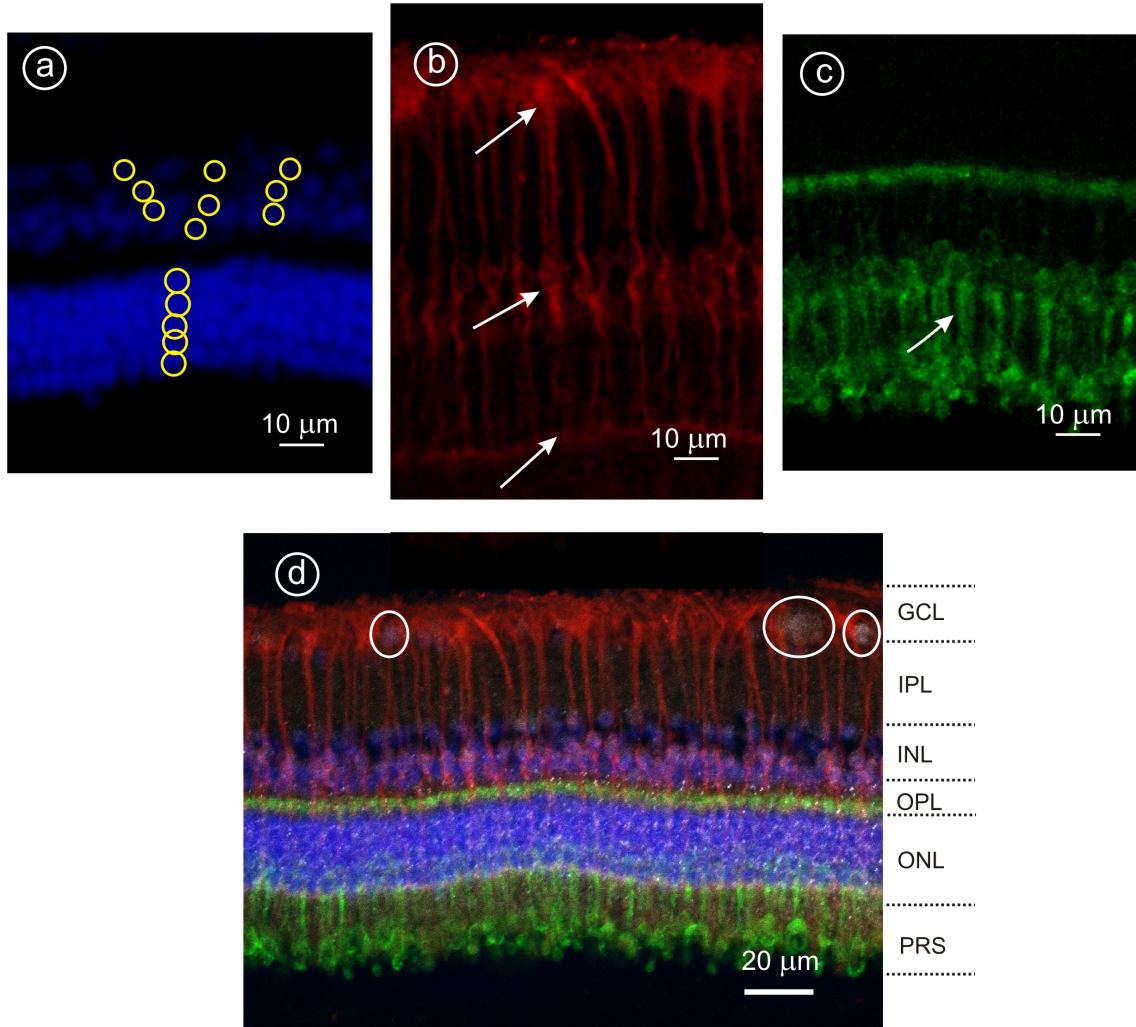
Figure 4.5: Detection of apoptotic cells in guinea pig retina cultured for 14 days on top of TiO_2 nanotube arrays. (a) The cultured retina maintained the structure of three rows of nuclei in the INL and five rows of nuclei in the ONL like in the fresh isolated retina (yellow circles). (b) The Müller cells conserved their shape spanning the entire thickness of the retinal tissue without any evident sign of damage. The arrows show the endfeet, the nucleus and the microvilli. (c) The photoreceptor cells are clearly discernible. Their synaptic connection and their inner and outer segments of the cone photoreceptors are well maintained (see arrows). (d) A merge picture of the retina cultures for 14 days and stained with hoechst for highlighting the nuclei (blue), peanut agglutinin for the cone photoreceptors (green), glutamin synthetase for the retinal radial glial cells (red) and caspase-3 for apoptotic cells (white). The stain with caspase-3 antibody shown that the dead cells are located mainly within the ganglion cells (white circles). GCL=ganglion cell layer, INL=inner nuclear layer, ONL=outer nuclear layer and PRS=photoreceptor segment layer.

The explants tended to flatten and to create strong adhesion sites to these arrays. Furthermore single cells were not recognizable anymore. At the upper limit of $d = 100$ nm the attachment of the retinal tissue to nanotubes arrays was very weak, compromising the integrity of the sample. In Figure 4.6 and 4.7 fluorescent images of retinal tissues cultured for 7 and 14 days on TiO_2 nanotube arrays with tube diameters between $30\,nm$ and $100\,nm$ are shown. The morphology of those cultured retinal explants was well maintained compared to the freshly isolated retinal tissue (see Figure 4.4) as asserted above.

Regarding the organotypic culture of slices of neo-cortex of the adult brain the results were successfully similar. After 7 and also 14 days of culture the neural network's architecture is conserved. The tissue was fluorescently labeled and it was shown that the density of cell nuclei is preserved, indeed the number of nuclei was consistent with the number of nuclei of the freshly isolated brain slices. The neurofilaments shown the typical arrangement of long axons conserving the neural networks (see Figure 4.8). TiO_2 substrates proved to satisfy the requirements for a long-term neural tissue survival (Dallacasagrande et al., 2012).
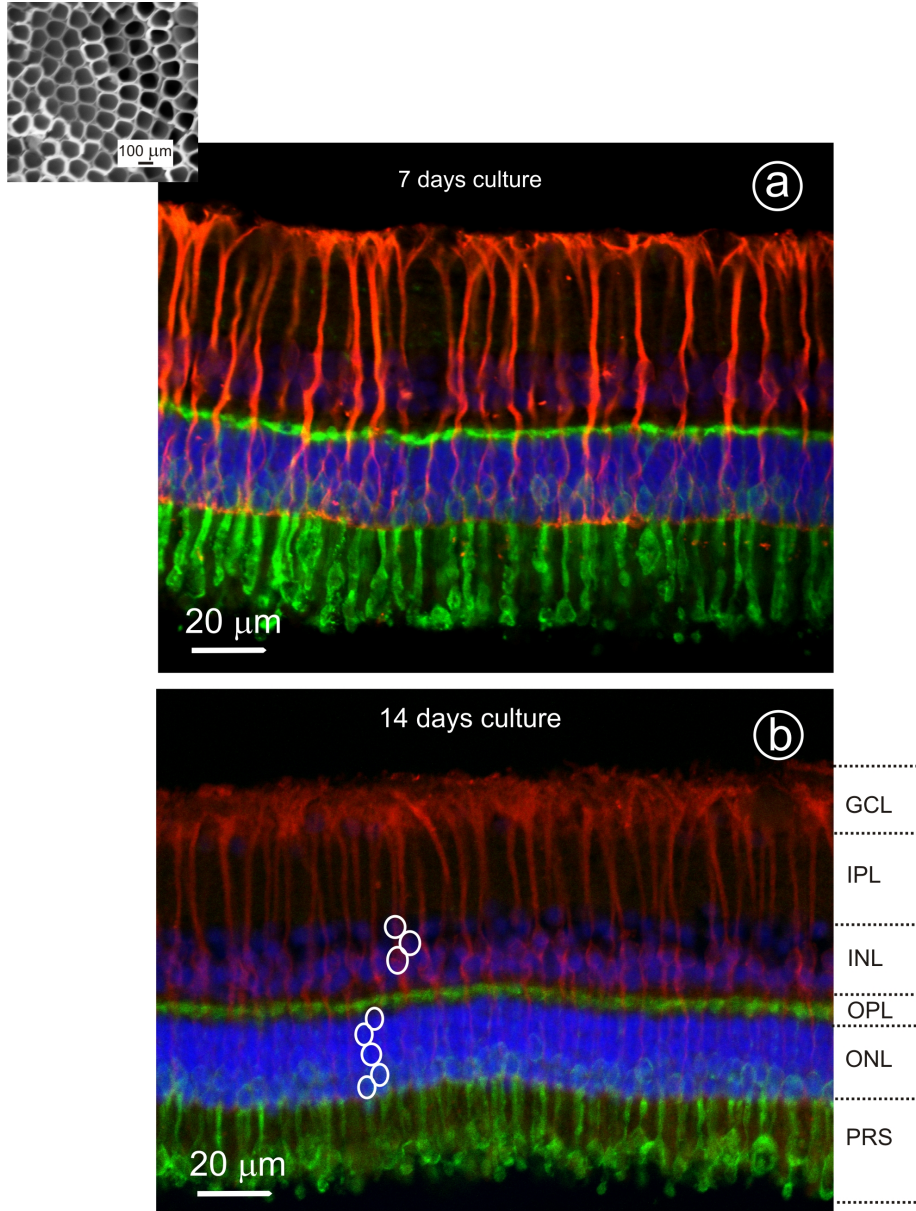
Figure 4.6: Fluorescent image of a cultured adult guinea pig retina on free-standing nanotubes. Müller glial cells are fluorescently labeled in red, photoreceptor cones in green and nuclei in blue. The retinal tissue was immunostained after 7 days (a) and 14 days (b) of culture on the free-standing nanotubes (Figure top left). GCL=ganglion cell layer, INL=inner nuclear layer, ONL=outer nuclear layer and PRS=photoreceptor segment layer. As for the freshly isolated retinal tissue the INL, ONL and PRS are clearly discernible. The number of nuclear rows in the INL and ONL is not altered.
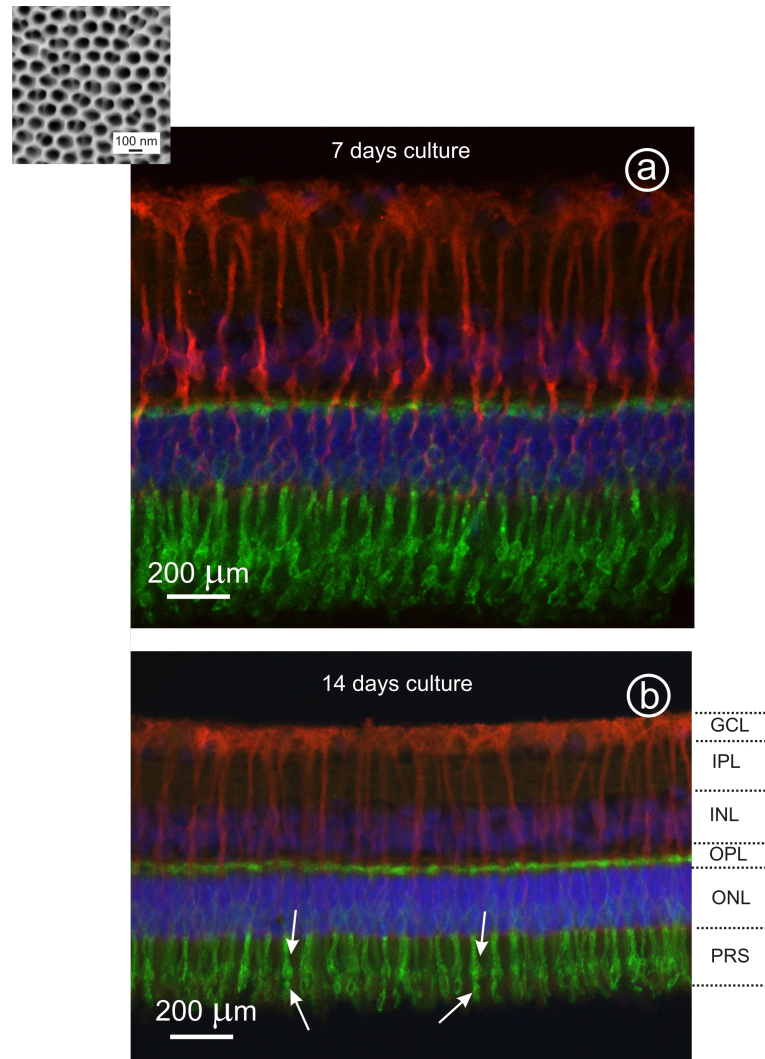
Figure 4.7: Fluorescent image of a cultured adult guinea pig retina on heterogeneous nanotube arrays. Müller glial cells are fluorescently labeled in red, photoreceptor cones in green and nuclei in blue. The retinal tissue was immunostained after 7 days (a) and 14 days (b) of culture on the nanotubes (Figure top left). GCL=ganglion cell layer, INL=inner nuclear layer, ONL=outer nuclear layer and PRS=photoreceptor segment layer.
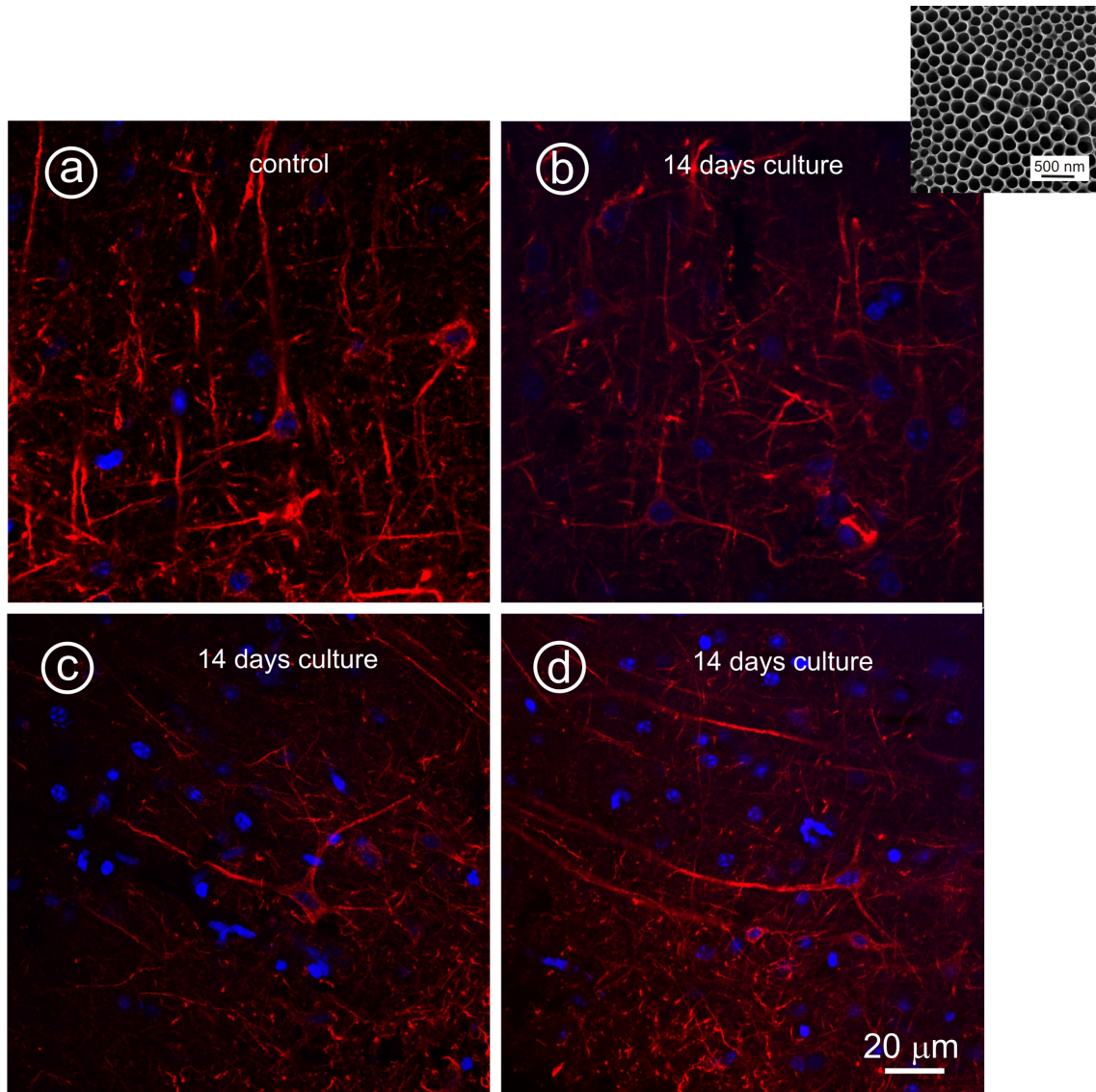
Figure 4.8: Fluorescent image of adult mouse brain slice of neo-cortex. The neurofilaments are labeled in red and the nuclei in blue. (a) The freshly isolated brain slices show a high density of nuclei and good spreading of the neuron axons as well as (b-c) the explants cultured for 14 days on the TiO$_2$ nanotube arrays shown in figure top right with the same experimental conditions.

4.2 A New Method to Mechanically probe Retinal Tissue

This part of my work focused in designing a new set-up and consequently in establishing a new method to mechanically stimulate the retinal tissue. The knowledge of the deformation which the neuroretina experiences when subjected to mechanical stress could help to understand, for example, how mechanics influences retinal development or how it is engaged in the generation of retinal diseases.

Different sets of experiments were performed trying to gather more information on the role of mechanics in retinal research. In the type of experiment presented here, the neurosensory retina undergoes short-term shear stress. Using this new set-up the retinal response to this type of stress can elucidate the mechanism involved in the retinal detachment, for example.

4.2.1 Behavior of the Retinal Tissue under Short-Term Shear Stress

In order to study the behavior of the retinal tissue under short-term shear stress a new set-up was designed as introduced in section 3.3.2. The setup is composed of a confocal microscope equipped with a motorized stage and a micromanipulator with the task of moving a ceramic rod towards the specimen. The sample employed consisted of isolated adult guinea pig retina (see Section 3.1.2). Handling the retinal tissue carefully was essential to avoid any alterations of the sample that could have influenced its response to the mechanical shear stress applied. The explant was thoroughly attached to a cellulose membrane (filter) with the photoreceptor cells side-down. To ensure that the coupling was uniform, the filter was briefly positioned on a paper towel allowing a strong adhesion of the retina due to the temporary absorption of the solution in excess. The retinal tissue was transferred in the PDMS chamber after having precisely been cut in slices and being stained with the vital dye MitoTracker Orange (see Section 3.1.4). The filter with the retinal piece attached was clamped to the chamber enabling the visualization of the retinal cross-section under the microscope (see Figure 4.9). The chamber was filled with physiological solution (see Table 3.1) to ensure the best conditions for the tissue survival and was positioned on top of the stage of the confocal microscope. As a result of the staining, it was possible to clearly identify the retinal slice and the filter to which the retina was attached. Another piece of filter stained with the same vital dye and glued to the ceramic rod was carefully approached to the retina from the other side (ganglion cells and Müller cell endfoot side). In this way the retinal slice was attached from both sides, to two separate pieces of the same filter material (see Figure 4.9).

The attachment of the second piece of filter to the retinal slice was the most delicate and critical step in this procedure. A large number of tests were performed before establishing the correct technique to guarantee that the retinal slices were not subjected to unnecessary
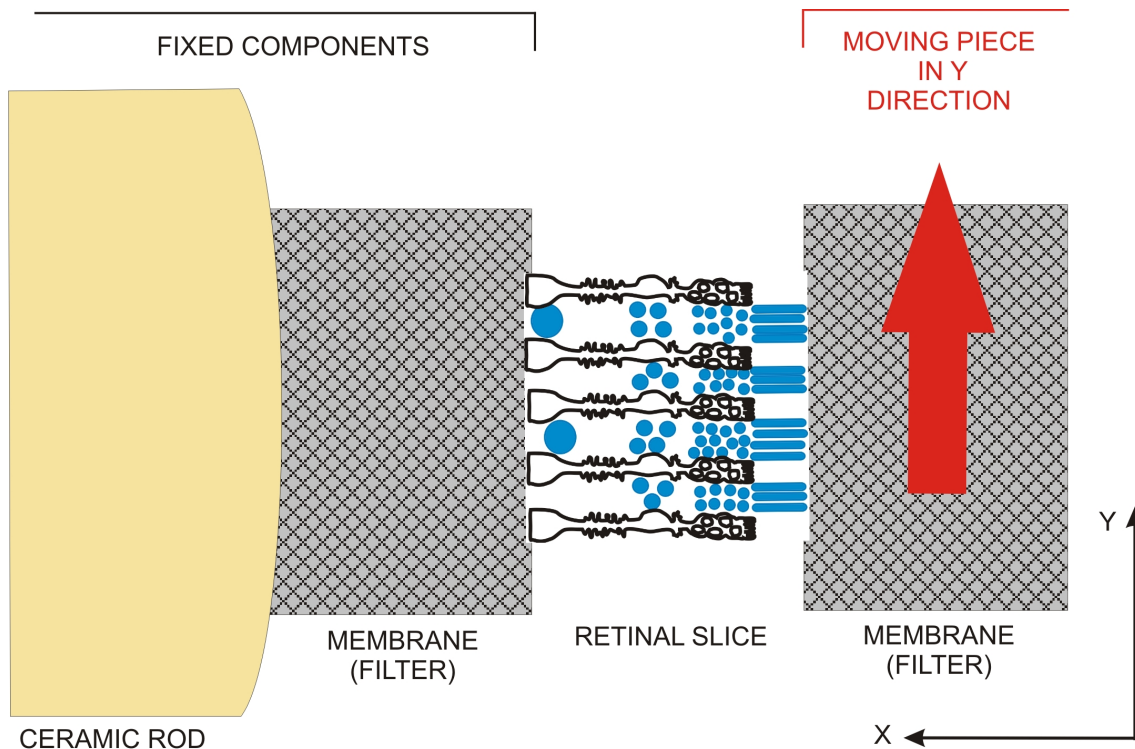
Figure 4.9: Schematic drawing of the set-up for short-term shear stress experiment. The retinal slice is trapped between two pieces of cellulose membrane (filter). One piece of filter is glued to the extremity of a ceramic rod (left) and the other is clamped to the chamber (right) (see Figure 3.9). The latter is moved in y-direction applying shear stress to the retinal slice. The Müller cells, the ganglion cell nuclei (big blue circles), the interneuron nuclei (medium blue circles), the photoreceptor nuclei (small blue circles) and the photoreceptor segments were highlighted in the retinal slice.

stress and that the attachment was correct. The advantage of using a confocal microscope was the possibility to obtain an high-resolution image and a z-section of the sample. Using the stack function of the confocal microscope it could be achieved to visualize exactly the area of the retinal tissue where the shear stress was applied. The confocal microscope was equipped with a motorized stage which moved the chamber and consequently the filter clamped to the chamber. In this way, the retinal slice was subjected to a controlled shear stress caused by the movement of the filter attached to the photoreceptor cell side. The entity of the movement was regulated by a customized Labview program. The motorized stage was moved with constant step sizes that were varying between $3\,\mu$m and $20\,\mu$m per minute depending on the experiment. Considering that the retinal explant survives up to 3 hours in solution at room temperature, the duration of the experiment was compatible with the time necessary to maintain an healthy retina.

The choice of using the MitoTracker orange, as a vital dye, was dictated by the fact that this dye, when used in the retinal tissue, clearly highlights the Müller cells. The retinal radial glial cells are a good indicator of the behavior of the layers since they span the entire thickness of the retina. In addition, the photoreceptor cells were visible under the fluorescent light because of their autofluorescence.

Observing the retinal cross-section, various zones were discernible because of the staining. The Müller cells and the photoreceptors together define the entire tissue thickness which can also be seen as the distance between the two filters at the initial conditions ($t = 0$). The Müller cells and the photoreceptors were considered separately as the indicator of the different layers that they span. The Müller cells were clearly visualized in their entirety and the photoreceptors were recognized by their outer segment layer attached to the filter. The Müller cells represent, compared to the photoreceptor cells, different retinal layers: ganglion cell layer, inner plexiform layer, inner nuclear layer, outer plexiform layer and outer nuclear layer. Instead the photoreceptors are the indicator only of the photoreceptors layer. When solely the Müller cells were taken into account, the analysis focused on comparing their inner part and their outer part.

For the analysis of the retinal tissue four points were used to extract the data: (1) the end-feet of the Müller cells, (2) the nucleus of the Müller cells, (3) the distal point (microvilli) of the Müller cells and (4) the distal point of the photoreceptor cell outer segment (see Figure 4.10 a).

In the analysis different types of strain were calculated to study the morphological alterations of the retinal tissue under shear stress caused by the movement of the microscopy stage. In general, the mechanical strain is defined with a mathematical expression of the shape changes resulting from experimental mechanical stresses (see Section 2.2.1). In the case of applied shear stress, the resulting shear strain was calculated as the tangent of the angle that the sheared element forms with its original orientation, depending on the time. The formula used, for example, to estimate the individual shear strain of the Müller cell is as following:

$$\gamma = \left| \tan \left[\arctan \left(\frac{y_3 - y_1}{x_3 - x_1} \right)_t - \arctan \left(\frac{y_3 - y_1}{x_3 - x_1} \right)_{t=0} \right] \right| \tag{4.1}$$

with the numbers referring to the different points: (1) Müller cell endfeet and (3) Müller cell distal point as shown in Figure 4.10 b. The absolute value was used to consider any shear stress applied independently by the direction. Although the retinal tissue was well attached to the cellulose membrane at both sides, during the experiment a slippage of the sample (at the ganglion cell side) was observed. To minimize errors arising from the shifting retina, the angle was measured observing each frame individually.
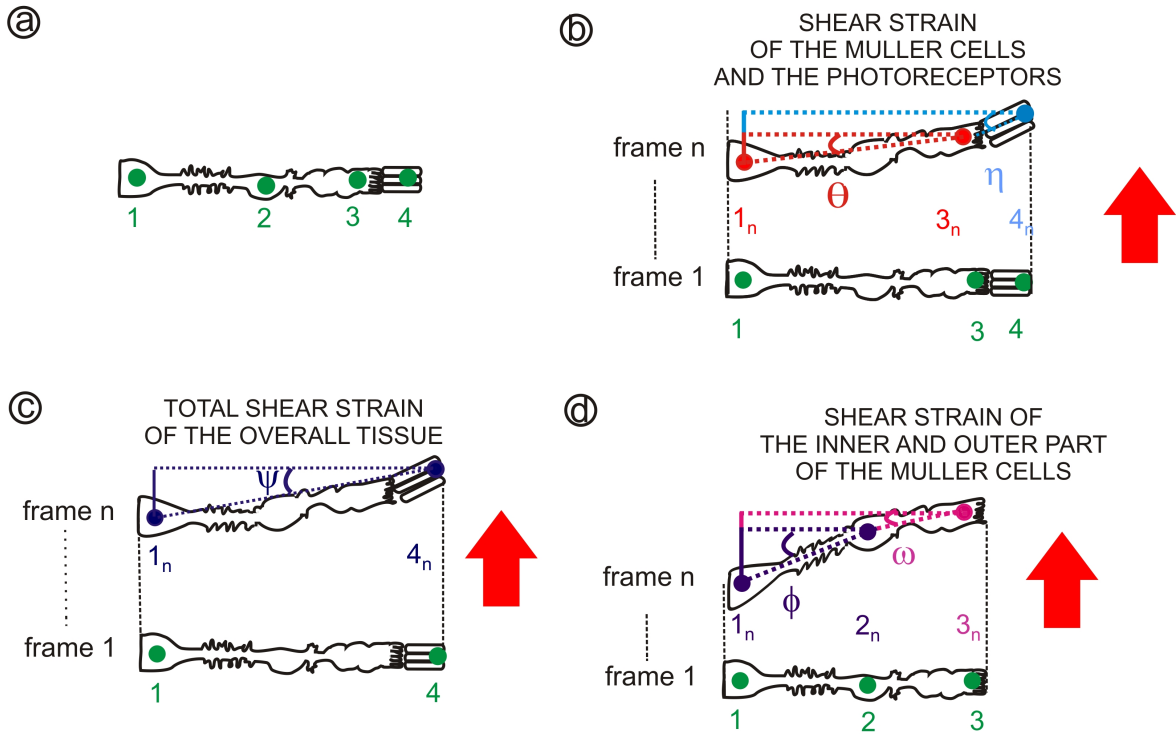
Figure 4.10: Schematic drawing illustrating the calculations. (a) In each figure, point *1* indicates the Müller cell end foot, point *2* the Müller cell nucleus, point *3* the distal part of the Müller cell and point *4* the photoreceptor outer segment. (b) The shear strain of the individual element of the tissue is calculated always referring to the frame of the considered elements. The individual elements considered are the Müller cell segment (red) and the photoreceptor cell segment (blue). The angles θ and η indicate the bending of the Müller cells and of the outer segment of the photoreceptors, respectively. (c) To calculate the shear strain considering the slipping of the tissue, the angle is measured directly referring to the frame-n. The angle ψ indicates the bending of the entire tissue. (d) To compare the behavior of the inner and outer part of the Müller cell, the photoreceptor outer segment (point *4*) was neglected. The angles ϕ and ω indicate the bending of the Müller cells and of the outer segment of the photoreceptors, respectively. The red arrow indicates the direction of the shear stress applied.

The tangent was calculated considering the angle formed by the line connecting the points of the specific segment analyzed in that particular frame and the line perpendicular to the shear stress applied (red arrow) passing through the distal point of the segment. To be more specific, the angles θ, η, ψ, ϕ and ω indicated the bending of the Müller cells, of the outer segment of the photoreceptors, of the entire tissue, of the inner and outer processes of the Müller cells, respectively (see Figure 4.10). The point *1* and *4*, corresponding to the endfeet of the Müller cells and to the outer segment of the photoreceptors, respectively, were considered for the evaluation of the shear strain of the entire tissue named total shear strain (γ_T) (see Figures 4.10 c).

The method was identical for the calculation of the individual shear strain (γ_I) for Müller cells (red) and photoreceptor cells (blue) (see Figures 4.10 b); and for the evaluation of the shear strain of the inner part (violet) and outer part (pink) of the Müller cells (see Figure 4.10 d).
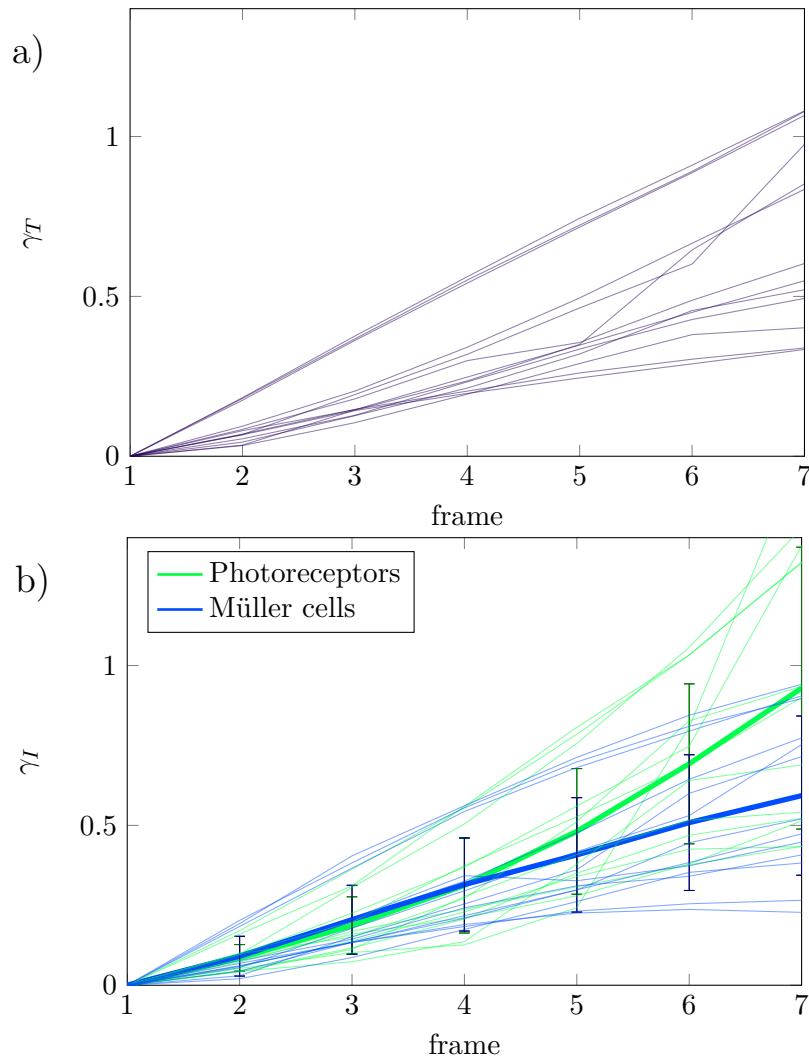
Figure 4.11: Shear strain depending on time. (a) Shear strain of the entire retinal tissue, called total shear strain (γ_T). (b) Individual shear strain (γ_I) for the Müller cell segments and outer photoreceptor segments. Each frame is taken every minute when the motorized stage moves 20 μm applying shear stress to the retinal slice. The thick lines are the averaged curves of the respective tissue part and the error bars are the standard deviation of the average.

First γ_T and γ_I were calculated for each frame (see Figure 4.11) giving an overview of the dependency of the strain with the time. These graphs do not have a physical meaning since the samples are living tissue acting slightly differently in each experiment, but they help to

understand the calculation. Therefore, each individual shear strain was normalized to the total shear strain (see Figure 4.12). The retinal tissue did not respond uniformly when a shear stress was applied. In fact, the Müller cells and the photoreceptor cells, representing distinct retinal layers, demonstrated different individual shear strain values starting from a critical total shear strain point. This critical value was defined as the minimal shear strain of the entire tissue that could cause the detachment of the retina from the membrane. It was calculated around 0.25 considering the slippage phenomenon.
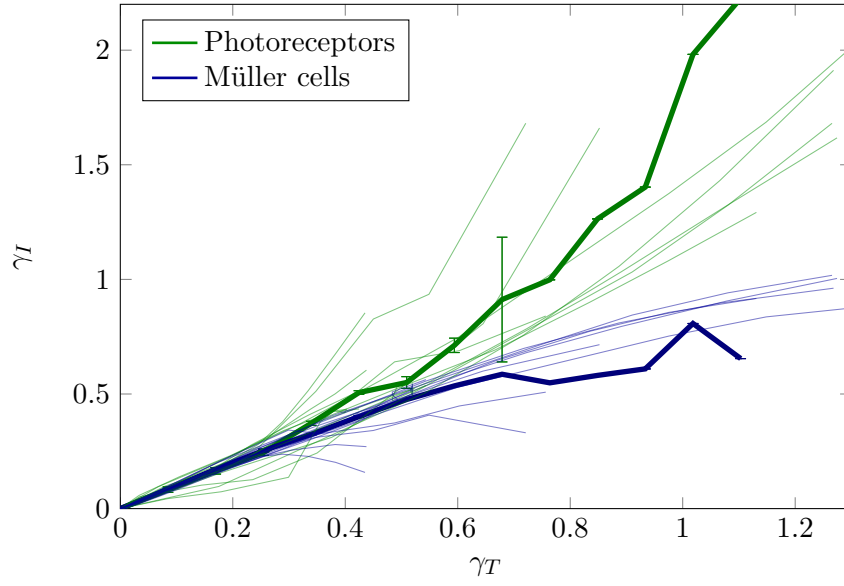
Figure 4.12: Shear strain of the Müller cells and the photoreceptor cells considering the slippage of the tissue along the filter at the photoreceptor side. The individual shear strain ($\gamma_I = individual\ shear\ strain$) was normalized to the total shear strain ($\gamma_T = total\ shear\ strain$). The graph shows a critical shear strain value around 0.25. This point can be interpreted as the minimal shear strain value from which the detachment of the retinal tissue from the filter can happen. The thick lines are the averaged curves of the respective tissue part and the error bars are the standard deviation of the average. Each thin lines show the shear strain of the individual segments considered for the calculation.

To calculate the shear strain it was necessary to first calculate the angular shear strain that is by definition the angle formed by the element after the shear and the element at its original position. The angular shear strain of the entire tissue considering the slippage phenomenon was calculated as following:

$$\gamma_\alpha = \left| \arctan \left(\frac{y_4 - y_1}{x_4 - x_1} \right)_t - \arctan \left(\frac{y_4 - y_1}{x_4 - x_1} \right)_{t=0} \right| \tag{4.2}$$

with the numbers referring to the different points (1) Müller cell endfeet and (4) photoreceptor cell outer segment as shown in Figure 4.10 c. The individual angular shear strain

normalized to the total angular shear strain highlighted the value of 15° as the maximal angle before the detachment of the retinal tissue from the filter could occur (see Figure 4.13).
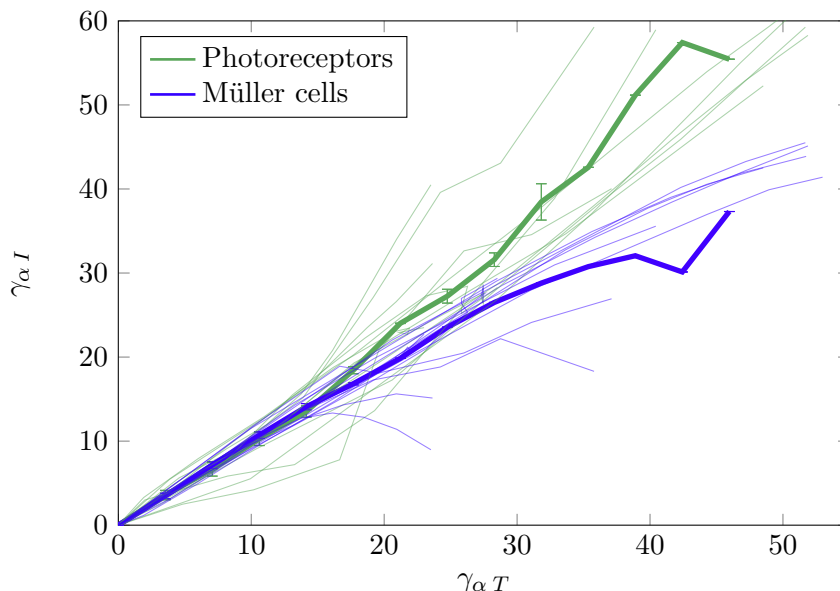
Figure 4.13: Angular shear strain of the Müller cells and the photoreceptors cells considering the slippage phenomenon. The individual angular shear strain ($\gamma_{\alpha\ I}$) was normalized to the total angular shear strain ($\gamma_{\alpha\ T}$). A critical angle value around 15° was observed as minimal value for the detachment of the retinal tissue from the filter. The thick lines are the averaged curves of the respective tissue part and the error bars are the standard deviation of the average. Each thin lines show the angular shear strain of the individual segments considered for the calculation.

The five retinal layers held together by the Müller cells seemed to resist more when a shear stress was applied showing a minimal deformation. In fact the angle between the Müller cells and the photoreceptors increases (see Figure 4.14) displaying an extensive reaction of the photoreceptors cells to the shear stress.

In addition to a deformation of the specimen in the parallel direction of the force exercised, an alteration of the morphology across to the retinal tissue, as an indirect effect of the shear stress applied, was observed.

In this case, it was more appropriate talking about axial/normal strain defined as the ratio of the displacement divided by reference length (see Section 2.2.1). In particular, the evaluation of this strain was made using the equation 2.4. It was calculated first over time (see Figure 4.15) and then was normalized to the total shear strain (see Figure 4.16). At the critical point of 0.25 total shear strain observed previously, the axial/normal strain of the Müller cells and the photoreceptor cells was shown to have a different trend highlighting a distinctive behavior of these two part of the retina tissue. The retinal radial
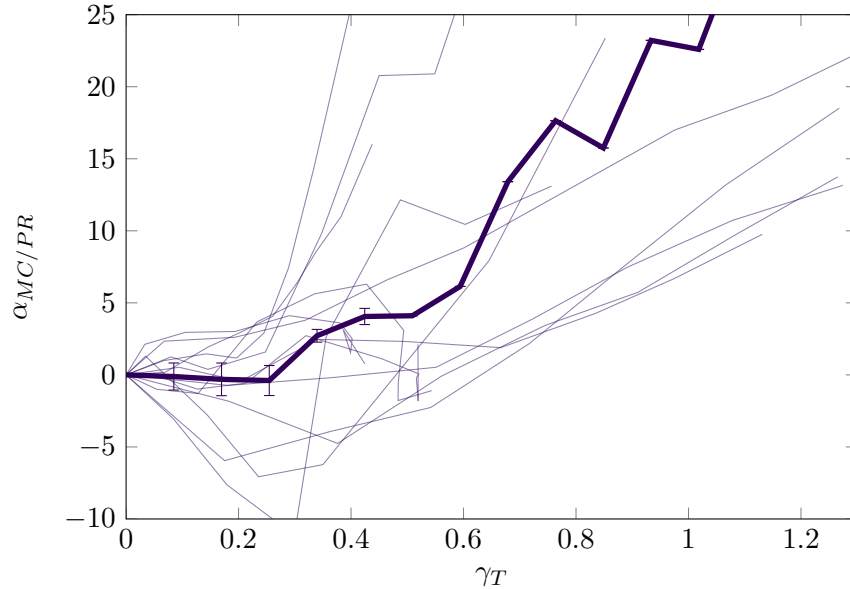
Figure 4.14: Angle between Müller cell segment and photoreceptor cell outer segment corrected for the slippage phenomenon. The angle remains zero until the shear strain value of 0.25. For $\gamma_T > 0.25$, the angle increases rapidly. That indicates that the Müller cells and photoreceptor cells react to the shear stress as a unit until a certain value of the shear strain. The behavior change probably arises from the detachment. The thick lines are the averaged curves of the angle between Müller cell segment and photoreceptor cell outer segment. The error bars are the standard deviation of the average. Each thin lines show the angle between Müller cell segment and photoreceptor cell outer segment of the individual segments considered for the calculation. $\alpha_{MC/PR} = $ *angle between Müller cells (MC) and photoreceptors (PR)*; $\gamma_T = $ *total shear strain.*

glial cells tended to maintain their strain almost constant demonstrating more resistance to deformation. On the contrary, the photoreceptors increased their strain linearly until the point they detached from the filter.

Focusing only on the measurements of the shear strain of the inner and outer part of the Müller cells, it was shown that the inner retina identified by the proximal part of the retinal radial glial cells reacted robustly to the shear stress applied, bending more compared to the outer part, represented by the pouter processes of the Müller cells (see Figure 4.17).

The ratio between the shear strain of inner and outer part the retina increases linearly and assumes the value of $1.2 - 1.25$ when it reaches a plateau at a total shear strain of around 0.4 near the minimum value of the total shear strain for the tissue detachment (see Figure 4.18).

These data are in accordance with the results obtained by stiffness measurements of the different retinal layers using an atomic force microscope (AFM). Freshly isolated guinea pig retina was embedded in agarose and sectioned in 400 μm thick slices. Using beads of 37 μm diameter that were attached to the cantilever and gave contact area of $5 - 10$ μm

and an indentation depth of 3 μm, it was possible to estimate the apparent elastic modulus $K = E/(1 - \nu^2)$ for each retinal layer. Here, E is the Young's modulus and ν the Poisson's ratio. Grouping the layer according to the division between inner and outer part of the Müller cells, the GCL and IPL represent the proximal part of the retina radial glia cells and the OPL, ONL and ROS approximately exemplify the distal segment of these cells. The apparent modulus estimated by AFM measurements resulted in 151 and 195, with a standard deviation of 130 and 160 and a standard error of 20 and 11, respectively. The ratio between the apparent modulus of the inner layer and the outer layers resulted 0.72. Assuming the shear stress applied to the retina to be constant for each area, the strain between the inner and outer part proves to be 1. The ratio between the inner and outer layers as defined previously resulted 0.72 giving a shear ratio around of 1.39. This is approximately the same value estimated in the shear stress experiments assuming a steady state (i.e. when the strain does not increase anymore with increasing of the total strain).
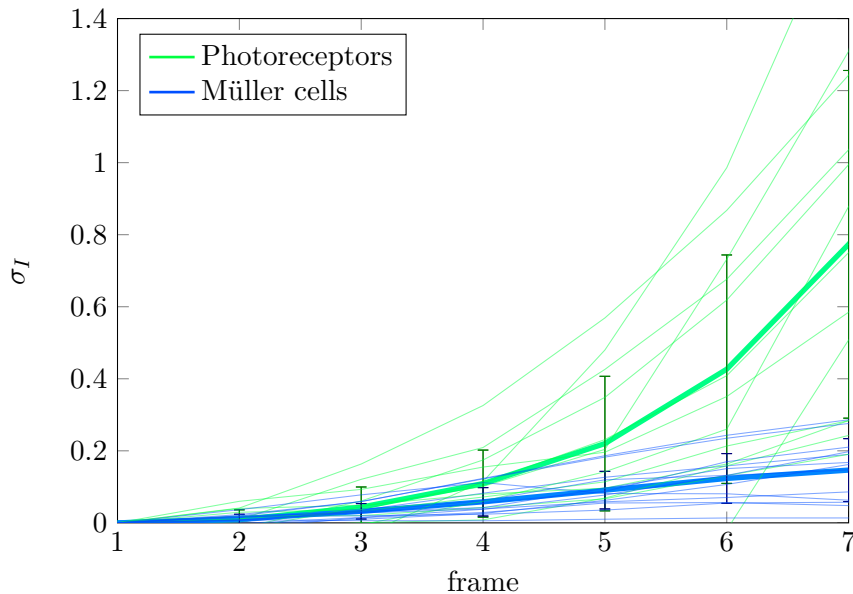
Figure 4.15: Strain of the Müller cell segment and outer photoreceptor segments depending on the time. In average, after the third frame the behavior of the individual segments changed. Each frame is taken every minute when the motorized stage moves 20 μm applying shear stress to the retinal slice. The photoreceptor outer segment shown a linear elongation until detachment, whereas the Müller cells maintain an almost constant strain. The thick lines are the averaged curves of the respective tissue part and the error bars are the standard deviation of the average. Each thin lines show the strain of the individual segments considered for the calculation in each frame. $\sigma_I = individual\ strain$.
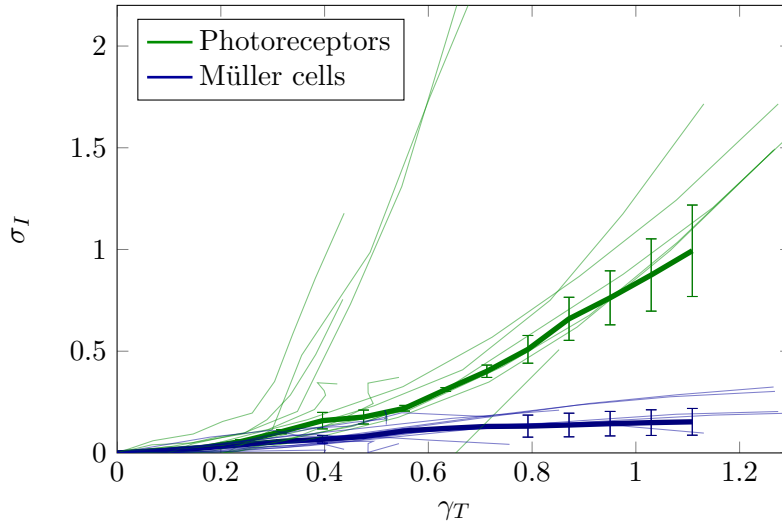
Figure 4.16: Strain of the Müller cells and the photoreceptors cells normalized to the total shear strain considering the slippage along the filter. The graph shows that the photoreceptor cells elongated more compared to the Müller cells, meaning that they are less resistant to the shear stress. The shear strain value of 0.25 is critical also when the axial/normal strain is investigated. At this point the behavior of the Müller cells and the photoreceptors cells changes. On one hand the retinal radial glial cells maintain an almost constant strain, on the other hand the photoreceptors react to the shear stress linearly increasing their length until detachment. The thick lines are the averaged curves of the respective tissue part and the error bars are the standard deviation of the average. Each thin lines show the strain of the individual segments considered for the calculation. $\sigma_I = individual\ strain$; $\gamma_T = total\ shear\ strain$.
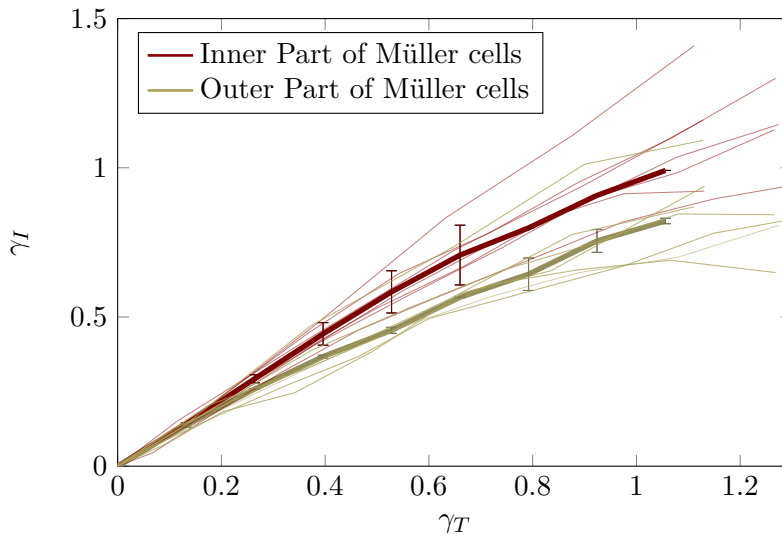
Figure 4.17: Shear strain of the inner and outer part of the Müller cells. The inner part of the retinal radial glial cells results to respond more decisively to the shear stress applied than the outer part. The bending of the inner part is more evident. Probably this is due the retinal morphology and not to the greater elasticity properties of the inner part of the retinal tissue. The individual shear strain is always normalized to the total shear strain. The thick lines are the averaged curves of the inner and outer part of the Müller cells. The error bars are the standard deviation of the average. Each thin lines show the shear strain of the individual segments considered for the calculation. $\gamma_T = total\ shear\ strain$; $\gamma_I = individual\ shear\ strain$.

77
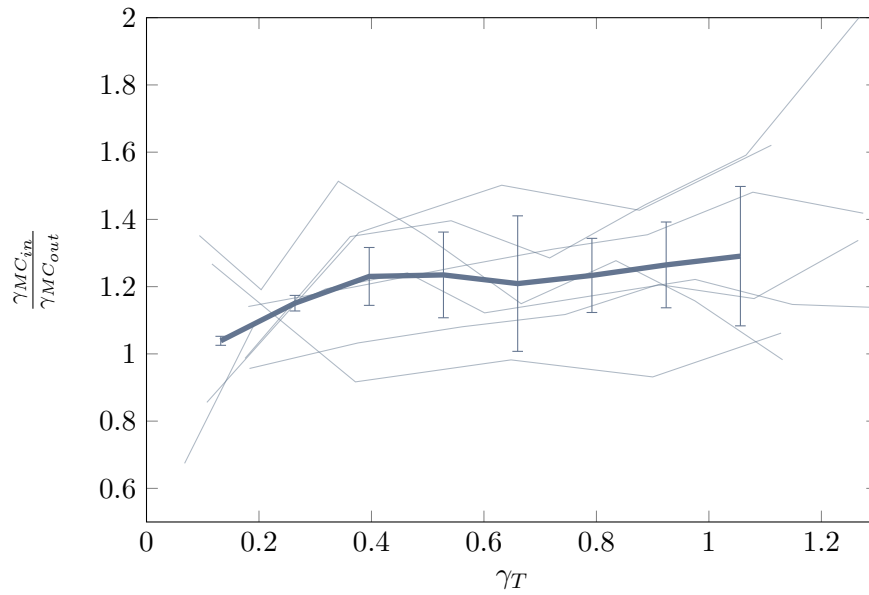
Figure 4.18: Ratio between the shear strain of the inner part and the outer part of the Müller cells normalized to the total shear strain. The ratio increases linearly until it reaches a plateau around 1.2 at approximately the total shear strain value of 0.25. The thick lines are the averaged curves of ration of the inner and outer part of the Müller cells. The error bars are the standard deviation of the average. Each thin lines show the ratio of the individual segments considered for the calculation normalized to the total shear strain. $MC_{in} = inner\ process\ of\ the\ Müller\ cells, MC_{out} = outer\ process\ of\ the\ Müller\ cells$.

When the slippage of the retinal tissue is not considered in the calculation

To evaluate the influence of the slippage phenomenon on the response of retinal tissue to the shear stress applied, the angle used to calculate the shear strain as tangent, it was estimated referring always to the first frame at time equal zero (see Figure 4.19). In this case, the shear strain of the entire retinal tissue was called total applied shear strain (see Figure 4.20).
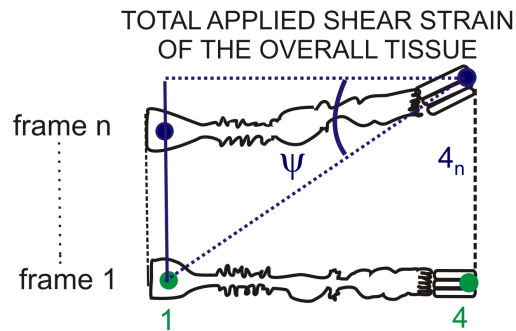
Figure 4.19: Schematic drawing of the calculation. Explanation of the calculation of the total applied shear strain of the entire tissue without considering the slippage. The angle ψ indicates the bending of the entire tissue referring to the first frame.
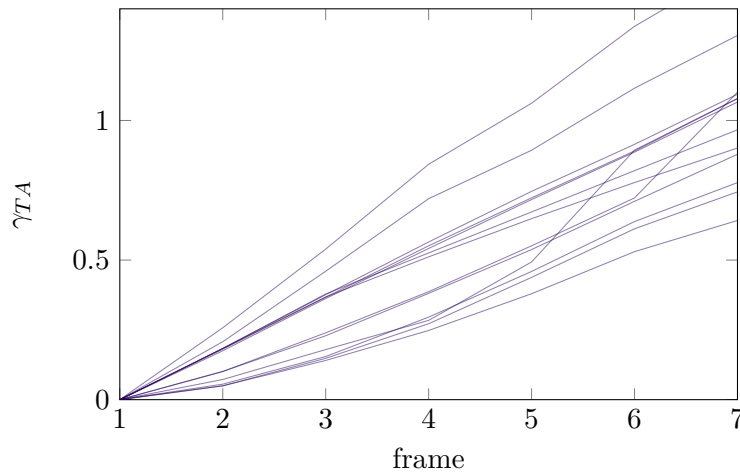
Figure 4.20: Shear strain of the entire retinal tissue depending on the time. Each frame is taken every minute when the motorized stage moves 20 μm applying shear stress to the retinal slice. The thick lines are the averaged curves of the respective tissue part and the error bars are the standard deviation of the average at different time. $\gamma_{TA} = total\ applied\ shear\ strain$.

Surprisingly, the retinal tissue reacted to the applied shear stress without being influenced on large scale by this phenomenon. In fact, without taking in account the shifting of the retinal tissue along the membrane at the Müller cell endfoot side, a critical point was

estimated to be 0.35, very closed to the value observed in the previous case (0.25)(see Figure 4.21).
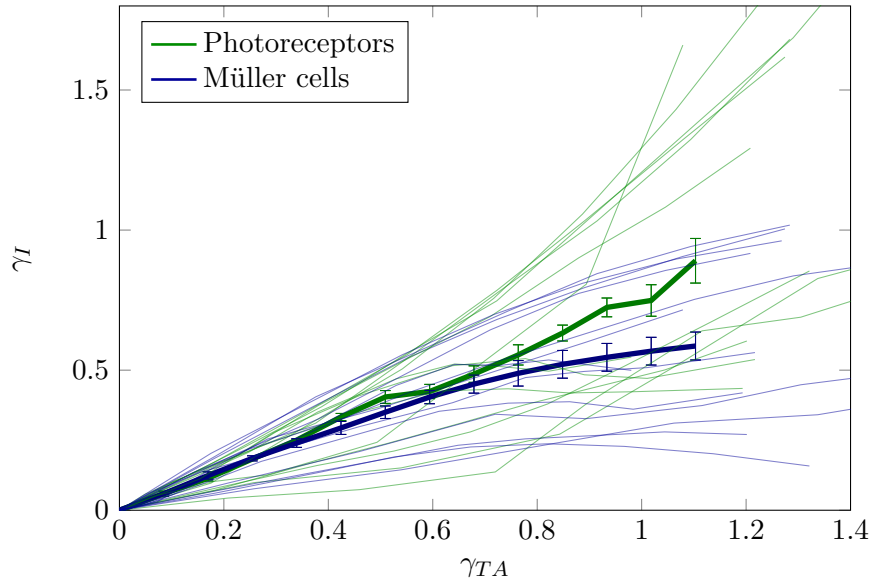
Figure 4.21: Shear strain of the Müller cells and the photoreceptors cells. The slipping of the tissue along the membrane was not considered. In this case, the critical shear strain value which induces detachment, was calculated to be around 0.35. The critical total shear strain values when considering or not the slippage, are very similar showing that the retinal tissue reacts to the shear stress applied without being influenced on the large scale by this phenomenon. The thick lines are the averaged curves of the respective tissue part and the error bars are the standard deviation of the average. Each thin lines show the shear strain of the individual segments considered for the calculation. $\gamma_{TA} = $ *total applied shear strain*; $\gamma_I = $ *individual shear strain*.

From a point of view of the angle, the results were comparable. The individual angular shear strains, normalized by the angular shear strain of the entire tissue, shown the same trend until the value of 15.5°(see Figure 4.22). The same behavior was observed when considering the slippage since the critical angle was measured to be 15°.

Calculation of the individual strain normalized by the total applied shear strain showed that starting from the critical total applied shear strain point of 0.35 the photoreceptor cells presented a more elastic behavior compared to the Müller cells (see Figure 4.24).

The angle formed between the Müller cells and the photoreceptor cells during the shear stress experiment oscillated around the zero until it increased linearly at the total shear strain of 0.5 without taking into account the shifting of the retinal tissue (see Figure 4.23). As previously explained the photoreceptor layer bent more showing the effect of the shear stress more relevant on this layer.
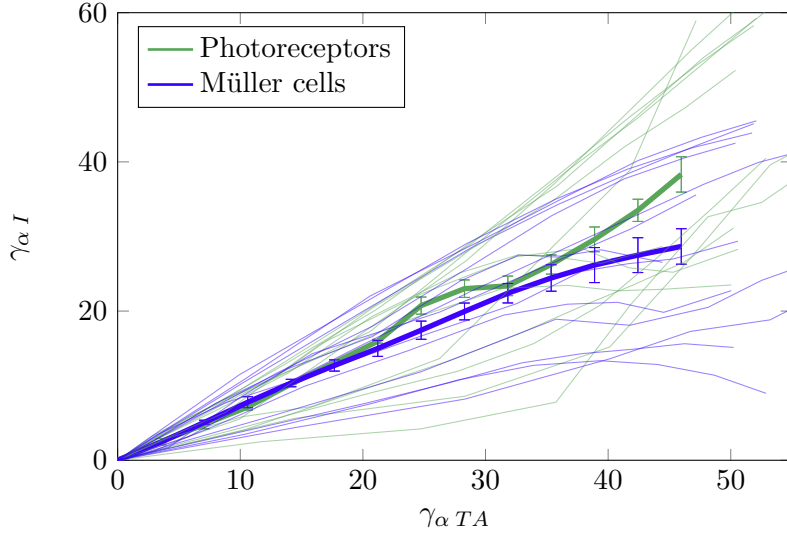
Figure 4.22: Angular shear strain of the Müller cells and the photoreceptors cells calculated without considering the slippage. As shown previously, the retinal response to the shear stress applied is not influenced in large scale by the shifting of the tissue. The critical angle value for the detachment of the retinal tissue from the membrane, was observed to be around 15.5°. This value resulted to be very similar to the value estimated considering the slipping of the tissue along the membrane. The thick lines are the averaged curves of the respective tissue part and the error bars are the standard deviation of the average. $\gamma_{\alpha I} = $ *individual angular shear strain*, $\gamma_{\alpha TA} = $ *total applied angular shear strain*.
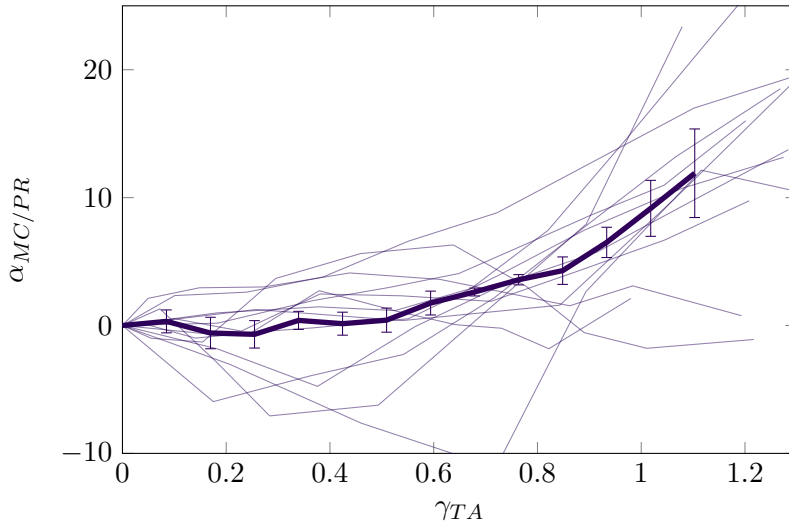
Figure 4.23: Angle between Müller cells and photoreceptor cells without considering the slippage phenomenon. The angle fluctuates around zero until it increases linearly at a shear strain value of 0.5. The thick lines are the averaged curves of the angle between Müller cell segment and photoreceptor cell outer segment. The error bars are the standard deviation of the average. Each thin lines show the angle between Müller cell segment and photoreceptor cell outer segment of the individual segments considered for the calculation, normalized to the total applied shear strain. $\alpha_{MC/PR} = $ *angle between Müller cells (MC) and photoreceptors (PR)*; $\gamma_{TA} = $ *total applied shear strain*.
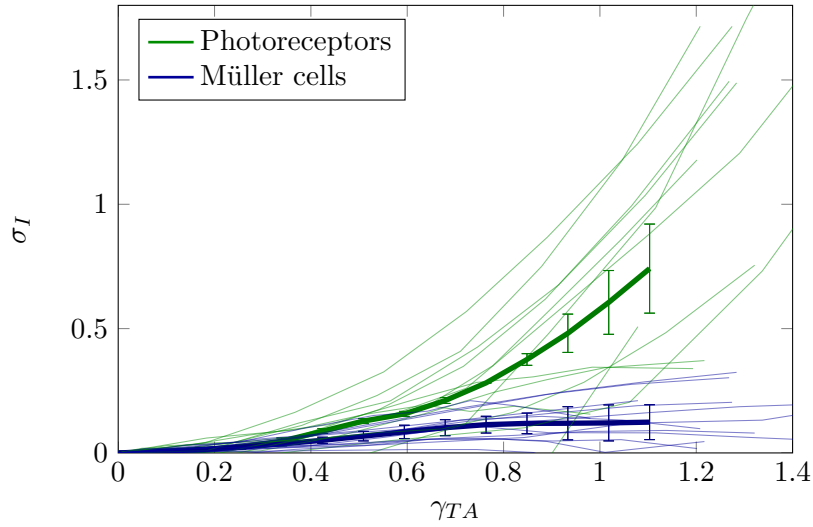
Figure 4.24: Strain of the Müller cell segments and the photoreceptor cell segment without considering the slippage phenomenon. The results are comparable to the other analysis (see figure 4.16). The photoreceptors shown a more elastic behavior compared to the Müller cells. Their behavior starts differentiating from a shear strain value of around 0.35. The thick lines are the averaged curves of the respective tissue part and the error bars are the standard deviation of the average. Each thin lines show the strain of the individual segments considered for the calculation normalized to the total applied angular shear strain. $\sigma_I = individual\ strain$; $\gamma_{TA} = total\ applied\ shear\ strain$.

In summary one can say that during this type of experiments two distinctive phenomena were observed: (i) the detachment of the retinal tissue from the cellulose filter at the photoreceptor cell side (see Figure 4.25) and (ii) the different bending of the inner and outer part of the Müller cells (see Figure 4.26). The observation of these phenomena provides new information on the response of the retinal tissue to an applied shear stress.
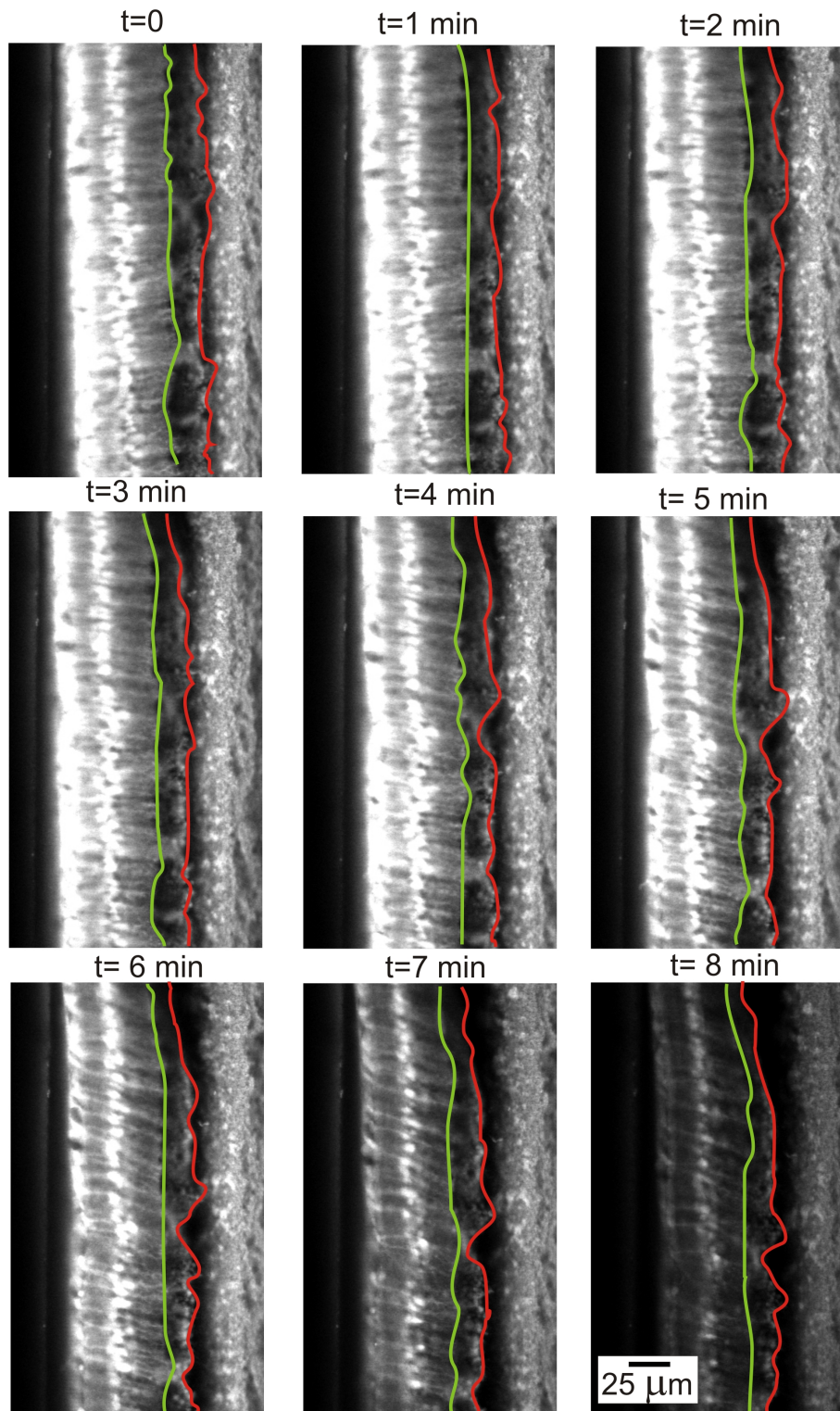
Figure 4.25: Short-term shear stress experiment highlighting the retina detachment. The green line points out the outer limiting membrane. Furthermore it indicates the distal part of the Müller cells. The red line marks the distal part of the photoreceptor cell outer segment and follows the detachment of the retinal from the membrane/filter.
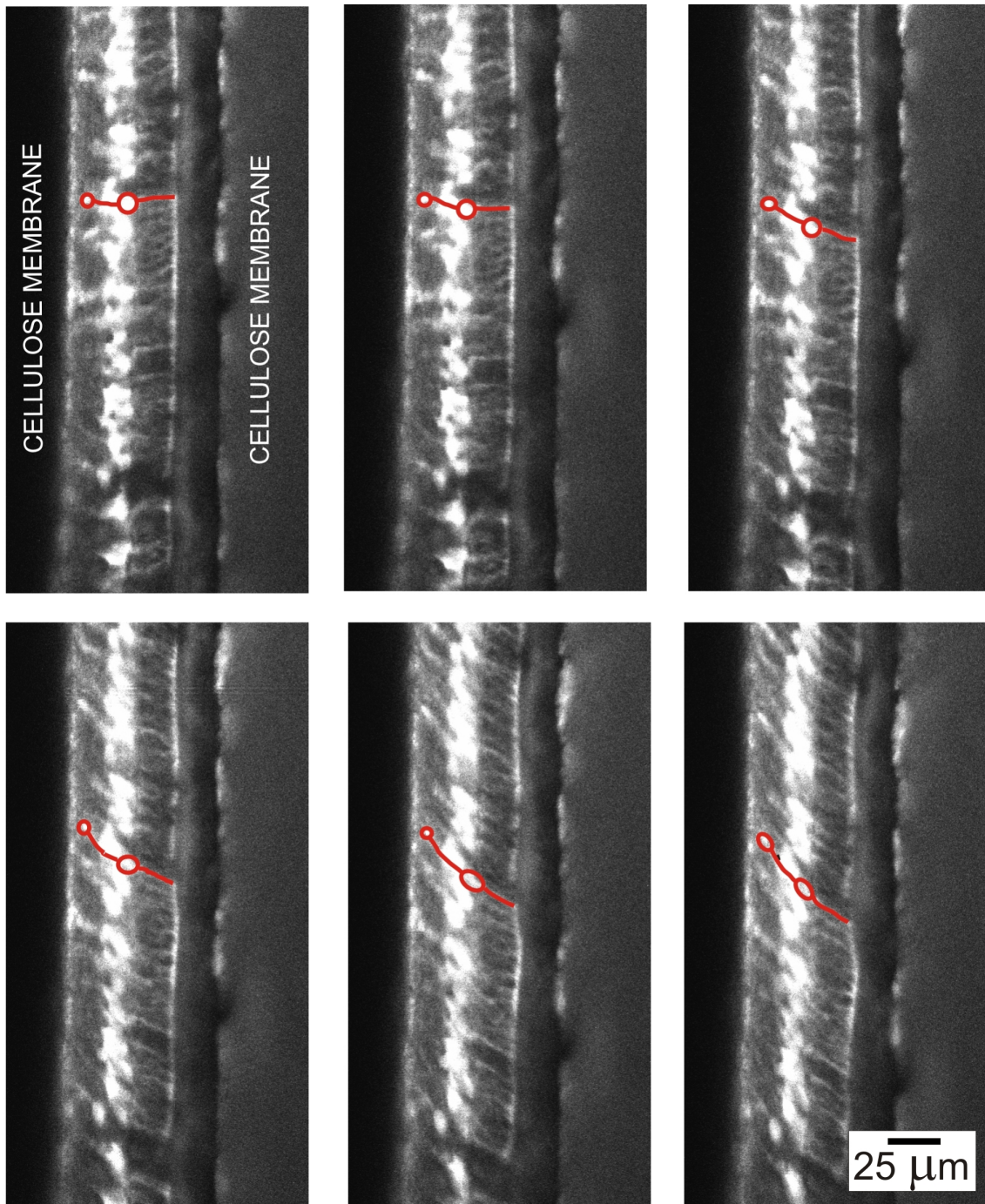
Figure 4.26: Short-term shear stress experiment highlighting the bending of the Müller cells. The red lines mark the inner (left) and outer (right) processes of the retinal radial cells. Instead the left circle locates the endfoot and the right circle the nucleus. The bending of the inner process is slightly more noticeble.

5 Discussion

In the following, the significance of the experimental results will be discussed. Firstly, I will elucidate the importance to study the tissue rather than a single cell; and I will emphasize the necessity to establish an organotypic culture for adult neural tissue. Additionally, the properties of TiO_2 nanotube arrays as substrate for long-term tissue culture, will be reviewed. In the second part, the potential of two new set-ups for mechanical probing of living tissue will be presented. Furthermore, the response of the retinal tissue to short-term and long-term shear stress will be examined. Finally, the nearly lack of knowledge regarding the mechanical properties of the retinal tissue together with the difficulty in gathering this information with the goal to understand retinal mechanisms such as retinal detachment or fovea development will be discussed.

5.1 A New Method for Long-Term Organotypic Culture of Neural Tissue

Cells are the smallest units of life. To give an idea of the complexity of the human body, the amount of human cells has been compared to the stars present in the universe. Indeed, the number of cells in each human organism have been estimated around $37400 \; x \; 10^{11}$ (Bianconi et al., 2013). This quantity is higher than the number of stars estimated to be present in the Milky Way ($4 \; x \; 10^{11}$). Focusing the attention on the vertebrate central nervous system (CNS) the number are remarkable. Roughly 100 billion (10^{11}) neurons and 2 to 10 times more glial cells populate the CNS (Kandel and Schwartz, 2013).

In nature, cells are not randomly clustered to form tissues. The tissue is a more complicated system composed of blood vessels, different types of cells with specific functions, and extracellular matrix filling the space in between cells. The functions of tissues go beyond what any single cell type could accomplish. In scientific research it is common practice to investigate single cells or conglomerate of cells in $2D$ (Vunjak-Novakovic and Freshney, 2006) and $3D$ culture environment (Abbott, 2003; Langer and Tirrell, 2004; Lavik and Langer, 2004; Lee et al., 2008). On the one hand, these are simplification of the *in vivo* model which can be useful for a basic study; on the other hand, this approach makes loses, or fails to gather information about the tissue. Animal physiology cannot be completely

reproduced and spatial-temporal organization are not maintained in these systems. Many biological responses such as receptor expression, transcriptional expression, cellular migration and apoptosis are altered (Haycock, 2011). In the central nervous system (CNS) tissue has a complex cytoarchitecture and organization with a very diverse cell population (Morrison et al., 2011). Therefore, in studying dissociated cells, we are loosing soma shape, neurite branching and glial-neuronal interaction.

The demand for *in vitro* models which can replace or reduce animal experiments is incessant. The animal testing has always been cross-examined for ethical reasons and for the high cost. For example, in drug screening to completely understand the mechanics of a particular compound usually only one animal is employed per drug, making the process long and expensive. In neuroscience, cell and tissue culture techniques can contribute in the understanding of physiological and biological mechanism involving the central nervous system, including biochemical and pharmacological investigations, mechanical stimulation and injury (Morrison et al., 2011). The common method for cell culture uses hard plastic or glass substrates that are not really representative of cellular environment found *in vivo* (Pampaloni et al., 2007). In the tissue culture called organotypic, the explanted tissues can be directly cultured without being dissociated into a suspension of single cells. This technology is a powerful tool allowing researchers to maintain with high accuracy the complex multicellular anatomy and the microenvironment of the original tissue (Sundstrom et al., 2005 Morrison et al., 2011). Unlike cell culture, organotypic tissue culture can preserve interregional cell connectivity, vascular coupling, allowing the study of long-term plasticity, and analyzing the long-term reactions to drugs and pathological conditions on the structure and function of the tissue (Gähwiler et al., 1997). Although organotypic cultures have certain limitations, they represent an efficient way to address many cellular and molecular mechanisms (Daviaud et al., 2013).

One of the limitations of the organotypic culture techniques has until recently been due to the ability to use only post-natal/juvenile tissues for long-term culture (Morrison et al., 2011). A cause of the reduced stability of the mature tissue after trauma or culturing procedure and the higher metabolic functions of the adult cells, the majority of the studies in neuroscience research are made on embryonic or neonatal neural tissue. In this stage, the animal cells are still developing, although they show an excellent vitality they cannot be used as a model for the fully differentiated adult tissue. For diseases that occur later, like Alzheimer or macular degeneration, it is not possible to have accurate experiments just probing young animals. The adult tissue has less resistance and weaker neuronal plasticity but it is in mature age when the majority of neurological diseases appear. (Daviaud et al., 2013).

The decision to focus on the neurosensory retina was dictated by the fact that is a very

convenient model for the central nervous system. Indeed, in neuroscience research the retina, as extension of the brain, is largely used because its accessibility. Furthermore the possibility of isolating and studying the entire tissue in comparison with the brain that has to be cut in slices for research purposes, is an advantage (London et al., 2013).

The organotypic culture of retinal tissue has been employed to study mechanisms of retinal injury and degenerative diseases (Wang et al., 2011), retinal development (Johnson and Martin, 2008, Wang et al., 2002b, Zhang et al., 2002, Mack et al., 2003), CNS regeneration (Gogia and Schneeweis, 2004, Leaver et al., 2006, Koriyama et al., 2007, Homma et al., 2007), cell death and neuroprotection (Manabe et al., 2002, McKernan et al., 2006, Xin et al., 2007), electrophysiology recording (Koizumi et al., 2007), genetic modification (Hatakeyama and Kageyama, 2002, Donovan and Dyer, 2007) and cell transplantation (Akagi et al., 2005, Liljekvist-Larsson and Johansson, 2005).

The majority of these studies are made on post-natal or juvenile retinas (Ogilvie et al., 1999; Pinzón-Duarte et al., 2000; Caffé et al., 2001) because of the limited survival of the adult neural tissue in culture, which mainly arises from the high-energy demands of the photoreceptor cells (Ames et al., 1992) and the decrease of plasticity of mature cells. In the past decades vision researchers from different laboratories have developed experiment-specific organotypic culture conditions for adult retinas. Koizumi et al. have maintained the adult retinal tissue in culture for up to six days (Koizumi et al., 2007; Lye et al., 2007). Kobuch et al. reached, with their perfusion system, 10 days culture, preparing the retinal tissue with the retinal pigment epithelium, a complicated procedure that requires special tools and constant monitoring (Kobuch et al., 2008). Kaempf et al. established another organotypic culture model using the mature retina with the RPE still attached testing only for 3 days (Kaempf et al., 2008; Johnson and Martin, 2008).

The necessity of establishing an efficient organotypic culture method for adult tissue that could allow mechanical probing has motivated this work. The interphase culture method introduced by Stoppini (Stoppini et al., 1991) is certainly a reliable and easy tool to culture the retinal tissue. The limitations of this system are observed in the survival of the adult tissue and the impossibility to apply mechanical stresses during the culture. The idea was to maintain the interphase technique and to replace the substrate in contact with the specimen. The cellulose filter commonly used favors the feeding but is not suitable for experiments involving mechanical stresses since it has the compactness of a wet piece of paper and cannot endure mechanical load without breaking. After testing substrate made of different materials, the titanium dioxide nanotubes arrays resulted to be the best membrane for this purpose. The first application of titanium and its alloys in biomedical field was as orthopedic or dental implants (40% of the implants in use are made of Ti) (Brammer et al., 2011; Long and Rack, 1998) due to their biocompatibility, strength, excellent corro-

sion resistance, drug eluting properties and high level of hemocompatibility (Rani et al., 2010). The *in vivo* and *in vitro* cellular response of osteoblasts, fibroblasts, chondrocytes, endothelial cells, epidermal keratocytes, vascular smooth muscle cells and mesenchymal stem cells on TiO_2 nanotube arrays were investigated by other scientific groups (Smith et al., 2011; Peng et al., 2009; Gongadze et al., 2013; Park et al., 2012; Laranjeira et al., 2013) (Huo et al., 2014). Although there are a numerous studies on cells interaction with TiO_2 nanotube arrays, nothing has been done at the tissue level. In the present research for the first time tissue, in particular neural tissue, was cultured on TiO_2 nanotube arrays. This current study shows that the new culture system, simply composed of a Petri dish and a stainless steal grid where the TiO_2 nanotube arrays are positioned (see Section 3.2, is optimal for organotypic culture of adult neural tissue because of its capability of reducing neuronal degeneration and glial hypertrophy that are usually observed in culture (Dallacasagrande et al., 2012; Mayr et al., 2013). When the retina is subjected to stress factors, as mechanical injury, an upregulation of intermediate filaments occurs (Fuchs and Cleveland, 1998; Lam et al., 2003; Lewis and Fisher, 2003; Lundkvist et al., 2004; Kaempf et al., 2008). The expression of vimentin, an intermediate filament in charge of maintaining cell shape, integrity of the cytoplasm and stabilizing the cytoskeleton interactions (Kaempf et al., 2008) did not increase when the adult neurosensory tissue was cultured on TiO_2 nanotube arrays. Actually it resulted very similar to the levels observed in freshly isolated retinas. Since the glutamate level is an important factor implicated in retinal degeneration (Dreyer EB et al., 1996; Rauen and WieÃner, 2000; Ristoff et al., 2007; Kaempf et al., 2008)), the expression of glutamine synthetase, a key enzyme in glutamate recycling (Kaempf et al., 2008), was checked. Its expression was in the range of the freshly isolated retina, indicating that the level of glutamate was normal even after 14 days of culture. Another efficient approach for verifying the health condition of the tissue is measuring the thickness of the sample before and after culture. A thinning of the retinal layers, in particular the inner and outer nuclear layers, and consequently of the tissue would suggest cell apoptosis and migration. This phenomenon was hardly observed after 14 days of culture, confirming the favorable properties of the TiO_2 nanotube arrays as substrate for long-term organotypic retinal tissue culture. The success of this culture system was better than expected especially considering that the neurosensory retina was kept without retinal pigment epithelium. In previous studies, the retinal cultured without retinal pigment epithelium (RPE) showed early ganglion cell apoptosis and photoreceptor degeneration (Kaempf et al., 2008; Caffé et al., 1989; Jablonski et al., 2001, Engelsberg et al., 2004, Katsuki et al., 2004, Kuhrt et al., 2004). Surprisingly, in this new culture system the photoreceptor inner and outer segments were well maintained (see Figure 5.1) without RPE. Usually the outer photoreceptor segments are lost during the retinal isolation

from the RPE or shortly after since the photoreceptors cells have a high metabolism and without the correct nutrition system quickly degenerate (Reidel et al., 2006).
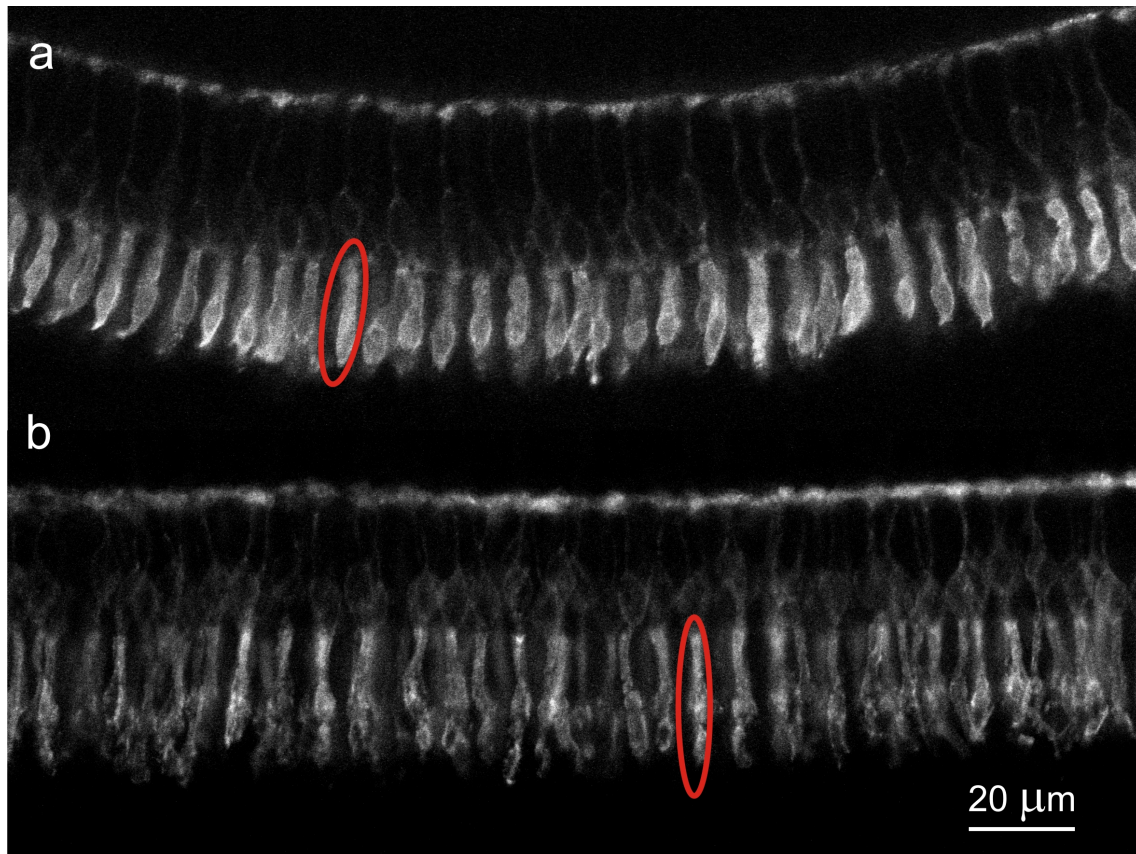
Figure 5.1: Cone photoreceptor cell comparison. Cones are stained with peanut agglutinin. (a) The retinal tissue is freshly isolated. (b) The neurosensory retina is cultured using the new system for 14 days. The morphology does not change and the maintenance of the outer segment layer in the cultured retina is clear (red circle).

To verify the universality of this culture method brain slices of adult mice were cultured 14 days using this organotypic culture system. The result and argumentation are similar. In general, organotypic brain slice cultures are prepared from animals at embryonic or postnatal stage because of their plasticity and resistance to mechanical trauma during the slice preparation (Cho et al., 2007). To understand the response of the adult brain in terms of neuronal architecture and synaptic circuity, and to create pathological models for stroke, epilepsy, Alzheimer's , Parkinson's and Huntington's diseases it is essential to study the mature slices *in vitro* (Cho et al., 2007).

The interactions between cells and biomaterials can affect cell/cell interplays, and consequently influence tissue development and function. Cell adhesion to biomaterials plays

an important role in the normal function of mammalian cells. It can be characterized in terms of specific and nonspecific interactions. Specific interactions implicate cell receptor to recognized and bind to proteins on the biomaterial surface forming focal adhesion sites, whereas nonspecific interactions consist in non-covalent attractive forces such as electrostatic interactions, hydrogen bonds and van-der-Waals forces (Israelachvili, 2011).

In previous studies, it was observed that the cellular behavior such as adhesion, proliferation, shape, migration, survival and differentiation (Huo et al., 2014) on TiO_2 nanotube arrays depends on the cell phenotypes and is influenced by the nanotubes diameter. The TiO_2 nanotube arrays with tube size ranging between 15 and 30 nm exhibited the larger degree of cell adhesion (Park et al., 2007; Huo et al., 2014). Nanostructured surfaces with $50 - 90$ nm adhesive pattern spacing resulted in a significant decrease in cell adhesion promoting cell fate (Selhuber-Unkel et al., 2010). Furthermore, cells cultured on TiO_2 nanotube arrays with pore sizes greater than 100 nm showed reduced adhesion and proliferation, an increase in apoptosis and they tended to send out cellular extensions (Oh et al., 2009; Park et al., 2009a; Mark et al., 2009; Park et al., 2009b; Bauer et al., 2009; Brammer et al., 2012; Moon et al., 2012).

The critical nanotube diameter value of $15 - 30$ nm can be explained considering that the focal adhesion cluster has approximately a size of 10 nm. A bigger diameter can prevent single cell adhesion and consequently it can induce to cell apoptosis (Kowalski et al., 2013) (see Figure 5.2).

In contrast to the cells, I have shown that the tissue prefers other optimum tube array parameters. The central nervous system tissue was successfully cultured on TiO_2 nanotube arrays with pore sizes greater than 30 nm. In particular, the best organotypic culture of retinal tissue was achieved on nanotubes and/or nanoporous arrays with diameter between 30 and 100 nm. Instead, the brain slices preferred to be cultured on nanoporous with smoother surface and pore sizes greater than 100 nm. The reason of this choice cannot be understood in term of cell's focal contact spacing or by the ability of cell receptors to connect to the membrane since the length scale does not match. The optimal tube parameters might be attributable to variations in structural organization of cells in the tissue. The heterogeneity and complexity of the neural tissue influence the cell surface area exposed to the nanotube arrays and the amount of extracellular matrix in between cells. Since the cells in the tissues present different size of the soma, they possess a distinctive ability to span the nanotube geometry. The observed organotypic conservation of the neocortex brain slice after culture on TiO_2 nanotube arrays with large diameter is likely caused by neurite formation promoted by the 100 nm pore size. Although the behavior of neurons on different nanotube arrays is unknown, studies on mesenchymal stem cells cultivated on 100 nm-nanotubes have shown that the cells form very few focal contacts
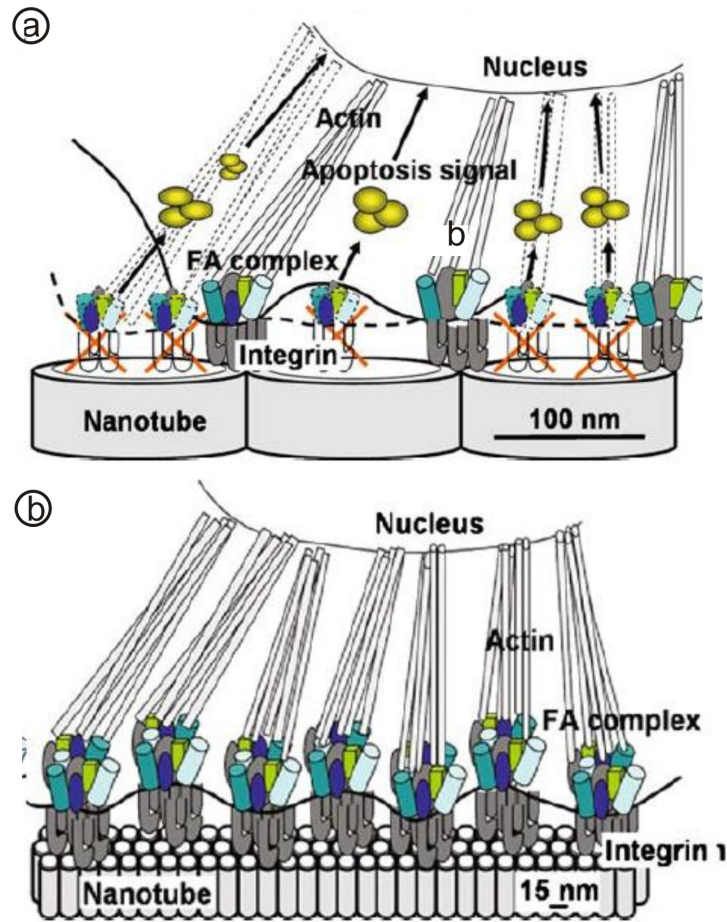
Figure 5.2: Hypothetical schema of the adhesion force between cells and TiO$_2$ nanotube arrays. (a) For a nanotube diameter of about 100 nm the cells loose focal adhesions and in culture is verify apoptosis. (b) The 15 nm nanotubes seem to be perfect for culture in terms of focal adhesion. Image from Park et al., 2007

and did not spread, instead they sent out filopodia, lamellopodia and cellular extension up to 200 nm (Park et al., 2007; Oh et al., 2009)

The weak focal contact formation within tissue and nanotubes with large diameter might be mainly due to van-der-Waals interactions (Loomis et al., 2012) and compensated by cellular adhesion within cells and extracellular matrix. In fact, I observed that single retinal cells (neurons and glial cells), cultivated on nanotube arrays with the same parameters that favored the culture of the corresponding tissue, die due to the loss of adhesion within 7 days. This confirms that the material properties of the nanotube arrays affect tissue viability and structural preservation. TiO$_2$ nanotube arrays employed as organotypic culture substrates facilitate adhesion of the tissue via van-der-Waals interactions and preserve the tissue integrity, while inhibiting migration of individual cells.

As mentioned previously, a prerequisite for a successful culture of neural tissue is the supply with nutrients by the culture medium. This is possible using the air-liquid interface technique. In the classical culture system introduced by Stoppini, the culture medium reaches the explant from the bottom through the cellulose membrane. In the method presented in this study this exchange is not possible since the TiO_2 nanotube membrane is closed at the bottom. Despite that, the full wettability and the superhydrophilicity of TiO_2 nanotube arrays (Balaur et al., 2005b; Balaur et al., 2005a; Shin et al., 2011; Song and Mano, 2013) ensure the adequate nutrient supply without bringing the tissue in direct contact with the bulk liquid avoiding the swelling and degeneration of the tissue. The supply is guaranteed by bringing the bottom and the sides of the nanotubes array in contact with the medium which is then wetting the entire substrate, providing fresh nutrition for the explant by diffusive transport.

5.2 New methods to study the Response of Retinal Tissue to Mechanical Stimuli

As described in section 2.2.2 the methods commonly used to mechanically probe the cells are numerous. Each method has a specific aim covering some aspects of cell mechanics. None of these methods was designed to experiment on living tissue because generally the scientific community addressed its research to single cell mechanics. Undoubtedly studying the mechanics of the single cell is the first step to acquire more knowledge in this field. However, *in vivo* cells are not functioning alone. They interact with the surrounding and with other cells in a elaborate agglomerate called tissue. The advantages of these methods are that they can produce statistically reliable and generalizable results. The complexity of the tissue structure makes it more challenging to work with it than with the single cells. In particular, for neural tissue one of the main issues is the survival of the explant, as discussed in the section 5.1. It is crucial to guarantee a suitable environment to avoid alteration of its intricate structure.

Traditionally, biomechanical eye research has focused on the parts of the eye that are more motile such as the lens. Recently, numerous studies have examined, in terms of mechanical properties, other parts of the eye such as the cornea (Woo et al., 1972, Hjortdal, 1994, Elsheikh et al., 2008, Last et al., 2009, Studer et al., 2010), the sclera (Curtin, 1969, Arciniegas and Amay, 1986, Phillips and McBrien, 1995, Ethier, 2006, Bisplinghoff et al., 2009, Eilaghi et al., 2010, Elsheikh et al., 2010 Norman et al., 2011, Lari et al., 2012, Grytz et al., 2014), and the choroid (Friberg and Lace, 1988, Del Priore, 2006). However, the retina is exposed to physiological and pathological stresses and the mechanism of propagation of these stresses is still not completely understood. A cause of the extremely delicate nature of the neurosensory retina, establishing a method to mechanically investigate this neural tissue is a challenge.

The approaches used to study the biomechanical of the eye are mainly addressed to create empirical models (Jones et al., 1992; Sigal et al., 2004; Sigal et al., 2005). These methods are extremely useful, although alone they can only describe mechanisms in an abstract manner.

At the beginning of the 80s, Kain performed an in vitro study on the mechanical properties of the retinal tissue drawing the conclusion that the adhesion forces between retina and retinal pigment epithelium are equal in all directions and that the neurosensory retina can be stretched reversibly possessing elastic properties (Kain HL, 1984). Later, Jones and colleagues calculated the Young's modulus of bovine retina of approximately 2×10^4 Pa using a realistic model of an incompressible solid. Jones himself thought this model to be not accurate since the real retina, although possessing elastic properties, is an inhomo-

geneous biological material (Jones et al., 1992). Recently Chen et al. demonstrated that the retina, compared to the other components of the posterior eye (choroid and sclera) is an inhomogeneous material and anisotropic along the surface (Chen et al., 2010; Chen and Weiland, 2010; Chen and Weiland, 2012; Chen et al., 2014). Lu et al. were the first focusing their attention on the mechanical behavior of the retinal glial cells. They studied the viscoelastic properties of individual Müller cells showing that these cells are softer than the neurons. They proved that in particular the inner and outer Müller cell processes are notably softer than soma and endfoot, and that the soma is stiffer than the endfoot. Furthermore they found that the elastic behavior was dominant for the intact retinal tissue (Lu et al., 2006). The retinal tissue was subjected to stretch in the study of Lindquist et al.. They reported the mechanosensory function of the Müller cells and showed that their inner and outer processes were elongated to a similar extent (Lindqvist et al., 2010). Franze et al. probed the inner retinal surface with scanning force microscopy discovering that it is mechanically inhomogeneous: stiffer in the mid-periphery and more compliant towards the optic nerve (Franze et al., 2011).

The necessity to gather more information on the retinal behavior under different stress conditions motivated this part of my work in designing new methods based on a qualitative analysis.

5.2.1 Inhomogeneous Behavior of the Retinal Tissue

In the first new set-up, the neurosensory tissue is under short-term shear stress (see Section 3.3.2 and Figure 4.9). The morphological changes of the Müller cells and indirectly the behavior of the retinal layers were monitored and analyzed.

For this type of experiment it was crucial to avoid additional stress to the sample and to keep the tissue intact and well conserved. Certainly the attachment of the specimen to the cellulose membrane is one of the most critical steps, requiring high precision. Particular consideration was made in the approaching the membrane to the side of the retina composed of ganglion cells and Müller cell endfeet (see Figure 4.9) since the photoreceptor cell side was already in contact with the cellulose filter (see Section 3.3.2). The possibility to squeeze the tissue while assuring a complete attachment is very high. At the same time in the attempt to prevent any crushing it could happen that the retinal is only weakly secured to the membrane. Using a confocal microscope was the best technique to control the attachment due to the possibility to scan through the entire tissue before and during the experiment.

In this work the neurosensory retina was not simplified to a homogeneous material to achieve a realistic understanding of this sophisticated and complex tissue. Three areas of the retina were analyzed: (1) the region composed of the retinal layers wrapped by the inner

process of the Müller cell (essentially the inner plexiform layer); (2) the section formed by the outer plexiform layer and the outer nuclear layer, and (3) the area constituted of photoreceptor segments (see Figure 5.3).
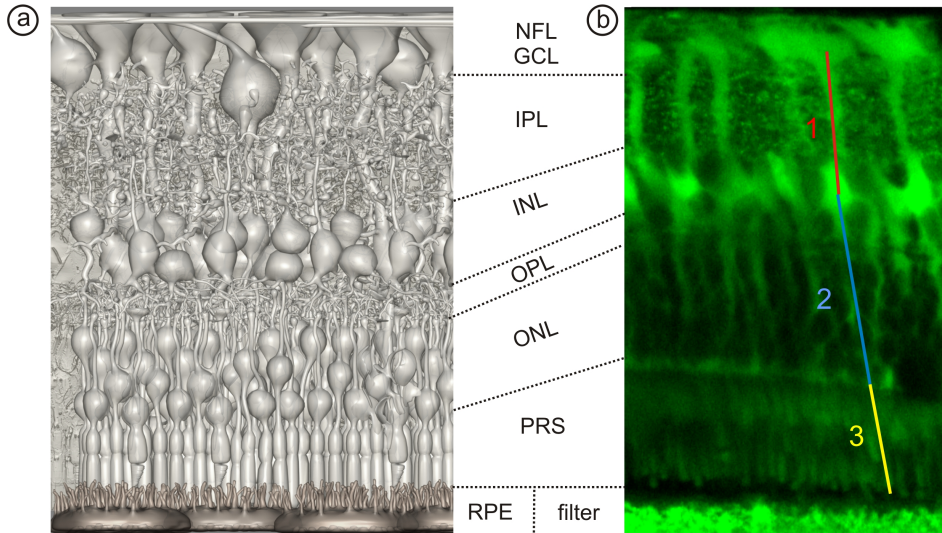
Figure 5.3: Illustration of the retinal segments considered in the calculation of the strain. (a) Illustration of the retinal cross-section. Image courtesy of J. Grosche. (b) Cross-section of an adult guinea pig retina stained with MitoTracker Orange. For the calculations of the strain three segments were considered. Segment 1 (red) connects the center of the Müller cells endfeet to the center of their nuclei. The area of the retina analyzed is mainly the inner plexiform layer (IPL). Segment 2 (blue) includes the rest of the glial cells from the center of their nuclei until their microvilli, that are not visible. In this case the segment wraps the outer plexiform layer (OPL) and the outer nuclear layer (ONL). Segment 3 (yellow) considers only the outer segment of the photoreceptor cells (PRS).

The forces applied to the retinal tissue could not be calculated but presumably are the following (see figure 5.4). Between the tissue and the membranes there are adhesion forces that help maintaining the retina anchored to the membranes. Furthermore, cells exercised forces to each other and to the extracellular matrix. These forces can be called internal forces although their distribution is not yet clear. In addition, there is the shear stress that is applied through the movement of the microscope stage.

Considering that the entity of the shear stress is unknown, the first step was to observe the dimensional adjustment of the retinal tissue due to this shear stress, calculating the strain. The resultant strain was measured as axial strain and normal strain for the reason that not only a shear stress is involved in the morphology change but also the adhesion forces and internal forces contributed to the displacement. The strain of the three segments were first examined in relation with the time and then normalized to the total shear strain.
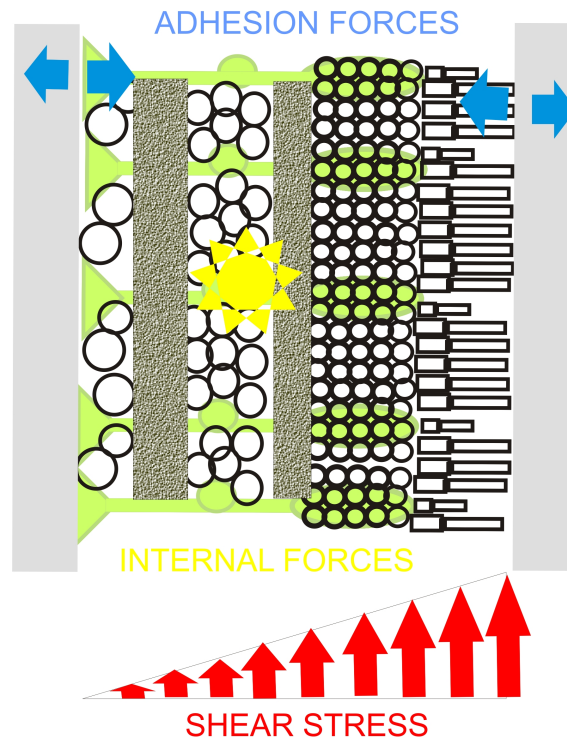
Figure 5.4: Schematic drawing of the forces acting on the retinal tissue during the shear stress experiment. Presumably the forces involved in the retinal behavior are the adhesion forces between the retinal tissue and the cellulose membrane, the internal forces that each cells exercised on the others and the shear stress applied due to the movement of the microscope stage. Since the shear stress is applied only in the photoreceptor side, these cells are the one that more are influenced. This shear stress is then transmitted to the rest of the retina tissue mainly through the radial glial cells.

The results showed that at a critical total shear strain value of 0.25 the retinal tissue started to detach from the cellulose filter (see Figure 4.12). This value was also obtained for the angular shear strain measurements (15 degrees)(see Figure 4.13). Before reaching this critical point the layers of the neurosensory retina act homogeneously like a block of the same material, but once passed that value their behavior changes. Precisely, the angle between the segments (1+2) and (3) that identify respectively the Müller cells and the photoreceptor cells increases (see Figure 4.14) indicating that the bending of the photoreceptor outer segments toward the direction of the shear strain applied is more noticeable. The calculation of the axial strain exhibits a pronounced elongation of the photoreceptor segment starting from the critical point. Indeed, the photoreceptor layer shows a more elastic behavior. On the contrary the Müller cells maintain their axial strain almost constant during the entire experiment (see Figure 4.16). Focusing only on the Müller cells, the analysis illustrates that individual shear strain of their inner segment

increases more rapidly than of their outer segment. This shows that the retinal tissue spanned by the inner processes of the Müller cells reacts strongly to the shear stress applied (see Figure 4.17).

The different behavior of the retinal layers can be accounted for by the heterogeneity in the retinal composition (see Figure 2.2). The retinal structure is unique considering that the Müller cells extend through the full thickness, the photoreceptors cells are vertically oriented, while the other layers are organized horizontally (Chen et al., 2014). The high packing of the retinal cells explains the transmission of the shear stress from the photoreceptors to the inner part of the retina. The plexiform layers certainly are the most compact layers since they form a tight synaptic network. Indeed, the neuronal cells extend their axons crosswise strengthening the retinal tissue structure. The processes of the Müller cells that span the plexiform layers are in contact to an increased number of synapses. The data show that the inner plexiform layer is the one more affected by the shear stress if compared to the outer plexiform layer. That does not necessarily imply that the inner retina is softer then the outer retina. This result is counterintuitive since it is the part of the retina situated further from the area where the shear stress is applied. The pronounced bending of this layer is explained once again by the crowding of the inner part of the retina. The structural heterogeneity of the inner retina mirrors the inhomogeneity of the mechanical properties of the inner retinal surface, result of complicated mechanical interactions between its components and the extracellular space (Franze et al., 2011). In the inner plexiform layer the connections are between a higher number of cells (bipolar cells, horizontal cells, amacrine cells and the Müller cells). Certainly, in this layer the intracellular forces play a decisive role in the response of the retinal tissue to external forces. Additionally, the inner retina looks pinned by the inner nuclear layer composed of the soma, the stiffest part of the retinal tissue containing endoplasmatic reticulum and nucleus (Lu et al., 2006). Interestingly, the outer limiting membrane seems to hold the distal part of the tissue tightly. The outer limiting membrane (OLM) is considered an important element for keeping the retinal structure through mechanical strength even if its function is not completely understood yet (Omri et al., 2010). The nuclear layers and the OLM seems to act like a pivot where the segments rotate since they oppose more resistance to the shear stress applied.

Although it was shown in previous AFM studies (Lu et al., 2006) that there is no difference in stiffness within the inner and the outer processes of the Müller cells, the processes possess different dominant cytoskeletal elements. The intermediate filament bundles prevail in the inner processes, whereas the microtubules are mainly present in the outer processes (Reichenbach et al., 1988a; Reichenbach et al., 1988b).

The intermediate filaments serve to maintain the basic integrity of the cell (Janmey et al.,

1991) and they contribute to the viscoelastic properties of the glial cells (Lu et al., 2010). Indeed, the resistance of the retina to mechanical stress is decreased in the case of absence of intermediate filaments (IFs) (Lundkvist et al., 2004). The Müller cells tend to become stiffer when their physiological condition is changed due to overexpression of vimentin (Lundkvist et al., 2004). This phenomenon is not instant, but requires a time period of days, thus it did not occur during my experiments. The intermediate filament networks compared to the microtubule organizations are easily deformed and withstand large stress and strain without rupture. This is probably why the deflection of the inner retinal layer is more notable under the influence of the shear stress and the internal forces.

The difference between the inner and outer processes of the Müller cells shown in my results does not seem to match the studies conducted separately by Lu (Lu et al., 2006) and Lindqvist (Lindqvist et al., 2010) where no difference in strength or stiffness was observed. Probably the reason is that in the first study only single Müller cells were probed and analyzed. Furthermore, in the second study the retinal tissue was stretched and not shear stressed as in my experiment. The force applied was directed across the retinal thickness, along the Müller cell axis and not perpendicular as in my study. Thus, the results do not contradict each other, but indicate that the mechanical response of the retina to external forces depends on the type of stress applied, on the microenvironment and it cannot be studied taking in consideration only the single building blocks, in this specific case the Müller cells.

Although during the experiment the retinal slice is attached at the top (ganglion cells and Müller cell endfeet side) and at the bottom (photoreceptor cell side) to the same type of cellulose membrane, the detachment after applied shear stress was noticed only at the photoreceptor side. The main reason can be that the traversal force is exercised directly to the rods and cones side. Another argumentation can be that the contact area of the photoreceptor cells is smaller compared to the area of the inner retina in contact with the cellulose membrane which probably influences the attachment (see Figure 5.5). Indeed, the inner limiting membrane, located on top of the nerve fiber, ganglion cells and Müller cells endfoot layer and composed of dense fibrillar meshwork (Heegaard et al., 1986), adheres completely to the cellulose filter, whereas the photoreceptor layer sticks to the substrate less than 80% caused by the fact that cones are shorter than rods and therefore to not adhere. Furthermore, the photoreceptor cells are free to move since they are attached to the retina only through the Müller cells that wrap the photoreceptor nuclei with their velate sheaths (see Figure 2.3). Normally, the photoreceptor cells are secured to the retinal pigment epithelium through microvilli (see Figure 5.11) and there are no physical connections between cones and/or rods, so they can be compared to the bristles of a brush. This morphological configuration facilitates the movement and the detachment

of the distal part of the retinal tissue.
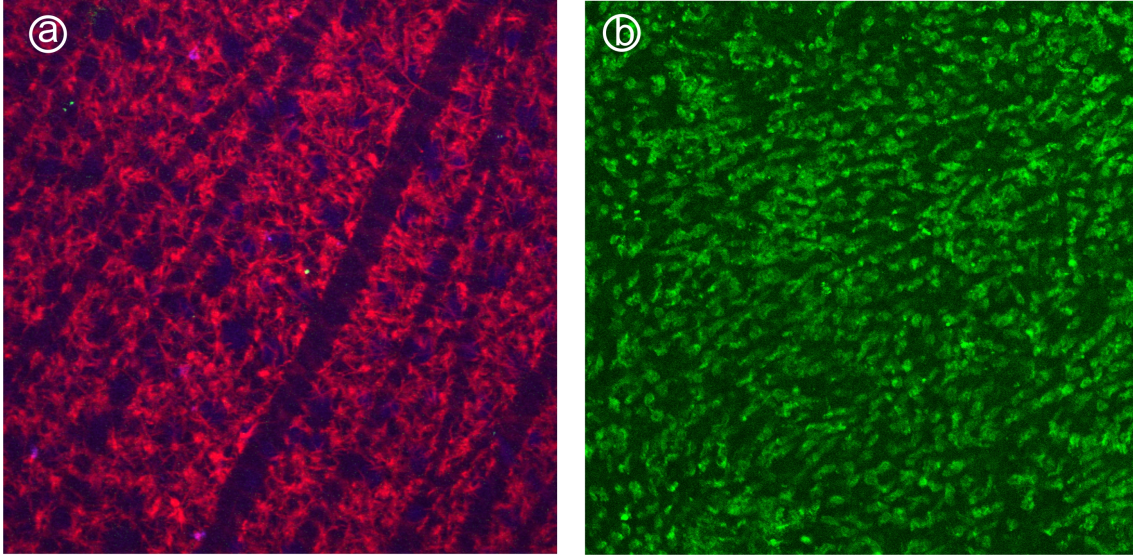
Figure 5.5: Immunostained guinea pig whole-mount retina. (a) The inner part of the retina is visualized with anti-vimentin antibody and Hoechst (ganglion cell nuclei). The black lines indicated the fiber layer (ganglion cell axons). (b) The cone photoreceptor cells are discernible through the peanut-agglitinin staining. Due to their loose attachment to the rest of the retina and the absence of mutual contact the photoreceptor bend easily. The reduced contact area between the filter and the photoreceptors during the experiment is caused by the cell morphology.

Nonetheless a slipping of the tissue along the membrane at both sides was observed. Even if the adhesion forces are unknown, the presence of friction forces between the tissue and the membrane can be one cause for the tissue shifting. Another explanation can arise from the fact that to protect the tissue from drying out and to allow its survival, it was necessary to totally immerse the retinal slice in a physiological solution during the entire duration of the experiment. It should be noticed that the retinal tissue in this experiment is not kept in culture but at room temperature. The air-liquid interface system is not necessary. The fluid penetrating the tissue can interfere and prevent a stable adhesion. Considering both scenarios (slipping and no slipping) the data showed that the shifting of the retinal tissue does not really influence the detachment. Indeed, the critical point calculated for both cases has very similar values (see Figures 4.21; 4.22; 4.24; 4.23)

5.2.2 A New Device to shear stress Retinal Whole-Mount

The last part of my research was dedicated to combining the knowledge gained on long-term organotypic neural tissue culture with the interest in applying shear stress to living retinal tissue. The aim was to design a new setup (see Section 3.3.1 and Figure 3.7) to

apply mechanical stress to retinal whole-mounts in culture. The main concern in designing this new device was to build a setup that could conserve the retinal tissue in a physiological environment mimicking the *in vivo* conditions. The purpose was to shear the retinal tissue over several days, so using the TiO_2 nanotube arrays as membrane to support the retina during the experiment was the best solution. The starting point was to incorporate the interface system into the design. As shown previously (Dallacasagrande et al., 2012) this culture system combined with the TiO_2 nanotube arrays ensures a long term organotypic culture of adult neural tissue.

One of the characteristics required was to avoid additional stress to the sample other than the stress actually applied. Since the device has to be moved from the laminar flow hood inside the incubator, the solution was to fix all the components on top of a heavy stainless steel tray (see Figure 3.8 (b)). All the metallic components were made of stainless steel to avoid the production of rust once in contact with the culture medium. In designing the device, particular attention was paid to the sterilization process. The number of elements were reduced to a minimum to facilitate the assembly and disassembly of the device for thorough cleaning. The sterilization of all the elements had to be easy and efficient. Indeed, one of the problems encountered in the first experiments was the contamination of the sample during the incubation time. The cause of contamination was individuated in the cleaning procedure of the device. This procedure was reevaluated and an efficacious cleaning routine was established (see Section 3.3.1 and Figure 3.8). Another problem to solve was the leaking of the device during the time the experiment was running. That was a major issue since the spill of the culture medium was consistently compromising the survival of the sample. After various attempts to prevent this phenomenon the device was modified. Initially the TiO_2 nanotube arrays were clamped to a support that glided on ceramic rods. For this setup three holes were made inside the Teflon chamber that caused leaking of the physiological solution. The gliding system was replaced with a more sophisticated structure made of stainless steal supports where the TiO_2 nanotube arrays were fixed with tissue glue, reducing in this way the components and removing the holes. An additional challenge was the placement of the retinal whole-mount on top of the TiO_2 nanotube membrane exactly at the point where the membranes touch each other without damaging the tissue. Originally, the TiO_2 nanotube arrays were suspended making it extremely complicated and unstable to position the sample. To facilitate the arrangement of the sample, a cross-like support was placed under the TiO_2 nanotube membranes. Another issue was presented by the removal of the sample from the TiO_2 nanotube membranes for the analysis. During the procedure of removal of the retinal tissue from the junction site of the TiO_2 nanotube arrays, the sample was fixed over night in 4% paraformaldehyde and finally embedded in 3% agarose with the purpose of wrapping the sample and maintaining

it intact during removal. Several devices were designed and tested before achieving the final result that satisfied the requirements and overcame all the challenges and issues.

Testing the device allowed to have some preliminary results regarding the morphological changes experienced by the sample. In particular, the attention was addressed to the behavior of the entire tissue after the application of long-term shear stress.

Once fixed and removed, the retinal tissue was immunostained as a whole-mount or as slices to allow to analysis the cross-section (see section 3.1.5).
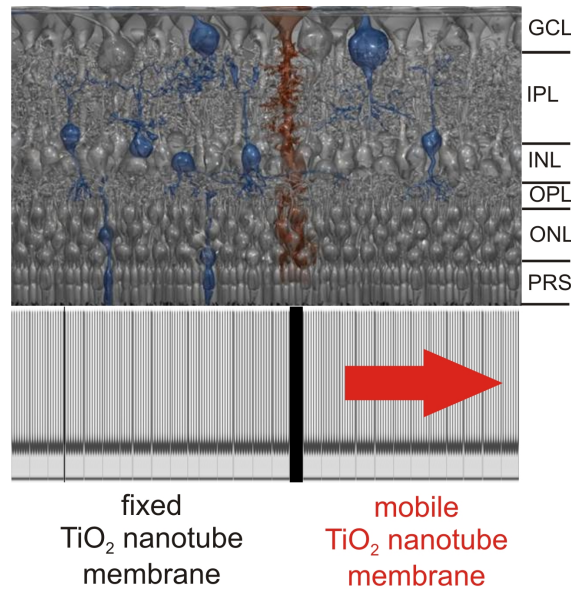
Figure 5.6: Lateral view of the set-up for long-term shear stress experiments. The retinal whole-mount lies at the junction between two TiO_2 nanotube membranes. The photoreceptor cell side is the part of the sample in direct contact with the arrays. One of the membranes is fixed and the other is moved by a stepping motor as previously described in section 3.3.1. GCL= ganglion cells layer; IPL= inner plexiform layer; INL= inner nuclear layer; OPL= outer plexiform layer; OLN= outer nuclear layer PRS= photoreceptor segment.

From the cross-section immunostained retina it was possible to observe that once the retina detaches from the membrane its reaction is to buckle like a rubber band, pulled and then released. The same behavior was shown in both cases, when either the photoreceptors or the ganglion cells were attached to the membrane.

Analyzing the staining of the whole-mount, the movement of the photoreceptor cell segment was clearly visible. It does not have a defined pattern but that confirms the mobility and flexibility of this part of the retina.

The results represent a good starting point, but more investigations are necessary to have a clear understanding of the retinal tissue under these conditions. Compared to the
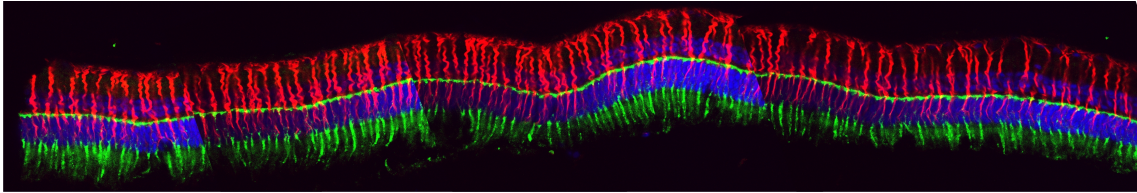
Figure 5.7: Fluorescent image of a whole-mount retina sheared in culture. Müller cells are stained with anti-vimentin (red), the photoreceptor cones with peanut agglutinin (green) and the nuclei with Hoechst (blue). The cross section indicates the whole-mount tissue placed on the TiO_2 nanotube arrays and shear stressed over 4 days in culture leaving a gap between the TiO_2 nanotube membranes of about 100 μ. The buckling of the tissue after release of the foce applied is more visible in the middle where the distance between the membranes was created by the movement of one of them. The retinal tissue acts like a rubber-band, showing global elastic behavior.

short-term stress experiments describe in section 5.2.1, this is a long-term experiment, consequently the parameters and conditions used were different. For example, in this case the membrane used is not a cellulose filter but TiO_2 nanotube arrays and the sample is attached to the membrane only on one side. Furthermore, the retinal tissue has time to settle down after each shear stress applied. The outcome is more an overview of the response of the retinal tissue to the release of the force applied.

Understanding the behavior of the retinal tissue under certain conditions is the key to acquire an in-depth knowledge of the mechanics involved in processes during retinal development and diseases, foveal formation and retinal detachment.

Mechanics in Retinal Development: Fovea Formation

During the human development, the tissue mechanics has an important role albeit the entity of the involvement is not completely well understood. For example, there is not a straightforward explanation for the formation of the primate fovea, the eye region which allows acuity vision (see Section 2.1.1)(Reichenbach and Bringmann, 2010). A variety of intrinsic molecular and extrinsic mechanical mechanisms are involved in the development of the primate fovea. The mechanical forces suggested to be implicated in this process are a tangential force produced by the ocular growth which stretches the retinal tissue like a glove by the fist (Mastronarde et al., 1984) and an orthogonal force generated by the intraocular pressure (Provis et al., 2013).

The shaping of the retinal tissue continues after the cell proliferation is concluded and after the retinal layers are formed. In general during the growth of the eye ball, the neurosensory retina becomes thinner since the retinal cells have more space to rearrange but it maintains the dimension of the plexiform layers. The moulding of the primate fovea occurs over an extensive period (pre- and post- natally). In humans, it starts at about 24 weeks of gestation (Hendrickson and Yuodelis, 1984; Provis et al., 1998)

The characteristic shape of the primate fovea is presumably due to a centripetal movement of the perifoveal photoreceptor cells and a centrifugal displacement of the inner retinal layers (see Figure 5.8). Since the Müller cells are embedded in the tissue, this rearrangement results in a formation of the foveal pit with the radial glial cells in a Z-configuration (see Figure 5.9). The neuronal cells of the (peri-)foveal columnar units are not reshaped but they passively pull the axons of the cones to keep the synaptic connections. In this way a "new" layer, the so-called Henle fiber layer is formed. This area, composed of photoreceptor cell axons and outer Müller cell processes arranged transversely, seems to act as a "sliding zone" comparable to the tectonic movement of the plates (see Figure 5.10) (Reichenbach and Bringmann, 2010).

No animal models have been developed yet that possess a foveal pit and that are easy to manipulate during development. A finite element analysis model has been proposed by Springer and Hedrickson (Springer and Hendrickson, 2004). They highlight the role of mechanical properties of the foveal avascular zone (FAZ). Indeed, this region is presumably more elastic and consequently more responsive to the mechanical forces, in particular to intraocular pressure, because of the lack of blood vessel. They also proposed that the tensile forces generated by the retinal stretch could cause axial "lifting" forces, which stimulate the elongation of the photoreceptor cells within the FAZ, to regulate the cone crowding. This point is controversial since the packing of the cones happens prior to the definition of this area.

Probably the mechanics of the different retinal layers, together with the different cell
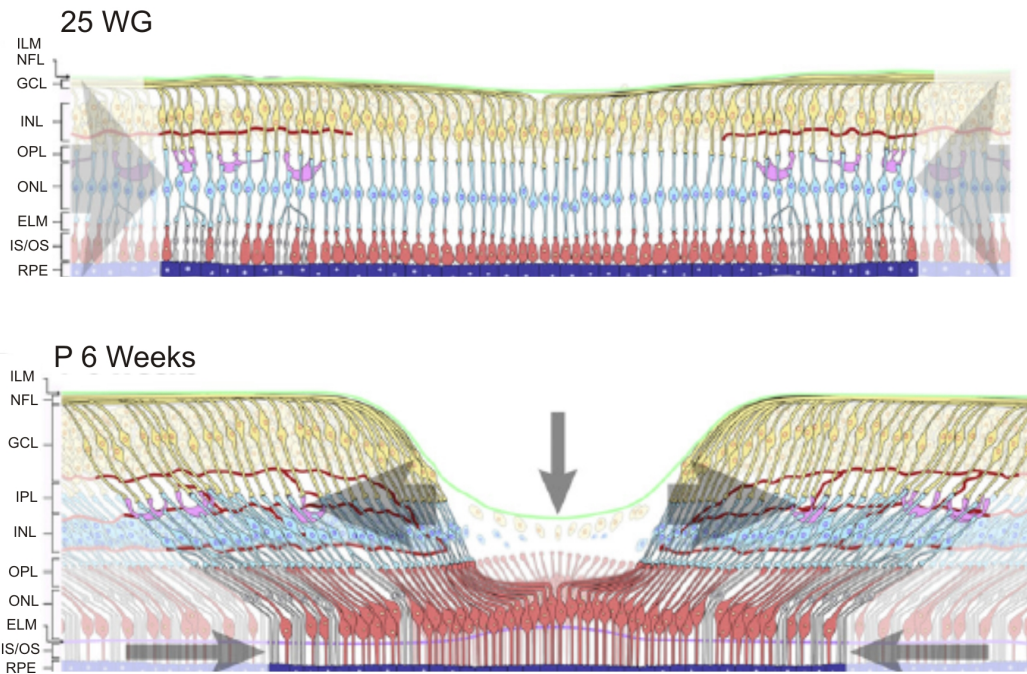
Figure 5.8: Drawing of the rearrangement of the retina due to fovea formation. In this diagram the Müller cells are omitted to clearly visualize the other retinal cells and distinguish the retinal layer. Cones are shown in red, rods in gray, bipolar cells in blue, amacrine cells in pink, and ganglion cells in yellow. The red lines indicate approximately the blood vessels. (a) Before the appearance of the fovea (25 weeks' gestation, WG) a centripetal force (gray big arrow) displaces all the retinal layer to the center. (b) The intraocular pressure intervenes around the 30 WG deforming the avascular zone of the retina creating first a shallow depression. In the first weeks after birth the cones differentiate and elongate forming the Henle fiber layer. The ganglion cells, the bipolar cells and the synaptic pedicles of the cones are pushed away from the center. ILM= inner limiting menbrane; NFL= nerve fiber layer; GCL=ganglion cell layer; IPL=inner plexiform layer; INL=inner nuclear layer; OPL=outer plexiform layer; ONL=outer nuclear layer; ELM=external limiting membrane; IS/OS=inner and outer segment; RPE= retinal pigment epithelium. Image modified from Provis et al., 2013

properties, intraocular pressure and eye growth, play a role in shaping of the primate fovea. As shown in my work, the photoreceptor segment exhibits a more elastic behavior that can facilitate the centripetal packing when an external force is applied. The outer limiting membrane results in a solid structure that helps maintain the integrity of the distal part of the retinal. Additionally, the distinct behavior of the layers wrapped by the inner and outer Müller cell processes could influence the centrifugal shifting.
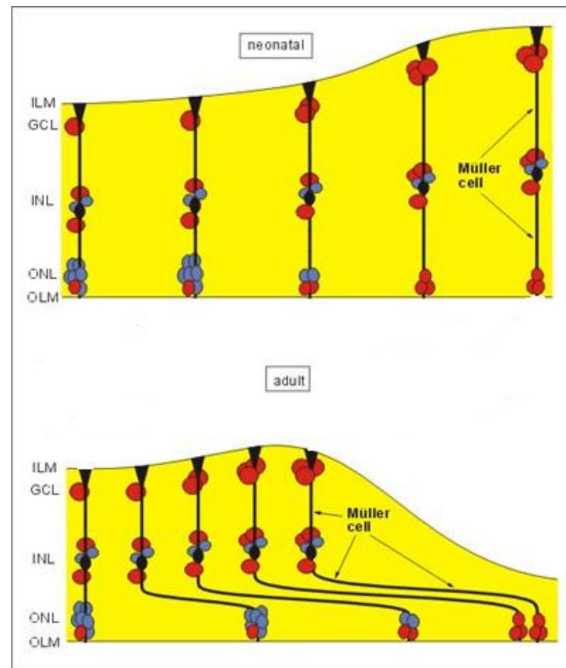
Figure 5.9: Schematic configuration of Müller cells in the primate fovea. In the adult fovea the Müller cells assuming the Z-shape. Their outer processes elongate together with the cone axons to maintain the functional connection with the interneurons. Image from Reichenbach and Bringmann, 2010
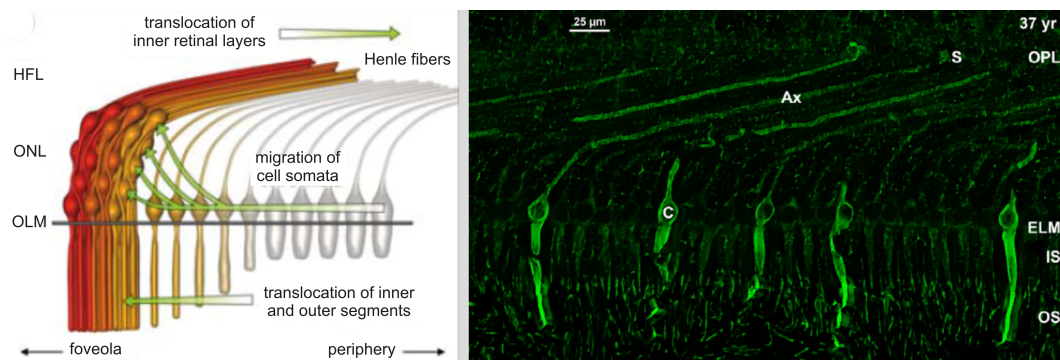
Figure 5.10: Morphology of the photoreceptor cells in the primate fovea. (a) Schematic drawing of the mechanical processes engaged in the development/shaping of the primate fovea. During this process the cones become thinner and move towards the center of the future fovea creating a stack of nuclei (ONL) on top of the outer limiting membrane (OLM). Instead the inner part of the retina drags centrifugally. To maintain the functionality of the columnar unit the axon of the cones elongate forming together with the outer processes of the Müller cells a so-called Henle fiber layer (HFL). This area is thought to be the 'sliding' zone. Image from Reichenbach and Bringmann, 2010. (b) The cones located in the fovea region of the retina of an adult male patient (37 years old) are stained with short-wavelength cone opsin. The long photoreceptor cell axons are clearly visible. Ax=axon; ELM=external (outer) limiting membrane; S=synapsis pedicles; IS=inner segment; OS=outer segment; OPL=outer plexiform layer. Image from Hendrickson et al., 2012

Mechanics in Retinal Pathologies: Retinal Detachment

The normal retinal adhesion depends on a combination of anatomic, physical and metabolic factors. There are no junctions which connect the gap between photoreceptor outer segments and retinal pigment epithelium (RPE) and the role of their physical interdigitation is not clear yet (see Figure 5.11).
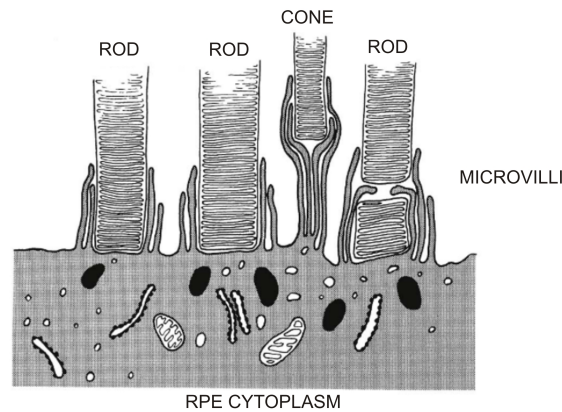
Figure 5.11: Interdigitation between photoreceptor outer segments and the microvilli of retinal pigment epithelium (RPE). This is the only physical connection of the retina to the back of the eye. Image from Marmor, 1993

The mammalian subretinal space remains tightly closed despite the continuous ocular movement and the pulling from the vitreous body. Indeed, the retina is kept in place by the balance between the intraocular pressure and osmotic pressure through the vitreous body and the negative pressure created by suction forces from water efflux through the RPE. The fluid pressure and vitreous pressure are external mechanical forces which strengthen or weaken retinal adhesion. The intraocular pressure and the osmotic pressure of the extracellular fluid present in the choroid (about 12 mmHg in the rabbit)(Bill, 1975) passively drive the fluid from the vitreous to the choroid. However, the posterior flow is very low and most fluid leaves the eye through anterior drainage (see Figure 5.12). Although, the pressure difference across the retina/RPE is small (only 0.52×10^{-3} mmHg)(Fatt and Shantinath, 1971) due to the fact that the intraocular pressure is contained by the sclera, this difference generates a force sufficient to pin the retina to the posterior eye (Marmor, 1993).

When these physiological forces are compromised or overwhelmed, a separation of the neurosensory retina from the underlying RPE could happen (Kirchhof et al., 2013). This phenomenon is known as retinal detachment.

The retinal detachment can lead to blindness since the outer retina after detachment be-
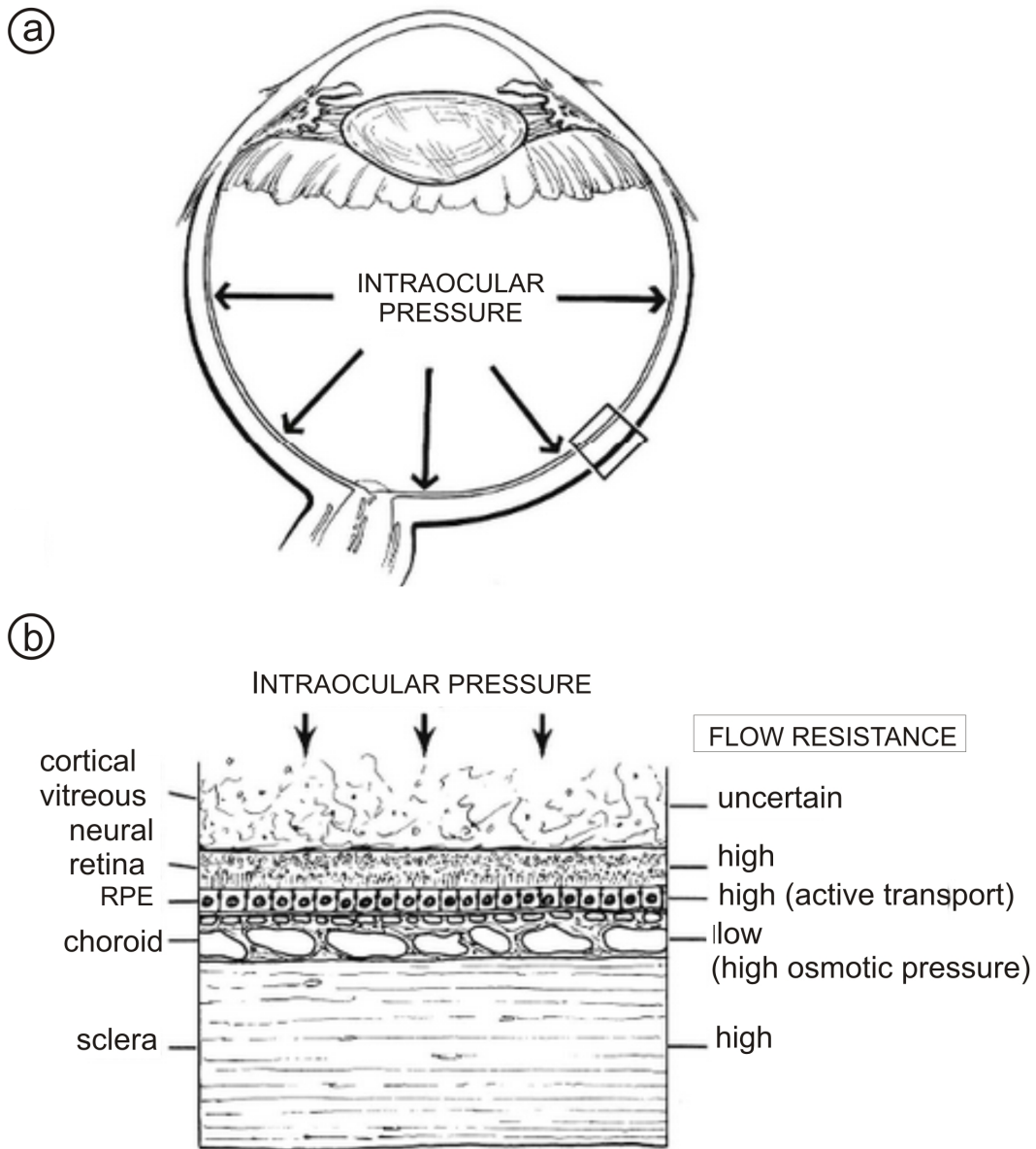
Figure 5.12: Intraocular pressure and flow resistance schema. (a) The intraocular pressure is the fluid pressure inside the eye. (b) Enlargement view of the posterior eye. Each layer has a different flow resistance. Additionally the RPE and the choroid can produce active transport of the fluid and osmotic pressure, respectively. Image from Marmor, 1993

comes ischemic due to the loss of blood supply from the choroid (Ghazi and Green, 2002). Cataract, surgery, myopia (David et al., 1997) and trauma can provoke retinal detachment (Bottega et al., 2013). Depending on the underlying causes, the retinal detachment

can be divided in three categories with the common denominator of an accumulation of subretinal fluid (Kirchhof et al., 2013). One of the most common form is rhegmatogeneous retinal detachment resulting from the formation of holes or tears in the retinal tissue (see Figure 5.13)(Chou and Siegel, 2012; Bottega et al., 2013). This form is characterized by a full thickness retinal break held open by vitroretinal traction that allows accumulation of liquefied vitreous in between retina and RPE (Ghazi and Green, 2002). When the retina is pulled off the RPE by tractional forces in absence of tears the disease is called tractional retinal detachment (Ghazi and Green, 2002). Instead the exudative (serous) retinal detachment is usually cause by tumor or inflammation without retinal breaks or traction (Kirchhof et al., 2013)
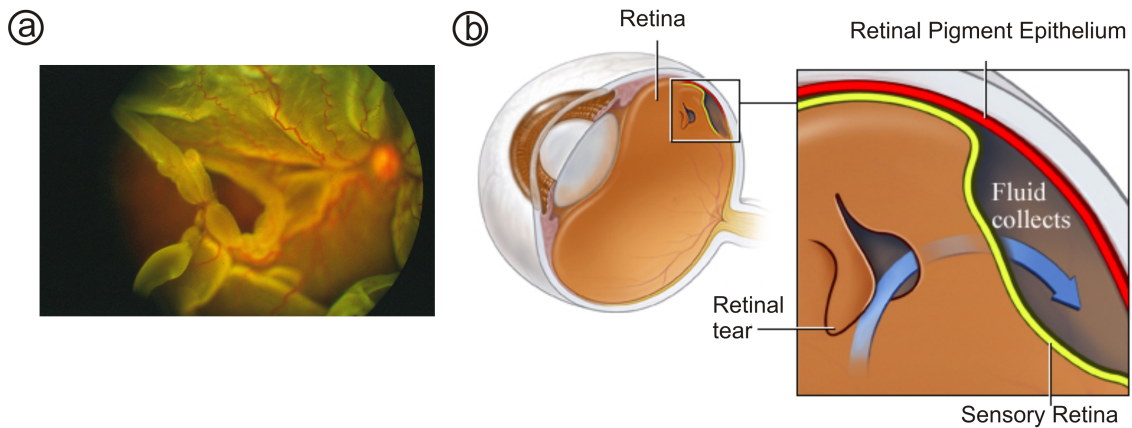
Figure 5.13: Retinal detachment. (a) Fundoscopic image of a detached human retina. (b) Schematic drawing of a cross section of an eye with detached retina. The retinal tear opens up space for the fluid to infiltrate between the retina and the RPE. Image from Healthwise, Incorporated.

Bottega et al. were the first to conduct an analytic study on the mechanics of a detaching retina developing a mechanics-based mathematical model (Bottega et al., 2013). Although Lakavicz et al. slightly modified this model, in literature this is the only study that takes in consideration the mechanical aspect of this disease (Lakawicz et al., 2014). These mathematical models can be developed without the employment of the tissue. In contrast, the widely used animals models (Lewis et al., 2002; Jackson et al., 2003; Zeng et al., 2012; Matsumoto et al., 2013) have the goal to study the molecular, immuno- and inflammatory response and are not interested in the mechanical aspect. The scarcity of knowledge in this area is certainly imputable to the difficulty in determining the material properties of the eye and in particular of the neurosensory retina (Bottega et al., 2013). The retinal detachment is caused first by a mechanical problem and therefore a cascade of signals that leads to degeneration and apoptosis. Although, the subject of retinal detachment is well known, the fundamental mechanics of the detachment propagation has not

been sufficiently described (Bottega et al., 2013). The present study can add new insights due to the direct employment of the tissue and the observation of the behavior of the different layers.

With my work I did not intend to create a model for retinal detachment, indeed the goal was to study the compartment of the retinal tissue when a short term shear stress was applied. Surprisingly, it was observed that although the retina behaves heterogeneously, it maintains its structure. This behavior prevents the rupture of the tissue and allows the possible reattachment. It therefore might act as a defense mechanism against a major damage that could lead to the loss of sight in the case the structure is compromised.

6 Conclusion

The research presented in this thesis was aimed at finding a novel substrate for long-term organotypic culture of adult neural tissue and to design new methods/set-ups to further investigate the mechanical properties of the retinal tissue.

The $3D$ culture systems bridge the gap between the petri-dish culture and the animal *in vivo* study. Although the $3D$ tissue models intended as cells in $3D$ environment are an extremely powerful tool (Griffith and Swartz, 2006; Lin and Chang, 2008; Justice et al., 2009; Derda et al., 2009), the organ culture has the advantages of providing specific information on growth patterns, differentiation and development. The limitation imposed by the age of animal used in the organotypic culture was overcome in this study. The key of the success of the culture system presented in this work is the employment of the titanium dioxide (TiO_2) nanotube array in combination with the interface technique introduce by Stoppini (Stoppini et al., 1991). Although, titanium and its alloys are commonly used in many biomedical applications such as dental and orthopedic implants, here, for the first time, TiO_2 nanotubes arrays were employed as substrate for organotypic culture of a tissue. In this work, I have shown that the TiO_2 nanotube arrays fulfill the requirements as substrate for obtaining long-term organotypic culture. Indeed, they discourage single cell adhesion and cell migration in favor of the overall tissue adhesion while preventing edema and degeneration. The full nanotube wettability and superhydrophylicity facilitate tissue adhesion and allow to supply the tissue with the essential nutrients while guaranteeing its correct oxygenation. Additionally, this system does not require special equipment and necessitates very little maintenance. The study revealed that the adult whole-mount mammalian retina and the mature brain slices survive up to 14 days cultured on TiO_2 nanotube substrates (Dallacasagrande et al., 2012; Mayr et al., 2013). This duration was previously never reached using as a culture substrate a cellulose filter or insert in the common interface culture system. The analysis was conducted in term of morphological changes and not from a functional point of view. Since the degeneration of the tissue is observed foremost when the tissue structure is corrupted, approaching the problem from this prospective is the first step for verifying the effectiveness of this methods. The results presented in this thesis show that the success of the TiO_2 nanotube arrays as a culture substrate strictly depends on the parameters used, such as diameter of the tubes and surface roughness. The optimal parameters are tissue/cell specific. Indeed the study illustrated

that the retina required a smaller diameter for the nanotubes ($30 - 85$ nm) compared to the one necessary for the brain slices (100 nm). However, the nanotube diameter required for a long-term tissue organotypic culture is bigger than the diameter used for culturing single cells ($10 - 30$ nm) as previous studies shown (Park et al., 2007; Huo et al., 2014). The characteristic that makes the TiO_2 nanotube arrays so attractive as culture substrate is their tunability. In fact, they can be easily adapted to different types of tissue to provide optimal culture conditions.

During the work of this thesis two different set-ups were designed to mechanically probe the retinal tissue. In the first device a shear stress was applied to the retinal slice stained with a vital dye that highlights the Müller cells. For the first time, the behavior of the retinal layers was observed. The study emphasizes that once a shear stress is applied, the retina behaves as an inhomogeneous material. This behavior was expected due to the complex structure of the neurosensory retina, nevertheless it was not verified for the overall tissue yet. The morphological structures and the internal forces influence the retinal layer response to the force applied although the mechanisms of the latter is still not well understood. The outer limiting membrane such as the outer and inner nuclear layers pin the retina in the neutral position. This leaves mainly three layers subjected to the shear stress: the photoreceptor segment layer,and the inner and outer plexiform layer. The results shown that the photoreceptor layer is more elastic compared to the rest of the retinal layers. This layer remarkably elongates and bends before detaching from the cellulose filter where the retinal tissue is placed in between. Certainly this layer is more affected by the shear stress because the force is directly applied to the outer part of the retina. However this does not justify why the Müller cells, a direct extension of the photoreceptor cells in the retinal cross-section, do not follow the same movement. Interestingly, the results displayed show that the inner plexiform layer wrapped by the inner radial glial cell processes are shown to be more affected by the shear stress compared to the outer plexiform layer, although is located further from the point where the force is applied. Furthermore, the study revealed that the retinal tissue can sustain up to 25% of shear strain before detaching from the substrate. This can be explain as a mechanism of defense against rupture that can be found *in vivo* situation. Once the retina detaches from the subretinal space it can be reattached and it can regain its functionality, instead the retinal rupture leads to a partial or complete blindness.

In the second set-up the whole mount retina was shear stressed for a few days in culture. The force was applied during a longer period of time allowing the retina to settle down and be rearranged. The observations were made on the immunostained tissue after removal from the TiO_2 nanotube membrane utilized in the design of this device. The results shown that the retina behaves overall as a rubber band buckling once the force applied is released.

112

Deepening in this area of research is needed thus these results could be the starting point for future work.

In conclusion, I demonstrated that the employment of the TiO_2 nanotube arrays improves the organotypic culture system of adult tissue (Dallacasagrande et al., 2012). For this reason future studies could be addressed to use these substrates in novel drug screening techniques for anti-cancer therapy and as platforms to model CNS diseases (traumatic, hypoxic and chemical CNS lesion). Furthermore, the TiO2 nanotube arrays represent an ideal substrate for mechanical testing or manipulation such as investigation of tissue elastic properties due to their very low elasticity and large achievable strains (Fischer and Mayr, 2011), as also shown in the present work. Additionally, my work made an effort to study the neural retina as a tissue composed of different parts avoiding the simplification of considering it as a homogeneous biological material. In fact, I have shown that the neurosensory retina is an inhomogeneous and anisotropic tissue due the complexity of its morphology. The attention has to be focused on investigating how the internal forces play a decisive role in the mechanical response of the tissue to external loading. Despite the new information acquired in this study more work has to be done to answer remaining open questions. The employment of genetically engineered animals, for example vimentin/GFAP deficient mice, can lead to understanding the importance of these cytoskeletal proteins while the retina is under stress. The second set-up is suitable for live recording since the lid has a hole that fits the objective of the microscope. To maintain the culture conditions a CO_2 chamber needs to be added to the confocal microscope. Although the analysis performed in this work was purely qualitative the potential of this setup is large. An in-depth knowledge of the mechanical properties of the neurosensory retina, as this work aimed to achieve, is urged in retina surgery.

"'Principles for the development of a complete mind: study the science of art, study the art of science, develop your senses-especially learn how to see and realize that everything connects to everything else"'

Leonardo da Vinci

7 Bibliography

Abbott, A. (2003). "Cell culture: Biology's new dimension". en. In: *Nature*, 4246951, pp. 870–872.

Agte, S., S. Junek, S. Matthias, E. Ulbricht, I. Erdmann, A. Wurm, D. Schild, J. A. Käs, and A. Reichenbach (2011). "Müller Glial Cell-Provided Cellular Light Guidance through the Vital Guinea-Pig Retina". In: *Biophysical Journal*, 10111, pp. 2611–2619.

Akagi, T., J. Akita, M. Haruta, T. Suzuki, Y. Honda, T. Inoue, S. Yoshiura, R. Kageyama, T. Yatsu, M. Yamada, and M. Takahashi (2005). "Iris-Derived Cells from Adult Rodents and Primates Adopt Photoreceptor-Specific Phenotypes". en. In: *Investigative Ophthalmology & Visual Science*, 469, pp. 3411–3419.

Alberts, B. (2008). *Molecular biology of the cell.* Garland Science.

Alcaraz, J., L. Buscemi, M. Grabulosa, X. Trepat, B. Fabry, R. Farré, and D. Navajas (2003). "Microrheology of Human Lung Epithelial Cells Measured by Atomic Force Microscopy". In: *Biophysical Journal*, 843, pp. 2071–2079.

Alenghat, F. J., B. Fabry, K. Y. Tsai, W. H. Goldmann, and D. E. Ingber (2000). "Analysis of Cell Mechanics in Single Vinculin-Deficient Cells Using a Magnetic Tweezer". In: *Biochemical and Biophysical Research Communications*, 2771, pp. 93–99.

Ames, A., Y. Y. Li, E. C. Heher, and C. R. Kimble (1992). "Energy metabolism of rabbit retina as related to function: high cost of Na^+ transport". en. In: *The Journal of Neuroscience*, 123, pp. 840–853.

Amos, L. A. and W. B. Amos (1991). *Molecules of the Cytoskeleton.* Macmillan Education, Limited.

Arciniegas, A. and L. E. Amay (1986). "Mechanical Behavior of the Sclera". en. In: *Ophthalmologica*, 1931-2, pp. 45–55.

Balaur, E., J. M. Macak, L. Taveira, and P. Schmuki (2005a). "Tailoring the wettability of TiO$_2$ nanotube layers". In: *Electrochemistry Communications*, 710, pp. 1066–1070.

Balaur, E., J. M. Macak, H. Tsuchiya, and P. Schmuki (2005b). "Wetting behaviour of layers of TiO$_2$ nanotubes with different diameters". en. In: *Journal of Materials Chemistry*, 1542, pp. 4488–4491.

Balland, M., N. Desprat, D. Icard, S. Féréol, A. Asnacios, J. Browaeys, S. Hénon, and F. Gallet (2006). "Power laws in microrheology experiments on living cells: Comparative analysis and modeling". In: *Physical Review E*, 742, p. 021911.

Bao, G. and S. Suresh (2003). "Cell and molecular mechanics of biological materials". en. In: *Nature Materials*, 211, pp. 715–725.

Bauer, S., J. Park, J. Faltenbacher, S. Berger, K. v. d. Mark, and P. Schmuki (2009). "Size selective behavior of mesenchymal stem cells on ZrO$_2$ and TiO$_2$ nanotube arrays". en. In: *Integrative Biology*, 18-9, pp. 525–532.

Bausch, A. R., F. Ziemann, A. A. Boulbitch, K. Jacobson, and E. Sackmann (1998). "Local Measurements of Viscoelastic Parameters of Adherent Cell Surfaces by Magnetic Bead Microrheometry". In: *Biophysical Journal*, 754, pp. 2038–2049.

Bausch, A. R., W. Möller, and E. Sackmann (1999). "Measurement of Local Viscoelasticity and Forces in Living Cells by Magnetic Tweezers". In: *Biophysical Journal*, 761, pp. 573–579.

Bhat, S., D. Jun, B. C., and T. E. S Dahms (2012). "Viscoelasticity in Biological Systems: A Special Focus on Microbes". In: *Viscoelasticity - From Theory to Biological Applications*. Ed. by J. De Vicente. InTech.

Bianconi, E., A. Piovesan, F. Facchin, A. Beraudi, R. Casadei, F. Frabetti, L. Vitale, M. C. Pelleri, S. Tassani, F. Piva, S. Perez-Amodio, P. Strippoli, and S. Canaider (2013). "An estimation of the number of cells in the human body". In: *Annals of Human Biology*, 406, pp. 463–471.

Bill, A. (1975). "Blood circulation and fluid dynamics in the eye". en. In: *Physiological Reviews*, 553, pp. 383–417.

Binnig, G., C. F. Quate, and C. Gerber (1986). "Atomic Force Microscope". In: *Physical Review Letters*, 569, pp. 930–933.

Bisplinghoff, J. A., C. McNally, S. J. Manoogian, and S. M. Duma (2009). "Dynamic material properties of the human sclera". In: *Journal of Biomechanics*, 4210, pp. 1493–1497.

Bottega, W. J., P. L. Bishay, J. L. Prenner, and H. F. Fine (2013). "On the mechanics of a detaching retina". en. In: *Mathematical Medicine and Biology*, 304, pp. 287–310.

Bouchaud, J. P. (1992). "Weak ergodicity breaking and aging in disordered systems". In: *Journal de Physique I*, 29, pp. 1705–1713.

Brammer, K. S., S. Oh, C. J. Frandsen, and S. Ji (2011). "Biomaterials and Biotechnology Schemes Utilizing TiO$_2$ Nanotube Arrays". en. In: *Biomaterials Science and Engineering*. Ed. by R. Pignatello. InTech.

Brammer, K. S., S. Oh, C. J. Frandsen, and S. Jin (2010). "TiO$_2$ nanotube structures for enhanced cell and biological functionality". en. In: *JOM*, 624, pp. 50–55.

Brammer, K. S., C. J. Frandsen, and S. Jin (2012). "TiO$_2$ nanotubes for bone regeneration". In: *Trends in Biotechnology*, 306, pp. 315–322.

Bringmann, A. and P. Wiedemann (2012). "Müller Glial Cells in Retinal Disease". In: *Ophthalmologica*, 2271, pp. 1–19.

Bringmann, A., I. Iandiev, T. Pannicke, A. Wurm, M. Hollborn, P. Wiedemann, N. N. Osborne, and A. Reichenbach (2009a). "Cellular signaling and factors involved in Müller cell gliosis: Neuroprotective and detrimental effects". In: *Progress in Retinal and Eye Research*, 286, pp. 423–451.

Bringmann, A., T. Pannicke, J. Grosche, M. Francke, P. Wiedemann, S. N. Skatchkov, N. N. Osborne, and A. Reichenbach (2006). "Müller cells in the healthy and diseased retina". In: *Progress in Retinal and Eye Research*, 254, pp. 397–424.

Bringmann, A., A. Reichenbach, and P. Wiedemann (2004). "Pathomechanisms of Cystoid-Macular Edema". In: *Ophthalmic Research*, 365, pp. 241–249.

Bringmann, A., T. Pannicke, B. Biedermann, M. Francke, I. Iandiev, J. Grosche, P. Wiedemann, J. Albrecht, and A. Reichenbach (2009b). "Role of retinal glial cells in neurotransmitter uptake and metabolism". In: *Neurochemistry International*, 543-4, pp. 143–160.

Brodland, G. W. and R. Gordon (1990). "Intermediate Filaments May Prevent Buckling of Compressively Loaded Microtubules". In: *Journal of Biomechanical Engineering*, 1123, pp. 319–321.

7 Bibliography

Bursac, P., G. Lenormand, B. Fabry, M. Oliver, D. A. Weitz, V. Viasnoff, J. P. Butler, and J. J. Fredberg (2005). "Cytoskeletal remodelling and slow dynamics in the living cell". en. In: *Nature Materials*, 47, pp. 557–561.

Buttery, R. G., C. F. Hinrichsen, W. L. Weller, and J. R. Haight (1991). "How thick should a retina be? A comparative study of mammalian species with and without intraretinal vasculature". In: *Vision research*, 312, pp. 169–187.

Caffé, A. R., H. Visser, H. G. Jansen, and S. Sanyal (1989). "Histotypic differentiation of neonatal mouse retina in organ culture". In: *Current Eye Research*, 810, pp. 1083–1092.

Caffé, A. R., P. Ahuja, B. Holmqvist, S. Azadi, J. Forsell, I. Holmqvist, A. K. Söderpalm, and T. van Veen (2001). "Mouse retina explants after long-term culture in serum free medium". eng. In: *Journal of Chemical Neuroanatomy*, 224, pp. 263–273.

Caffé, A. R., A Söderpalm, and T van Veen (1993). "Photoreceptor-specific protein expression of mouse retina in organ culture and retardation of rd degeneration in vitro by a combination of basic fibroblast and nerve growth factors". eng. In: *Current eye research*, 128, pp. 719–726.

Campbell, I. C., B. Coudrillier, and C. Ross Ethier (2014). "Biomechanics of the Posterior Eye: A Critical Role in Health and Disease". In: *Journal of Biomechanical Engineering*, 1362, pp. 021005–021005.

Chen, J, Y Kanai, N. J. Cowan, and N Hirokawa (1992). "Projection domains of MAP2 and tau determine spacings between microtubules in dendrites and axons". eng. In: *Nature*, 3606405, pp. 674–677.

Chen, K. and J. D. Weiland (2010). "Anisotropic and inhomogeneous mechanical characteristics of the retina". In: *Journal of Biomechanics*, 437, pp. 1417–1421.

Chen, K. and J. D. Weiland (2012). "Mechanical Characteristics of the Porcine Retina in low temperatures". In: *Retina April 2012*, 324, pp. 844–847.

Chen, K., A. P. Rowley, J. D. Weiland, and M. S. Humayun (2014). "Elastic properties of human posterior eye". en. In: *Journal of Biomedical Materials Research Part A*, 1026, pp. 2001–2007.

Chen, K., A. P. Rowley, and J. D. Weiland (2010). "Elastic properties of porcine ocular posterior soft tissues". en. In: *Journal of Biomedical Materials Research Part A*, 93A2, pp. 634–645.

120

Cho, S., A. Wood, and M. R. Bowlby (2007). "Brain Slices as Models for Neurodegenerative Disease and Screening Platforms to Identify Novel Therapeutics". In: *Current Neuropharmacology*, 51, pp. 19–33.

Chou, T. and M. Siegel (2012). "A mechanical model of retinal detachment". en. In: *Physical Biology*, 94, p. 046001.

Conde, C. and A. Caceres (2009). "Microtubule assembly, organization and dynamics in axons and dendrites". en. In: *Nature Reviews Neuroscience*, 105, pp. 319–332.

Coughlin, M. F. and D. Stamenović (2003). "A Prestressed Cable Network Model of the Adherent Cell Cytoskeleton". In: *Biophysical Journal*, 842, pp. 1328–1336.

Crick, F. and A. Hughes (1950). "The physical properties of cytoplasm". In: *Experimental Cell Research*, 11, pp. 37–80.

Crocker, J. C., M. T. Valentine, E. R. Weeks, T. Gisler, P. D. Kaplan, A. G. Yodh, and D. A. Weitz (2000). "Two-Point Microrheology of Inhomogeneous Soft Materials". In: *Physical Review Letters*, 854, pp. 888–891.

Curtin, B. J. (1969). "Physiopathologic aspects of scleral stress-strain." In: *Transactions of the American Ophthalmological Society*, 67, pp. 417–461.

Dallacasagrande, V., M. Zink, S. Huth, A. Jakob, M. Müller, A. Reichenbach, J. A. Käs, and S. G. Mayr (2012). "Tailoring Substrates for Long-Term Organotypic Culture of Adult Neuronal Tissue". In: *Advanced Materials*, 2418, pp. 2399–2403.

Daviaud, N., E. Garbayo, P. C. Schiller, M. Perez-Pinzon, and C. N. Montero-Menei (2013). "Organotypic cultures as tools for optimizing central nervous system cell therapies". In: *Experimental Neurology*, 248, pp. 429–440.

David, T., S. Smye, T. James, and T. Dabbs (1997). "Time-dependent stress and displacement of the eye wall tissue of the human eye". In: *Medical Engineering & Physics*, 192, pp. 131–139.

Davson, H. (1972). "Part I-retinal structure and organization". In: *The Physiology of the Eye (Third Edition)*. Academic Press, pp. 115–127.

Del Priore, L. V. (2006). "Stiffness of Retinal and Choroidal Tissue: A Surface Wrinkling Analysis of Epiretinal Membranes and Choroidal Folds". In: *American Journal of Ophthalmology*, 1423, 435–440.e1.

Delaey, C. and J. Van de Voorde (2000). "Regulatory mechanisms in the retinal and choroidal circulation". In: *Ophthalmic research*, 326, pp. 249–256.

Deng, L., X. Trepat, J. P. Butler, E. Millet, K. G. Morgan, D. A. Weitz, and J. J. Fredberg (2006). "Fast and slow dynamics of the cytoskeleton". en. In: *Nature Materials*, 58, pp. 636–640.

Derda, R., A. Laromaine, A. Mammoto, S. K. Y. Tang, T. Mammoto, D. E. Ingber, and G. M. Whitesides (2009). "Paper-supported 3D cell culture for tissue-based bioassays". en. In: *Proceedings of the National Academy of Sciences*, 10644, pp. 18457–18462.

Desprat, N., A. Richert, J. Simeon, and A. Asnacios (2005). "Creep Function of a Single Living Cell". In: *Biophysical Journal*, 883, pp. 2224–2233.

Discher, D. E., P. Janmey, and Y.-l. Wang (2005). "Tissue Cells Feel and Respond to the Stiffness of Their Substrate". en. In: *Science*, 3105751, pp. 1139–1143.

Donovan, S. L. and M. A. Dyer (2007). "Preparation and square wave electroporation of retinal explant cultures". en. In: *Nature Protocols*, 16, pp. 2710–2718.

Dreher, Z., S. R. Robinson, and C. Distler (1992). "Müller cells in vascular and avascular retinae: a survey of seven mammals". In: *Journal of Comparative Neurology*, 3231, pp. 59–80.

Dreyer EB, Zurakowski D, Schumer RA, Podos SM, and Lipton SA (1996). "ELevated glutamate levels in the vitreous body of humans and monkeys with glaucoma". In: *Archives of Ophthalmology*, 1143, pp. 299–305.

Eilaghi, A., J. G. Flanagan, I. Tertinegg, C. A. Simmons, G. Wayne Brodland, and C. Ross Ethier (2010). "Biaxial mechanical testing of human sclera". In: *Journal of Biomechanics*, 439, pp. 1696–1701.

Elsheikh, A., D. Alhasso, and P. Rama (2008). "Biomechanical properties of human and porcine corneas". In: *Experimental Eye Research*, 865, pp. 783–790.

Elsheikh, A., B. Geraghty, D. Alhasso, J. Knappett, M. Campanelli, and P. Rama (2010). "Regional variation in the biomechanical properties of the human sclera". In: *Experimental Eye Research*, 905, pp. 624–633.

Engelsberg, K., B. Ehinger, J. Wassélius, and K. Johansson (2004). "Apoptotic cell death and microglial cell responses in cultured rat retina". en. In: *Graefe's Archive for Clinical and Experimental Ophthalmology*, 2423, pp. 229–239.

Engler, A. J., S. Sen, H. L. Sweeney, and D. E. Discher (2006). "Matrix Elasticity Directs Stem Cell Lineage Specification". In: *Cell*, 1264, pp. 677–689.

Ethier, C. R. (2006). "Scleral biomechanics and glaucomaâa connection?" In: *Canadian Journal of Ophthalmology / Journal Canadien d'Ophtalmologie*, 411, pp. 9–14.

Ethier, C. R. and C. A. Simmons (2007). *Introductory Biomechanics: From Cells to Organisms*. en. Cambridge University Press.

Evans, E and A Yeung (1989). "Apparent viscosity and cortical tension of blood granulocytes determined by micropipet aspiration." In: *Biophysical Journal*, 561, pp. 151–160.

Fabry, B., G. N. Maksym, R. D. Hubmayr, J. P. Butler, and J. J. Fredberg (1999). "Implications of heterogeneous bead behavior on cell mechanical properties measured with magnetic twisting cytometry". In: *Journal of Magnetism and Magnetic Materials*, 1941-3, pp. 120–125.

Fabry, B., G. N. Maksym, J. P. Butler, M. Glogauer, D. Navajas, and J. J. Fredberg (2001a). "Scaling the Microrheology of Living Cells". In: *Physical Review Letters*, 8714, p. 148102.

Fabry, B., G. N. Maksym, S. A. Shore, P. E. Moore, R. A. Panettieri, J. P. Butler, and J. J. Fredberg (2001b). "Selected Contribution: Time course and heterogeneity of contractile responses in cultured human airway smooth muscle cells". en. In: *Journal of Applied Physiology*, 912, pp. 986–994.

Fabry, B., G. Maksym, J. Butler, M. Glogauer, D. Navajas, N. Taback, E. Millet, and J. Fredberg (2003). "Time scale and other invariants of integrative mechanical behavior in living cells". In: *Physical Review E*, 684.

Fatt, I. and K. Shantinath (1971). "Flow conductivity of retina and its role in retinal adhesion". In: *Experimental Eye Research*, 122, pp. 218–226.

Felder, S. and E. L. Elson (1990). "Mechanics of fibroblast locomotion: quantitative analysis of forces and motions at the leading lamellas of fibroblasts." en. In: *The Journal of Cell Biology*, 1116, pp. 2513–2526.

7 Bibliography

Fernández, P., P. A. Pullarkat, and A. Ott (2006). "A Master Relation Defines the Nonlinear Viscoelasticity of Single Fibroblasts". In: *Biophysical Journal*, 9010, pp. 3796–3805.

Fischer, K. and S. G. Mayr (2011). "In-Plane Mechanical Response of TiO$_2$ Nanotube Arrays - Intrinsic Properties and Impact of Adsorbates for Sensor Applications". en. In: *Advanced Materials*, 2333, pp. 3838–3841.

Fletcher, D. A. and R. D. Mullins (2010). "Cell mechanics and the cytoskeleton". In: *Nature*, 4637280, pp. 485–492.

Flitney, E. W., E. R. Kuczmarski, S. A. Adam, and R. D. Goldman (2009). "Insights into the mechanical properties of epithelial cells: the effects of shear stress on the assembly and remodeling of keratin intermediate filaments". en. In: *The FASEB Journal*, 237, pp. 2110–2119.

Franze, K., J. Grosche, S. N. Skatchkov, S. Schinkinger, C. Foja, D. Schild, O. Uckermann, K. Travis, A. Reichenbach, and J. Guck (2007). "Müller cells are living optical fibers in the vertebrate retina". en. In: *Proceedings of the National Academy of Sciences*, 10420, pp. 8287–8292.

Franze, K., M. Francke, K. Günter, A. F. Christ, N. Körber, A. Reichenbach, and J. Guck (2011). "Spatial mapping of the mechanical properties of the living retina using scanning force microscopy". en. In: *Soft Matter*, 77, p. 3147.

Friberg, T. R. and J. W. Lace (1988). "A comparison of the elastic properties of human choroid and sclera". In: *Experimental Eye Research*, 473, pp. 429–436.

Fuchs, E. and D. W. Cleveland (1998). "A Structural Scaffolding of Intermediate Filaments in Health and Disease". en. In: *Science*, 2795350, pp. 514–519.

Fung, Y. C. (1993). *Biomechanics: Mechanical Properties of Living Tissues*. Springer.

Gähwiler, B. H, M Capogna, D Debanne, R. A McKinney, and S. M Thompson (1997). "Organotypic slice cultures: a technique has come of age". In: *Trends in Neurosciences*, 2010, pp. 471–477.

Gardel, M. L., J. H. Shin, F. C. MacKintosh, L. Mahadevan, P. Matsudaira, and D. A. Weitz (2004). "Elastic Behavior of Cross-Linked and Bundled Actin Networks". en. In: *Science*, 3045675, pp. 1301–1305.

Geiger, B., J. P. Spatz, and A. D. Bershadsky (2009). "Environmental sensing through focal adhesions". en. In: *Nature Reviews Molecular Cell Biology*, 101, pp. 21–33.

Ghazi, N. G. and W. R. Green (2002). "Pathology and pathogenesis of retinal detachment". en. In: *Eye*, 164, pp. 411–421.

Gogia, P. and D. M. Schneeweis (2004). "Neurite extension from rod bipolar cells in retinal cell and explant cultures". In: *26th Annual International Conference of the IEEE Engineering in Medicine and Biology Society, 2004. IEMBS '04*. Vol. 2, pp. 4229–4232.

Gongadze, E., D. Kabaso, S. Bauer, J. Park, P. Schmuki, and A. Iglic (2013). "Adhesion of Osteoblasts to a Vertically Aligned TiO$_2$ Nanotube Surface". en. In: *Mini-Reviews in Medicinal Chemistry*, 132, pp. 194–200.

Greaves, G. N., A. L. Greer, R. S. Lakes, and T. Rouxel (2011). "Poisson's ratio and modern materials". en. In: *Nature Materials*, 1011, pp. 823–837.

Griffith, L. G. and M. A. Swartz (2006). "Capturing complex 3D tissue physiology in vitro". en. In: *Nature Reviews Molecular Cell Biology*, 73, pp. 211–224.

Grytz, R., M. A. Fazio, M. J. A. Girard, V. Libertiaux, L. Bruno, S. Gardiner, C. A. Girkin, and J. Crawford Downs (2014). "Material properties of the posterior human sclera". In: *Journal of the Mechanical Behavior of Biomedical Materials*, 29, pp. 602–617.

Guck, J, R Ananthakrishnan, H Mahmood, T. J. Moon, C. C. Cunningham, and J Kas (2001). "The optical stretcher: a novel laser tool to micromanipulate cells." In: *Biophysical Journal*, 812, pp. 767–784.

Guck, J., S. Schinkinger, B. Lincoln, F. Wottawah, S. Ebert, M. Romeyke, D. Lenz, H. M. Erickson, R. Ananthakrishnan, D. Mitchell, J. Kas, S. Ulvick, and C. Bilby (2005). "Optical Deformability as an Inherent Cell Marker for Testing Malignant Transformation and Metastatic Competence". In: *Biophysical Journal*, 885, pp. 3689–3698.

Guck, J., R. Ananthakrishnan, C. C. Cunningham, and J. Käs (2002). "Stretching biological cells with light". In: *Journal of Physics: Condensed Matter*, 1419, pp. 4843–4856.

Hatakeyama, J. and R. Kageyama (2002). "Retrovirus-mediated gene transfer to retinal explants". In: *Methods*, 284, pp. 387–395.

7 Bibliography

Haycock, J. W. (2011). "3D Cell Culture: A Review of Current Approaches and Techniques". en. In: *3D Cell Culture.* Ed. by J. W. Haycock. Methods in Molecular Biology 695. Humana Press, pp. 1–15.

Heegaard, S., O. A. Jensen, and J. U. Prause (1986). "Structure and composition of the inner limiting membrane of the retina". en. In: *Graefe's Archive for Clinical and Experimental Ophthalmology*, 2244, pp. 355–360.

Helmholtz, H. v. (2005). *Treatise on Physiological Optics.* Dover Publications.

Henderson, E., P. G. Haydon, and D. S. Sakaguchi (1992). "Actin filament dynamics in living glial cells imaged by atomic force microscopy". en. In: *Science*, 2575078, pp. 1944–1946.

Hendrickson, A. (2005). "Organization of the adult primate fovea". In: *Macular degeneration.* Springer, pp. 1–23.

Hendrickson, A., D. Possin, L. Vajzovic, and C. A. Toth (2012). "Histologic Development of the Human Fovea From Midgestation to Maturity". In: *American Journal of Ophthalmology*, 1545, 767–778.e2.

Hendrickson, A. E. and C. Yuodelis (1984). "The Morphological Development of the Human Fovea". In: *Ophthalmology*, 916, pp. 603–612.

Hjortdal, J. . (1994). "Young's Modulus of Elasticity for the Human Cornea". In: *Journal of Cataract & Refractive Surgery*, 206, p. 672.

Hochmuth, R. M. (2000). "Micropipette aspiration of living cells". In: *Journal of Biomechanics*, 331, pp. 15–22.

Hoffman, B. D. and J. C. Crocker (2009). "Cell Mechanics: Dissecting the Physical Responses of Cells to Force". In: *Annual Review of Biomedical Engineering*, 111, pp. 259–288.

Homma, K., Y. Koriyama, K. Mawatari, Y. Higuchi, J. Kosaka, and S. Kato (2007). "Early downregulation of IGF-I decides the fate of rat retinal ganglion cells after optic nerve injury". In: *Neurochemistry International*, 505, pp. 741–748.

Howard, J. (2001). *Mechanics of motor proteins and the cytoskeleton.* Sinauer Associates, Publishers.

126

Hubel, D. H. (1995). *Eye, Brain, and Vision.* Henry Holt and Company.

Huo, K., B. Gao, J. Fu, L. Zhao, and P. K. Chu (2014). "Fabrication, modification, and biomedical applications of anodized TiO$_2$ nanotube arrays". en. In: *RSC Advances*, 433, pp. 17300–17324.

Ingber, D. E. (1997). "Tensegrity: the architectural basis of cellular mechanotransduction". eng. In: *Annual review of physiology*, 59, pp. 575–599.

Ingber, D. E. (1993). "Cellular tensegrity: defining new rules of biological design that govern the cytoskeleton". en. In: *Journal of Cell Science*, 1043, pp. 613–627.

Ishijima, A., T. Doi, K. Sakurada, and T. Yanagida (1991). "Sub-piconewton force fluctuations of actomyosin in vitro". en. In: *Nature*, 3526333, pp. 301–306.

Israelachvili, J. N. (2011). "Chapter 13 - Van der Waals Forces between Particles and Surfaces". In: *Intermolecular and Surface Forces (Third Edition).* San Diego: Academic Press, pp. 253–289.

Jablonski, M. M., J. Tombran-Tink, D. A. Mrazek, and A. Iannaccone (2001). "Pigment epithelium-derived factor supports normal Müller cell development and glutamine synthetase expression after removal of the retinal pigment epithelium". en. In: *Glia*, 351, pp. 14–25.

Jackson, T. L., J. Hillenkamp, T. H. Williamson, K. W. Clarke, A. I. Almubarak, and J. Marshall (2003). "An Experimental Model of Rhegmatogenous Retinal Detachment: Surgical Results and Glial Cell Response". en. In: *Investigative Ophthalmology & Visual Science*, 449, pp. 4026–4034.

Janmey, P. A., U. Euteneuer, P. Traub, and M. Schliwa (1991). "Viscoelastic properties of vimentin compared with other filamentous biopolymer networks." en. In: *The Journal of Cell Biology*, 1131, pp. 155–160.

Janmey, P. and C. Schmidt (2006). "Experimental measurements of intracellular mechanics". In: *Cytoskeletal Mechanics.* Cambridge Texts in Biomedical Engineering. Cambridge University Press.

Jiang, Y., P. J. Swart, A. Saxena, M. Asipauskas, and J. A. Glazier (1999). "Hysteresis and avalanches in two-dimensional foam rheology simulations". In: *Physical Review E*, 595, pp. 5819–5832.

Johansson, K. and B. Ehinger (2005). "Structural changes in the developing retina maintained in vitro". In: *Vision Research*, 4525-26, pp. 3235–3243.

Johnson, T. V. and K. R. Martin (2008). "Development and Characterization of an Adult Retinal Explant Organotypic Tissue Culture System as an In Vitro Intraocular Stem Cell Transplantation Model". en. In: *Investigative Ophthalmology & Visual Science*, 498, pp. 3503–3512.

Jonas, M., H. Huang, R. D. Kamm, and P. T. C. So (2008). "Fast Fluorescence Laser Tracking Microrheometry, I: Instrument Development". In: *Biophysical Journal*, 944, pp. 1459–1469.

Jones, I. L., M. Warner, and J. D. Stevens (1992). "Mathematical modelling of the elastic properties of retina: A determination of Young's modulus". en. In: *Eye*, 66, pp. 556–559.

Justice, B. A., N. A. Badr, and R. A. Felder (2009). "3D cell culture opens new dimensions in cell-based assays". In: *Drug Discovery Today*, 141-2, pp. 102–107.

Kaempf, S., P. Walter, A. K. Salz, and G. Thumann (2008). "Novel organotypic culture model of adult mammalian neurosensory retina in co-culture with retinal pigment epithelium". In: *Journal of Neuroscience Methods*, 1731, pp. 47–58.

Kain HL (1984). "A new model for examining chorioretinal adhesion experimentally". In: *Archives of Ophthalmology*, 1024, pp. 608–611.

Kamimura, S and K Takahashi (1981). "Direct measurement of the force of microtubule sliding in flagella". eng. In: *Nature*, 2935833, pp. 566–568.

Kamm, R., J. Lammerding, and M. Mofrad (2010). "Cellular Nanomechanics". In: *Springer Handbook of Nanotechnology*. Ed. by P. B. Bhushan. Springer Berlin Heidelberg, pp. 1171–1200.

Kandel, E. and J. Schwartz (2013). *Principles of Neural Science, Fifth Edition*. McGraw Hill Professional.

Karcher, H., J. Lammerding, H. Huang, R. T. Lee, R. D. Kamm, and M. R. Kaazempur-Mofrad (2003). "A Three-Dimensional Viscoelastic Model for Cell Deformation with Experimental Verification". In: *Biophysical Journal*, 855, pp. 3336–3349.

Katsuki, H., R. Yamamoto, D. Nakata, T. Kume, and A. Akaike (2004). "Neuronal Nitric Oxide Synthase Is Crucial for Ganglion Cell Death in Rat Retinal Explant Cultures". en. In: *Journal of Pharmacological Sciences*, 941, pp. 77–80.

Kelly, P. (2013). *Solid Mechanics Part I: An Introduction to Solid Mechanics.* Univeristy of Auckland.

Khademhosseini, A. (2008). *Micro and Nanoengineering of the Cell Microenvironment: Technologies and Applications.* Artech House.

Kirchhof, B., K. T. Oh, M. E. Hartnett, and M. B. Landers III (2013). "Chapter 95 - Pathogenetic Mechanisms of Retinal Detachment". In: *Retina (Fifth Edition).* London: W.B. Saunders, pp. 1616–1621.

Kirmizis, D. and S. Logothetidis (2010). "Atomic force microscopy probing in the measurement of cell mechanics". In: *International Journal of Nanomedicine*, 5, pp. 137–145.

Kishino, A. and T. Yanagida (1988). "Force measurements by micromanipulation of a single actin filament by glass needles". en. In: *Nature*, 3346177, pp. 74–76.

Kobuch, K., W. A. Herrmann, C. Framme, H. G. Sachs, V.-P. Gabel, and J. Hillenkamp (2008). "Maintenance of adult porcine retina and retinal pigment epithelium in perfusion culture: Characterisation of an organotypic in vitro model". In: *Experimental Eye Research*, 864, pp. 661–668.

Koehler, S. A., S. Hilgenfeldt, and H. A. Stone (1999). "Liquid Flow through Aqueous Foams: The Node-Dominated Foam Drainage Equation". In: *Physical Review Letters*, 8221, pp. 4232–4235.

Koizumi, A., G. Zeck, Y. Ben, R. H. Masland, and T. C. Jakobs (2007). "Organotypic Culture of Physiologically Functional Adult Mammalian Retinas". In: *PLoS ONE*, 22, e221.

Kolb, H. (2003). "How the retina works". In: *American Scientist*, 911, pp. 28–35.

Kollmannsberger, P. and B. Fabry (2009). "Active soft glassy rheology of adherent cells". en. In: *Soft Matter*, 59, pp. 1771–1774.

Kollmannsberger, P. and B. Fabry (2007). "High-force magnetic tweezers with force feedback for biological applications". In: *Review of Scientific Instruments*, 7811, p. 114301.

7 Bibliography

Kollmannsberger, P. and B. Fabry (2011). "Linear and Nonlinear Rheology of Living Cells". In: *Annual Review of Materials Research*, 411, pp. 75–97.

Koriyama, Y., K. Homma, K. Sugitani, Y. Higuchi, T. Matsukawa, D. Murayama, and S. Kato (2007). "Upregulation of IGF-I in the goldfish retinal ganglion cells during the early stage of optic nerve regeneration". In: *Neurochemistry International*, 505, pp. 749–756.

Kowalski, D., D. Kim, and P. Schmuki (2013). "TiO$_2$ nanotubes, nanochannels and mesosponge: Self-organized formation and applications". In: *Nano Today*, 83, pp. 235–264.

Kuhrt, H., M. Walski, A. Reichenbach, and J. Albrecht (2004). "Rabbit retinal organ culture as an in-vitro model of hepatic retinopathy". en. In: *Graefe's Archive for Clinical and Experimental Ophthalmology*, 2426, pp. 512–522.

Lakawicz, J. M., W. J. Bottega, J. L. Prenner, and H. F. Fine (2014). "An analysis of the mechanical behaviour of a detaching retina". en. In: *Mathematical Medicine and Biology*, dqt023.

Lam, T. T., J. M. K. Kwong, and M. O. M. Tso (2003). "Early Glial Responses after Acute Elevated Intraocular Pressure in Rats". en. In: *Investigative Ophthalmology & Visual Science*, 442, pp. 638–645.

Langer, R. and D. A. Tirrell (2004). "Designing materials for biology and medicine". en. In: *Nature*, 4286982, pp. 487–492.

Laranjeira, M. S., M. H. Fernandes, and F. J. Monteiro (2013). "Response of Monocultured and Co-Cultured Human Microvascular Endothelial Cells and Mesenchymal Stem Cells to Macroporous Granules of Nanostructured-Hydroxyapatite Agglomerates". In: *Journal of Biomedical Nanotechnology*, 99, pp. 1594–1606.

Lari, D. R., D. S. Schultz, A. S. Wang, O.-T. Lee, and J. M. Stewart (2012). "Scleral mechanics: Comparing whole globe inflation and uniaxial testing". In: *Experimental Eye Research*, 941, pp. 128–135.

Last, J. A., S. J. Liliensiek, P. F. Nealey, and C. J. Murphy (2009). "Determining the mechanical properties of human corneal basement membranes with atomic force microscopy". In: *Journal of Structural Biology*, 1671, pp. 19–24.

Laughlin, S. B., R. R. de Ruyter van Steveninck, and J. C. Anderson (1998). "The metabolic cost of neural information". en. In: *Nature Neuroscience*, 11, pp. 36–41.

Lavik, E. and R. Langer (2004). "Tissue engineering: current state and perspectives". In: *Applied Microbiology & Biotechnology*, 651, pp. 1–8.

Leaver, S., A. Harvey, and G. Plant (2006). "Adult olfactory ensheathing glia promote the long-distance growth of adult retinal ganglion cell neurites in vitro". en. In: *Glia*, 535, pp. 467–476.

Lee, J., M. J. Cuddihy, and N. A. Kotov (2008). "Three-Dimensional Cell Culture Matrices: State of the Art". In: *Tissue Engineering Part B: Reviews*, 141, pp. 61–86.

Lewis, G. P., D. G. Charteris, C. S. Sethi, and S. K. Fisher (2002). "Animal models of retinal detachment and reattachment: identifying cellular events that may affect visual recovery". en. In: *Eye*, 164, pp. 375–387.

Lewis, G. P., K. A. Linberg, and S. K. Fisher (1998). "Neurite outgrowth from bipolar and horizontal cells after experimental retinal detachment." en. In: *Investigative Ophthalmology & Visual Science*, 392, pp. 424–434.

Lewis, G. P. and S. K. Fisher (2003). "Up-Regulation of Glial Fibrillary Acidic Protein in Response to Retinal Injury: Its Potential Role in Glial Remodeling and a Comparison to Vimentin Expression". In: *International Review of Cytology.* Vol. Volume 230. Academic Press, pp. 263–290.

Li, S. Z. and A. K. Jain (2009). *Encyclopedia of Biometrics: I-Z.* Vol. 2. Springer.

Liljekvist-Larsson, I. and K. Johansson (2005). "Retinal neurospheres prepared as tissue for transplantation". In: *Developmental Brain Research*, 1602, pp. 194–202.

Lim, C. T., E. H. Zhou, A. Li, S. R. K. Vedula, and H. X. Fu (2006). "Experimental techniques for single cell and single molecule biomechanics". In: *Materials Science and Engineering: C*, 268, pp. 1278–1288.

Lin, R.-Z. and H.-Y. Chang (2008). "Recent advances in three-dimensional multicellular spheroid culture for biomedical research". en. In: *Biotechnology Journal*, 39-10, pp. 1172–1184.

Lin, Y.-C., G. H. Koenderink, F. C. MacKintosh, and D. A. Weitz (2011). "Control of non-linear elasticity in F-actin networks with microtubules". en. In: *Soft Matter*, 73, pp. 902–906.

Lindqvist, N., Q. Liu, J. Zajadacz, K. Franze, and A. Reichenbach (2010). "Retinal Glial (Muller) Cells: Sensing and Responding to Tissue Stretch". en. In: *Investigative Ophthalmology & Visual Science*, 513, pp. 1683–1690.

Linsenmeier, R. A. and L. Padnick-Silver (2000). "Metabolic Dependence of Photoreceptors on the Choroid in the Normal and Detached Retina". en. In: *Investigative Ophthalmology & Visual Science*, 4110, pp. 3117–3123.

Lodish, H. (2013). *Molecular cell biology*. Freeman.

London, A., I. Benhar, and M. Schwartz (2013). "The retina as a window to the brain-from eye research to CNS disorders". en. In: *Nature Reviews Neurology*, 91, pp. 44–53.

Long, M. and H. J Rack (1998). "Titanium alloys in total joint replacement-a materials science perspective". In: *Biomaterials*, 1918, pp. 1621–1639.

Loomis, W. F., D. Fuller, E. Gutierrez, A. Groisman, and W.-J. Rappel (2012). "Innate Non-Specific Cell Substratum Adhesion". In: *PLoS ONE*, 78, e42033.

Lu, Y.-B., I. Iandiev, M. Hollborn, N. Korber, E. Ulbricht, P. G. Hirrlinger, T. Pannicke, E.-Q. Wei, A. Bringmann, H. Wolburg, U. Wilhelmsson, M. Pekny, P. Wiedemann, A. Reichenbach, and J. A. Käs (2010). "Reactive glial cells: increased stiffness correlates with increased intermediate filament expression". In: *The FASEB Journal*, 252, pp. 624–631.

Lu, Y.-B, T. Pannicke, E.-Q. Wei, A. Bringmann, P. Wiedemann, G. Habermann, E. Buse, J. A. Käs, and A. Reichenbach (2013). "Biomechanical properties of retinal glial cells: Comparative and developmental data". In: *Experimental Eye Research*, 113, pp. 60–65.

Lu, Y.-B., K. Franze, G. Seifert, C. Steinhäuser, F. Kirchhoff, H. Wolburg, J. Guck, P. Janmey, E.-Q. Wei, and J. Käs (2006). "Viscoelastic properties of individual glial cells and neurons in the CNS". In: *Proceedings of the National Academy of Sciences*, 10347, pp. 17759–17764.

Lundkvist, A., A. Reichenbach, C. Betsholtz, P. Carmeliet, H. Wolburg, and M. Pekny (2004). "Under stress, the absence of intermediate filaments from Müller cells in the

retina has structural and functional consequences". en. In: *Journal of Cell Science*, 11716, pp. 3481–3488.

Lye, M. H., T. C. Jakobs, R. H. Masland, and A. Koizumi (2007). "Organotypic Culture of Adult Rabbit Retina". In: *Journal of Visualized Experiments : JoVE*, 3.

Lythgoe, M. F., N. R. Sibson, and N. G. Harris (2003). "Neuroimaging of animal models of brain disease". en. In: *British Medical Bulletin*, 651, pp. 235–257.

Ma, K. and S. Tc (1995). "Morphogenesis of retinal ganglion cells: a model of dendritic, mosaic, and foveal development." eng. In: *Perspectives on developmental neurobiology*, 33, pp. 177–194.

Mack, A. F., D. Uhlmann, A. Germer, Á. Szél, V. Enzmann, and A. Reichenbach (2003). "Differentiation of cones in cultured rabbit retina: effects of retinal pigment epithelial cell-conditioned medium". In: *Neuroscience Letters*, 3411, pp. 53–56.

MacKintosh, F. C., J. Käs, and P. A. Janmey (1995). "Elasticity of Semiflexible Biopolymer Networks". In: *Physical Review Letters*, 7524, pp. 4425–4428.

Maggs, D. J., P. Miller, and R. Ofri (2012). *Slatter's Fundamentals of Veterinary Ophthalmology*. en. Elsevier Health Sciences.

Mahaffy, R. E., C. K. Shih, F. C. MacKintosh, and J. Käs (2000). "Scanning Probe-Based Frequency-Dependent Microrheology of Polymer Gels and Biological Cells". In: *Physical Review Letters*, 854, pp. 880–883.

Maksym, G. N., B. Fabry, J. P. Butler, D. Navajas, D. J. Tschumperlin, J. D. Laporte, and J. J. Fredberg (2000). "Mechanical properties of cultured human airway smooth muscle cells from 0.05 to 0.4 Hz". en. In: *Journal of Applied Physiology*, 894, pp. 1619–1632.

Manabe, S.-i., S. Kashii, Y. Honda, R. Yamamoto, H. Katsuki, and A. Akaike (2002). "Quantification of axotomized ganglion cell death by explant culture of the rat retina". In: *Neuroscience Letters*, 3341, pp. 33–36.

Mandadapu, K. K., S. Govindjee, and M. R. Mofrad (2008). "On the cytoskeleton and soft glassy rheology". In: *Journal of Biomechanics*, 417, pp. 1467–1478.

Mark, K. v. d., S. Bauer, J. Park, and P. Schmuki (2009). "Another look at 'Stem cell fate dictated solely by altered nanotube dimension'". en. In: *Proceedings of the National Academy of Sciences*, 10624, E60–E60.

7 Bibliography

Marmor, M. F. (1993). "Chapter 8 Mechanisms of retinal adhesion". In: *Progress in Retinal Research*, 12, pp. 179–204.

Mastronarde, D. N., M. A. Thibeault, and M. W. Dubin (1984). "Non-uniform postnatal growth of the cat retina". en. In: *The Journal of Comparative Neurology*, 2284, pp. 598–608.

Matsumoto, H., J. W. Miller, and D. G. Vavvas (2013). "Retinal Detachment Model in Rodents by Subretinal Injection of Sodium Hyaluronate". In: *Journal of Visualized Experiments : JoVE*, 79.

Mayr, S. G., M. Moske, and K. Samwer (1999). "Identification of key parameters by comparing experimental and simulated growth of vapor-deposited amorphous $Zr_{65}Al_{7.5}Cu_{27.5}$ films". In: *Physical Review B*, 6024, pp. 16950–16955.

Mayr, S., M. Zink, V. Dallacasagrande, J. Käs, and A. Reichenbach (2013). "Nanotube carrier substrate for primary tissue culture". Pat. US20130017607 A1.

McKernan, D. P., C. Caplis, M. Donovan, C. J. O'Brien, and T. G. Cotter (2006). "Age-Dependent Susceptibility of the Retinal Ganglion Cell Layer to Cell Death". en. In: *Investigative Ophthalmology & Visual Science*, 473, pp. 807–814.

Metea, M. R. and E. A. Newman (2006). "Glial Cells Dilate and Constrict Blood Vessels: A Mechanism of Neurovascular Coupling". en. In: *The Journal of Neuroscience*, 2611, pp. 2862–2870.

Mitchison, J. M. and M. M. Swann (1954). "The Mechanical Properties of the Cell Surface I. The Cell Elastimeter". en. In: *Journal of Experimental Biology*, 313, pp. 443–460.

Mofrad, M. R. (2009). "Rheology of the Cytoskeleton". In: *Annual Review of Fluid Mechanics*, 411, pp. 433–453.

Mogil, J. S. (2009). "Animal models of pain: progress and challenges". In: *Nature Reviews Neuroscience*, 104, pp. 283–294.

Moon, K.-S., S.-H. Yu, J.-M. Bae, and S. Oh (2012). "Biphasic Osteogenic Characteristics of Human Mesenchymal Stem Cells Cultured on Nanotubes of Different Diameters". en. In: *Journal of Nanomaterials*, 2012, e252481.

Moritoh, S., K. F. Tanaka, H. Jouhou, K. Ikenaka, and A. Koizumi (2010). "Organotypic Tissue Culture of Adult Rodent Retina Followed by Particle-Mediated Acute Gene Transfer In Vitro". In: *PLoS ONE*, 59, e12917.

Morrison, B., D. K. Cullen, and M. LaPlaca (2011). "In Vitro Models for Biomechanical Studies of Neural Tissues". en. In: *Neural Tissue Biomechanics*. Ed. by L. E. Bilston. Studies in Mechanobiology, Tissue Engineering and Biomaterials 3. Springer Berlin Heidelberg, pp. 247–285.

Mosinger Ogilvie, J., J. D. Speck, J. M. Lett, and T. T. Fleming (1999). "A reliable method for organ culture of neonatal mouse retina with long-term survival". In: *Journal of Neuroscience Methods*, 871, pp. 57–65.

Müller Holt, B. (2011). "Challenge of the Soft-tissue to Device Interface: A Rheology-based Approach to Biomaterial Development". PhD thesis. Brown University.

Newman, E. A. (2003). "New roles for astrocytes: Regulation of synaptic transmission". In: *Trends in Neurosciences*, 2610, pp. 536–542.

Norman, R. E., J. G. Flanagan, I. A. Sigal, S. M. K. Rausch, I. Tertinegg, and C. R. Ethier (2011). "Finite element modeling of the human sclera: Influence on optic nerve head biomechanics and connections with glaucoma". In: *Experimental Eye Research*, 931, pp. 4–12.

Odell, I. D. and D. Cook (2013). "Immunofluorescence Techniques". en. In: *Journal of Investigative Dermatology*, 1331, e4.

Ofri, R. (2008). "Chapter 15 - Retina". In: *Slatter's Fundamentals of Veterinary Ophthalmology (Fourth Edition)*. Ed. by D. J. Maggs, P. E. Miller, and R. Ofri. Saint Louis: W.B. Saunders, pp. 285–317.

Ogilvie, J. M., J. D. Speck, J. M. Lett, and T. T. Fleming (1999). "A reliable method for organ culture of neonatal mouse retina with long-term survival". eng. In: *Journal of Neuroscience Methods*, 871, pp. 57–65.

Oh, S., K. S. Brammer, Y. S. J. Li, D. Teng, A. J. Engler, S. Chien, and S. Jin (2009). "Stem cell fate dictated solely by altered nanotube dimension". en. In: *Proceedings of the National Academy of Sciences*, 1067, pp. 2130–2135.

Omri, S, B Omri, M Savoldelli, L Jonet, B Thillaye-Goldenberg, G Thuret, P Gain, J. C. Jeanny, P Crisanti, and F. Behar-Cohen (2010). "The outer limiting membrane (OLM)

revisited: clinical implications". In: *Clinical Ophthalmology (Auckland, N.Z.)* 4, pp. 183–195.

Otterbein, L. R., C. Cosio, P. Graceffa, and R. Dominguez (2002). "Crystal structures of the vitamin D-binding protein and its complex with actin: structural basis of the actin-scavenger system". eng. In: *Proceedings of the National Academy of Sciences of the United States of America*, 9912, pp. 8003–8008.

Pampaloni, F., E. G. Reynaud, and E. H. K. Stelzer (2007). "The third dimension bridges the gap between cell culture and live tissue". en. In: *Nature Reviews Molecular Cell Biology*, 810, pp. 839–845.

Pang, I.-H. and A. F. Clark (2010). *Animal Models for Retinal Diseases*. Neuromethods.

Park, J., S. Bauer, K. von der Mark, and P. Schmuki (2007). "Nanosize and Vitality : TiO$_2$ Nanotube Diameter Directs Cell Fate". In: *Nano Letters*, 76, pp. 1686–1691.

Park, J., S. Bauer, P. Schmuki, and K. von der Mark (2009a). "Narrow Window in Nanoscale Dependent Activation of Endothelial Cell Growth and Differentiation on TiO$_2$ Nanotube Surfaces". In: *Nano Letters*, 99, pp. 3157–3164.

Park, J., S. Bauer, A. Pittrof, M. S. Killian, P. Schmuki, and K. von der Mark (2012). "Synergistic Control of Mesenchymal Stem Cell Differentiation by Nanoscale Surface Geometry and Immobilized Growth Factors on TiO$_2$ Nanotubes". en. In: *Small*, 81, pp. 98–107.

Park, J., S. Bauer, K. A. Schlegel, F. W. Neukam, K. von der Mark, and P. Schmuki (2009b). "TiO$_2$ Nanotube Surfaces: 15 nm-An Optimal Length Scale of Surface Topography for Cell Adhesion and Differentiation". en. In: *Small*, 56, pp. 666–671.

Pelletier, V., N. Gal, P. Fournier, and M. Kilfoil (2009). "Microrheology of Microtubule Solutions and Actin-Microtubule Composite Networks". In: *Physical Review Letters*, 10218.

Peng, L., M. L. Eltgroth, T. J. LaTempa, C. A. Grimes, and T. A. Desai (2009). "The effect of TiO$_2$ nanotubes on endothelial function and smooth muscle proliferation". In: *Biomaterials*, 307, pp. 1268–1272.

Peng, L., A. J. Barczak, R. A. Barbeau, Y. Xiao, T. J. LaTempa, C. A. Grimes, and T. A. Desai (2010). "Whole Genome Expression Analysis Reveals Differential Effects of TiO$_2$ Nanotubes on Vascular Cells". In: *Nano Letters*, 101, pp. 143–148.

Pevsner, J. (2002). "Leonardo da Vinci's contributions to neuroscience". In: *Trends in Neurosciences*, 254, pp. 217–220.

Phillips, J. R. and N. A. McBrien (1995). "Form deprivation myopia: elastic properties of sclera". en. In: *Ophthalmic and Physiological Optics*, 155, pp. 357–362.

Piccoli, C., D. Boffoli, and N. Capitanio (2004). "Comparative analysis of mitochondria selective dyes in different cell types detected by Confocal Laser Scanning Microscopy: methods and applications". In: *Comp. Gen. Pharmacol*, 2, pp. 130–139.

Pinzón-Duarte, G., K. Kohler, B. Arango-González, and E. Guenther (2000). "Cell differentiation, synaptogenesis, and influence of the retinal pigment epithelium in a rat neonatal organotypic retina culture". In: *Vision Research*, 4025, pp. 3455–3465.

Pipkin, A. C (1986). *Lectures on Viscoelasticity Theory*. Springer New York.

Pollard, T. D. and G. G. Borisy (2003). "Cellular Motility Driven by Assembly and Disassembly of Actin Filaments". In: *Cell*, 1124, pp. 453–465.

Polyak, L. (1941). *The retina: the anatomy and the histology of the retina in man, ape, and monkey, including the consideration of visual functions, the history of physiological optics, and the histological laboratory technique.* University of Chicago Press: Chicago.

Pournaras, C. J., E. Rungger-Brändle, C. E. Riva, S. H. Hardarson, and E. Stefansson (2008). "Regulation of retinal blood flow in health and disease". In: *Progress in Retinal and Eye Research*, 273, pp. 284–330.

Provis, J. M., A. M. Dubis, T. Maddess, and J. Carroll (2013). "Adaptation of the central retina for high acuity vision: Cones, the fovea and the avascular zone". In: *Progress in Retinal and Eye Research*, 35, pp. 63–81.

Provis, J. M., C. M. Diaz, and B. Dreher (1998). "Ontogeny of the primate fovea: a central issue in retinal development". In: *Progress in neurobiology*, 545, pp. 549–581.

Puig-De-Morales, M., M. Grabulosa, J. Alcaraz, J. Mullol, G. N. Maksym, J. J. Fredberg, and D. Navajas (2001). "Measurement of cell microrheology by magnetic twisting cytometry with frequency domain demodulation". en. In: *Journal of Applied Physiology*, 913, pp. 1152–1159.

Pullarkat, P. A., P. A. Fernández, and A. Ott (2007). "Rheological properties of the Eukaryotic cell cytoskeleton". In: *Physics Reports*, 4491-3, pp. 29–53.

Radmacher, M, M Fritz, C. M. Kacher, J. P. Cleveland, and P. K. Hansma (1996). "Measuring the viscoelastic properties of human platelets with the atomic force microscope." In: *Biophysical Journal*, 701, pp. 556–567.

Rand, R. P. (1964). "Mechanical Properties of the Red Cell Membrane". In: *Biophysical Journal*, 44, pp. 303–316.

Rani, S., S. C. Roy, M. Paulose, O. K. Varghese, G. K. Mor, S. Kim, S. Yoriya, T. J. LaTempa, and C. A. Grimes (2010). "Synthesis and applications of electrochemically self-assembled titania nanotube arrays". en. In: *Physical Chemistry Chemical Physics*, 1212, p. 2780.

Rauen, T. and M. Wießner (2000). "Fine tuning of glutamate uptake and degradation in glial cells: common transcriptional regulation of GLAST1 and GS". In: *Neurochemistry International*, 372-3, pp. 179–189.

Reichenbach, A. and S. R. Robinson (1995). "Phylogenetic constraints on retinal organisation and development". In: *Progress in Retinal and Eye Research*, 151, pp. 139–171.

Reichenbach, A., E. Hagen, K. Schippel, G. Brückner, W. Reichelt, and L. Leibnitz (1988a). "Cytotopographical specialization of enzymatically isolated rabbit retinal Müller (glial) cells: structure, ultrastructure, and 3H-ouabain binding sites". eng. In: *Zeitschrift Für Mikroskopisch-Anatomische Forschung*, 1026, pp. 897–912.

Reichenbach, A., W. Eberhardt, R. Scheibe, C. Deich, B. Seifert, W. Reichelt, K. Dähnert, and M. Rödenbeck (1991). "Development of the rabbit retina. IV. Tissue tensility and elasticity in dependence on topographic specializations". In: *Experimental Eye Research*, 532, pp. 241–251.

Reichenbach, A., E. Hagen, K. Schippel, and W. Eberhardt (1988b). "Quantitative electron microscopy of rabbit Müller (glial) cells in dependence on retinal topography". eng. In: *Zeitschrift Für Mikroskopisch-Anatomische Forschung*, 1025, pp. 721–755.

Reichenbach, A. and A. Bringmann (2010). *Müller Cells in the Healthy and Diseased Retina.* Springer New York.

Reichenbach, A. and A. Bringmann (2013). "New functions of Müller cells". en. In: *Glia*, 615, pp. 651–678.

Reidel, B., W. Orisme, T. Goldmann, W. C. Smith, and U. Wolfrum (2006). "Photoreceptor vitality in organotypic cultures of mature vertebrate retinas validated by light-dependent molecular movements". In: *Vision Research*, 4627, pp. 4464–4471.

Reinelt, D. A. and A. M. Kraynik (1993). "Large Elastic Deformations of Three-Dimensional Foams and Highly Concentrated Emulsions". In: *Journal of Colloid and Interface Science*, 1592, pp. 460–470.

Renner, W., W. W. Franke, E. Schmid, N. Geisler, K. Weber, and E. Mandelkow (1981). "Reconstitution of intermediate-sized filaments from denatured monomeric vimentin". In: *Journal of Molecular Biology*, 1492, pp. 285–306.

Ristoff, E., M. Burstedt, A. Larsson, and L. Wachtmeister (2007). "Progressive retinal dystrophy in two sisters with glutathione synthetase (GS) deficiency". en. In: *Journal of Inherited Metabolic Disease*, 301, pp. 102–102.

Rotsch, C. and M. Radmacher (2000). "Drug-Induced Changes of Cytoskeletal Structure and Mechanics in Fibroblasts: An Atomic Force Microscopy Study". In: *Biophysical Journal*, 781, pp. 520–535.

Roy, P., S. Berger, and P. Schmuki (2011). "TiO$_2$ Nanotubes: Synthesis and Applications". In: *Angewandte Chemie International Edition*, 5013, pp. 2904–2939.

Sasaki, N. (2012). "Viscoelastic Properties of Biological Materials". In: *Viscoelasticity - From Theory to Biological Applications*. Ed. by J. De Vicente. InTech.

Satcher Jr, R. L. and C. F. Dewey Jr (1996). "Theoretical estimates of mechanical properties of the endothelial cell cytoskeleton". In: *Biophysical Journal*, 711, pp. 109–118.

Schrag, M., S. Sharma, H. Brown-Borg, and O. Ghribi (2008). "Hippocampus of Ames dwarf mice is resistant to β-amyloid-induced tau hyperphosphorylation and changes in apoptosis-regulatory protein levels". en. In: *Hippocampus*, 183, pp. 239–244.

Schramm, G. A. (1994). *A Practical Approach to Rheology and Rheometry*. en. Haake.

Schweizer, J., P. E. Bowden, P. A. Coulombe, L. Langbein, E. B. Lane, T. M. Magin, L. Maltais, M. B. Omary, D. A. D. Parry, M. A. Rogers, and M. W. Wright (2006). "New consensus nomenclature for mammalian keratins". en. In: *The Journal of Cell Biology*, 1742, pp. 169–174.

Selhuber-Unkel, C., T. Erdmann, M. López-García, H. Kessler, U. S. Schwarz, and J. P. Spatz (2010). "Cell Adhesion Strength Is Controlled by Intermolecular Spacing of Adhesion Receptors". In: *Biophysical Journal*, 984, pp. 543–551.

Semmrich, C., T. Storz, J. Glaser, R. Merkel, A. R. Bausch, and K. Kroy (2007). "Glass transition and rheological redundancy in F-actin solutions". en. In: *Proceedings of the National Academy of Sciences*, 10451, pp. 20199–20203.

Shao, J.-Y. (2001). "Measuring piconewton forces and its application in cellular and molecular biomechanics". In: *Advances in Biomechanics*, pp. 47–51.

Shin, D. H., T. Shokuhfar, C. K. Choi, S.-H. Lee, and C. Friedrich (2011). "Wettability changes of TiO$_2$ nanotube surfaces". en. In: *Nanotechnology*, 2231, p. 315704.

Sigal, I. A., J. G. Flanagan, and C. R. Ethier (2005). "Factors Influencing Optic Nerve Head Biomechanics". en. In: *Investigative Ophthalmology & Visual Science*, 4611, pp. 4189–4199.

Sigal, I. A., J. G. Flanagan, I. Tertinegg, and C. R. Ethier (2004). "Finite Element Modeling of Optic Nerve Head Biomechanics". en. In: *Investigative Ophthalmology & Visual Science*, 4512, pp. 4378–4387.

Smith, B. S., S. Yoriya, T. Johnson, and K. C. Popat (2011). "Dermal fibroblast and epidermal keratinocyte functionality on titania nanotube arrays". In: *Acta Biomaterialia*, 76, pp. 2686–2696.

Smith, B. A., B. Tolloczko, J. G. Martin, and P. Grütter (2005). "Probing the Viscoelastic Behavior of Cultured Airway Smooth Muscle Cells with Atomic Force Microscopy: Stiffening Induced by Contractile Agonist". In: *Biophysical Journal*, 884, pp. 2994–3007.

Smith, S. B., L Finzi, and C Bustamante (1992). "Direct mechanical measurements of the elasticity of single DNA molecules by using magnetic beads". eng. In: *Science (New York, N.Y.)* 2585085, pp. 1122–1126.

Sollich, P. (1998). "Rheological constitutive equation for a model of soft glassy materials". In: *Physical Review E*, 581, pp. 738–759.

Song, W. and J. F. Mano (2013). "Interactions between cells or proteins and surfaces exhibiting extreme wettabilities". en. In: *Soft Matter*, 911, pp. 2985–2999.

Springer, A. D. and A. E. Hendrickson (2004). "Development of the primate area of high acuity. 1. Use of finite element analysis models to identify mechanical variables affecting pit formation". In: *Visual neuroscience*, 2101, pp. 53–62.

Stamenović, D. (2008). "Rheological behavior of mammalian cells". en. In: *Cellular and Molecular Life Sciences*, 6522, pp. 3592–3605.

Stamenović, D. (1991). "A model of foam elasticity based upon the laws of plateau". In: *Journal of Colloid and Interface Science*, 1451, pp. 255–259.

Stamenović, D. (2005). "Effects of cytoskeletal prestress on cell rheological behavior". In: *Acta Biomaterialia*, 13, pp. 255–262.

Stamenović, D., Z. Liang, J. Chen, and N. Wang (2002). "Effect of the cytoskeletal prestress on the mechanical impedance of cultured airway smooth muscle cells". en. In: *Journal of Applied Physiology*, 924, pp. 1443–1450.

Stevens, J. D., I. L. Jones, M Warner, M. J. Lavin, and P. K. Leaver (1992). "Mathematical modelling of retinal tear formation: Implications for the use of heavy liquids". In: *Eye*, 61, pp. 69–74.

Stoppini, L., P. A. Buchs, and D. Muller (1991). "A simple method for organotypic cultures of nervous tissue". In: *Journal of Neuroscience Methods*, 372, pp. 173–182.

Studer, H., X. Larrea, H. Riedwyl, and P. Büchler (2010). "Biomechanical model of human cornea based on stromal microstructure". In: *Journal of Biomechanics*, 435, pp. 836–842.

Su, T., B. Paradiso, Y.-S. Long, W.-P. Liao, and M. Simonato (2011). "Evaluation of cell damage in organotypic hippocampal slice culture from adult mouse: A potential model system to study neuroprotection". In: *Brain Research*, 1385, pp. 68–76.

Sundstrom, L., A. Pringle, B. Morrison, and M. Bradley (2005). "Organotypic cultures as tools for functional screening in the CNS". In: *Drug Discovery Today*, 1014, pp. 993–1000.

Sung, K. L., C. Dong, G. W. Schmid-Schönbein, S. Chien, and R. Skalak (1988). "Leukocyte relaxation properties". In: *Biophysical Journal*, 542, pp. 331–336.

Taylor, L., D. Moran, K. Arér, E. Warrant, and F. Ghosh (2013). "Stretch to See: Lateral Tension Strongly Determines Cell Survival in Long-Term Cultures of Adult Porcine Retina". en. In: *Investigative Ophthalmology & Visual Science*, 543, pp. 1845–1856.

Thoumine, O. and A. Ott (1997). "Time scale dependent viscoelastic and contractile regimes in fibroblasts probed by microplate manipulation". en. In: *Journal of Cell Science*, 11017, pp. 2109–2116.

Tout, S., T. Chan-Ling, H. Holländer, and J. Stone (1993). "The role of Müller cells in the formation of the blood-retinal barrier". In: *Neuroscience*, 551, pp. 291–301.

Trepat, X., M. Grabulosa, L. Buscemi, F. Rico, B. Fabry, J. J. Fredberg, and R. Farré (2003). "Oscillatory magnetic tweezers based on ferromagnetic beads and simple coaxial coils". In: *Review of Scientific Instruments*, 749, pp. 4012–4020.

Trepat, X., L. Deng, S. S. An, D. Navajas, D. J. Tschumperlin, W. T. Gerthoffer, J. P. Butler, and J. J. Fredberg (2007). "Universal physical responses to stretch in the living cell". en. In: *Nature*, 4477144, pp. 592–595.

Trepat, X., G. Lenormand, and J. J. Fredberg (2008). "Universality in cell mechanics". en. In: *Soft Matter*, 49, pp. 1750–1759.

Tsacopoulos, M. and P. J. Magistretti (1996). "Metabolic coupling between glia and neurons". en. In: *The Journal of Neuroscience*, 163, pp. 877–885.

Tseng, Y., T. P. Kole, and D. Wirtz (2002). "Micromechanical Mapping of Live Cells by Multiple-Particle-Tracking Microrheology". In: *Biophysical Journal*, 836, pp. 3162–3176.

Uchio, E., S. Ohno, J. Kudoh, K. Aoki, and L. T. Kisielewicz (1999). "Simulation model of an eyeball based on finite element analysis on a supercomputer". en. In: *British Journal of Ophthalmology*, 8310, pp. 1106–1111.

Uckermann, O., I. Iandiev, M. Francke, K. Franze, J. Grosche, S. Wolf, L. Kohen, P. Wiedemann, A. Reichenbach, and A. Bringmann (2004). "Selective staining by vital dyes of Müller glial cells in retinal wholemounts". In: *Glia*, 451, pp. 59–66.

Uga, S. and G. K. Smelser (1973). "Comparative study of the fine structure of retinal Müller cells in various vertebrates". In: *Investigative Ophthalmology & Visual Science*, 126, pp. 434–448.

Valiron, O, N Caudron, and D Job (2001). "Microtubule dynamics". eng. In: *Cellular and molecular life sciences: CMLS*, 5814, pp. 2069–2084.

Van Vliet, K., G Bao, and S Suresh (2003). "The biomechanics toolbox: experimental approaches for living cells and biomolecules". In: *Acta Materialia*, 5119, pp. 5881–5905.

Vincent, J. (2012). *Structural biomaterials*. Princeton University Press.

Vliet, K. J. V., G. Bao, and S. Suresh (2003). *The biomechanics toolbox: experimental approaches for living cells and biomolecules.*

Vonna, L., A. Wiedemann, M. Aepfelbacher, and E. Sackmann (2003). "Local force induced conical protrusions of phagocytic cells". en. In: *Journal of Cell Science*, 1165, pp. 785–790.

Vunjak-Novakovic, G. and R. I. Freshney (2006). *Culture of Cells for Tissue Engineering.* en. John Wiley & Sons.

Wang, J., A. M. Kolomeyer, M. A. Zarbin, and E. Townes-Anderson (2011). "Organotypic culture of full-thickness adult porcine retina". eng. In: *Journal of Visualized Experiments: JoVE*, 49.

Wang, N, J. P. Butler, and D. E. Ingber (1993). "Mechanotransduction across the cell surface and through the cytoskeleton". eng. In: *Science (New York, N.Y.)* 2605111, pp. 1124–1127.

Wang, N., I. M. Tolić-Nørrelykke, J. Chen, S. M. Mijailovich, J. P. Butler, J. J. Fredberg, and D. Stamenović (2002a). "Cell prestress. I. Stiffness and prestress are closely associated in adherent contractile cells". en. In: *American Journal of Physiology - Cell Physiology*, 2823.

Wang, N., K. Naruse, D. Stamenović, J. J. Fredberg, S. M. Mijailovich, I. M. Tolić-Nørrelykke, T. Polte, R. Mannix, and D. E. Ingber (2001). "Mechanical behavior in living cells consistent with the tensegrity model". en. In: *Proceedings of the National Academy of Sciences*, 9814, pp. 7765–7770.

Wang, S. W., X. Mu, W. J. Bowers, and W. H. Klein (2002b). "Retinal ganglion cell differentiation in cultured mouse retinal explants". In: *Methods*, 284, pp. 448–456.

Waugh, R. E. and R. G. Bauserman (1995). "Physical measurements of bilayer-skeletal separation forces". eng. In: *Annals of biomedical engineering*, 233, pp. 308–321.

7 Bibliography

Weale, R. A. (1974). "The Vertebrate Retina. Principles of Structure and Function". In: *The British Journal of Ophthalmology*, 5811, pp. 948–949.

Weitz, D. A. (2001). "Condensed matter: Memories of paste". en. In: *Nature*, 4106824, pp. 32–33.

Wen, Q. and P. A. Janmey (2011). "Polymer physics of the cytoskeleton". In: *Current Opinion in Solid State and Materials Science*, 155, pp. 177–182.

Wiche, G. (1998). "Role of plectin in cytoskeleton organization and dynamics". en. In: *Journal of Cell Science*, 11117, pp. 2477–2486.

Willoughby, C. E., D. Ponzin, S. Ferrari, A. Lobo, K. Landau, and Y. Omidi (2010). "Anatomy and physiology of the human eye: effects of mucopolysaccharidoses disease on structure and function - a review: Anatomy and physiology of the eye". In: *Clinical & Experimental Ophthalmology*, 38, pp. 2–11.

Wirtz, D. (2009). "Particle-Tracking Microrheology of Living Cells: Principles and Applications". In: *Annual Review of Biophysics*, 381, pp. 301–326.

Wollensak, G. (2006). "Biomechanical properties of retina". In: *Journal of Biomechanics*. Abstracts of the 5th World Congress of Biomechanics, 39, Supplement 1, S634–S635.

Woo, S. L.-Y., A. S. Kobayashi, W. A. Schlegel, and C. Lawrence (1972). "Nonlinear material properties of intact cornea and sclera". In: *Experimental Eye Research*, 141, pp. 29–39.

Worthington, K. S., L. A. Wiley, A. M. Bartlett, E. M. Stone, R. F. Mullins, A. K. Salem, C. A. Guymon, and B. A. Tucker (2014). "Mechanical properties of murine and porcine ocular tissues in compression". In: *Experimental Eye Research*, 121, pp. 194–199.

Wottawah, F., S. Schinkinger, B. Lincoln, R. Ananthakrishnan, M. Romeyke, J. Guck, and J. Käs (2005). "Optical Rheology of Biological Cells". In: *Physical Review Letters*, 949, p. 098103.

Wu, W., I. W. H. Peters, and M. E. Hammer (1987). "Basic Mechanical Properties of Retina in Simple Elongation". In: *Journal of Biomechanical Engineering*, 1091, pp. 65–67.

Xin, H., J.-A. S. Yannazzo, R. S. Duncan, E. V. Gregg, M. Singh, and P. Koulen (2007). "A novel organotypic culture model of the postnatal mouse retina allows the study of

glutamate-mediated excitotoxicity". In: *Journal of Neuroscience Methods*, 1591, pp. 35–42.

Yamada, S., D. Wirtz, and S. C. Kuo (2000). "Mechanics of Living Cells Measured by Laser Tracking Microrheology". In: *Biophysical Journal*, 784, pp. 1736–1747.

Yao, X. Y., G. S. Hageman, and M. F. Marmor (1994). "Retinal adhesiveness in the monkey." en. In: *Investigative Ophthalmology & Visual Science*, 352, pp. 744–748.

Yoon, J. J., L. F. B. Nicholson, S. X. Feng, J. C. Vis, and C. R. Green (2010). "A novel method of organotypic brain slice culture using connexin-specific antisense oligodeoxynu-cleotides to improve neuronal survival". In: *Brain Research*, 1353, pp. 194–203.

Yu, D. Y., S. J. Cringle, V. A. Alder, E. N. Su, and P. K. Yu (1996). "Intraretinal oxygen distribution and choroidal regulation in the avascular retina of guinea pigs". en. In: *American Journal of Physiology - Heart and Circulatory Physiology*, 2703.

Zeng, R., Y. Zhang, F. Shi, and F. Kong (2012). "A Novel Experimental Mouse Model of Retinal Detachment: Complete Functional and Histologic Recovery of the Retina". en. In: *Investigative Ophthalmology & Visual Science*, 533, pp. 1685–1695.

Zhang, S. S.-M., X.-Y. Fu, and C. J. Barnstable (2002). "Tissue culture studies of retinal development". In: *Methods*, 284, pp. 439–447.

Acknowledgements

First and foremost I would like to express my gratitude to my supervisors, Prof. Andreas Reichenbach and Prof. Josef Käs for welcoming in their research teams, for their support and guidance during the past four years and for giving me the tools and the freedom to become a scientist. I would like to thank Dr. Mareike Zink and Prof. Stefan Mayr for introducing me to the world of TiO_2 nanotube arrays. This definitely made a huge impact in my research. Moreover, my acknowledgment goes to Dr. Kristian Franze for letting me spend some time in his lab in Cambridge, for the motivating discussions and for the AFM measurements.

Starting this "adventure" in Leipzig meant also being part of the Marie Curie ITN eduGLIA. I am really grateful for the people I met, for the stimulating conversation and interesting courses attended. Thank to all the fellows: Hannah, Cai, Ciaran, Ilaria, Györgyi, David, Joanna, Mina, Priyanka, Rebekah, Ciro, Kristi, Craig and Xiaoguang and of course above all Isabell! We shared a lot of unforgettable moments in amazing locations. It has truly been an amazing experience from a scientific and social point of view. Thank you, Sigrid and Thomas for listening to us and for organizing everything beautifully.

I was lucky enough to work in two research groups with different backgrounds allowing me to to take the best from both worlds. In each lab I have always found support and motivation. Thanks to my fellows labmates in the Paul-Flechsig Institute: Lysann, Annett, Claudi, Steffi, Heidi, Nicole and Martina and Dr. Antje Grosche. A special thanks goes to Colle for dealing with administration problems, to Dr. Elke Ulbricht for teaching me about immunostaining, to Dr. Petra Hirrlinger for passing on her knowledge about the isolation of neural tissue, and last but not least to Dr. Thomas Pannike for being always there to answer to my questions and to diligently proofreading this manuscript. Thanks to all my labmates in the Soft Matter Physics department, in particular Philipp, Lydia, Melanie, Tobias and David. I would like to thank Roland Stange and Thomas Fuhs for introducing me to Labview. A huge thank to Susanne Rönicke for her perseverance in speaking with me only in German forcing me to learn this challenging language, for her advises and for proofreading this manuscript. I am really grateful to Jürgen Lippoldt for listening to my requests, for being patient and especially for helping me in the last months with the Matlab, LaTex and the challenging analysis. Furthermore, I would like to thank the people whose indispensable work always keeps the lab running: Claudia Brück, Ms. Jungmann, Elke Westphal and Dr. Undine Dietrich. I also would like to acknowledge Dr. Bernd Biedermann and Berd Kohlstrunk for their technical assistance.

Selbstständigkeitserklärung

Hiermit versichere ich, dass die vorliegende Arbeit ohne unzulässige Hilfe und ohne Benutzung anderer als der angegebenen Hilfsmittel angefertigt und dass die aus fremden Quellen direkt oder indirekt übernommenen Gedanken in der Arbeit als solche kenntlich gemacht wurden. Alle Personen von denen bei der Auswahl und Auswertung des Materials sowie bei der Herstellung des Manuskripts Unterstützungsleistungen erhalten wurde sind namentlich genannt. Außer den in der Arbeit Genannten, waren keine weiteren Personen bei der geistigen Herstellung der vorliegenden Arbeit beteiligt, insbesondere haben keine Personen von dem Bewerber oder in seinem Auftrag weder unmittelbar noch mittelbar geldwerte Leistungen für Arbeiten erhalten, die im Zusammenhang mit dem Inhalt der vorgelegten Dissertation stehen. Es wird weiterhin versichert, dass die vorgelegte Arbeit weder im Inland noch im Ausland in gleicher oder in ähnlicher Form einer anderen Prüfungsbehörde zum Zwecke einer Promotion oder eines anderen Prüfungsverfahrens vorgelegt und in ihrer Gesamtheit noch nicht veröffentlicht wurde. Es haben keine früheren erfolglosen Promotionsversuche stattgefunden.

Leipzig, den 19. September 2014 ....